Preliminary Development of a Three-Dimensional Numerical Model for Reservoir Hydrodynamics

by Robert S. Bernard

19960124 116

DTIC QUALITY INSPECTED 1

The contents of this report are not to be used for advertising, publication, or promotional purposes. Citation of trade names does not constitute an official endorsement or approval of the use of such commercial products.

Preliminary Development of a Three-Dimensional Numerical Model for Reservoir Hydrodynamics

by Robert S. Bernard

U.S. Army Corps of Engineers
Waterways Experiment Station
3909 Halls Ferry Road
Vicksburg, MS   39180-6199

Final report

**US Army Corps
of Engineers**
Waterways Experiment
Station

N

INFORMATION
TECHNOLOGY
LABORATORY

GEOTECHNICAL
LABORATORY

HEADQUARTERS
BUILDING

COASTAL ENGINEERING
RESEARCH CENTER

MAIN
ENTRANCE

HYDRAULICS
LABORATORY

ENVIRONMENTAL
LABORATORY

STRUCTURES
LABORATORY

FOR INFORMATION CONTACT:
PUBLIC AFFAIRS OFFICE
U. S. ARMY ENGINEER
WATERWAYS EXPERIMENT STATION
3909 HALLS FERRY ROAD
VICKSBURG, MISSISSIPPI 39180-6199
PHONE : (601)634-2502

SCALE
800   0   800 m

AREA OF RESERVATION = 2.7 sq km

Contents

Preface

This report presents the results of research and development conducted from April 1991 through May 1994 by personnel of the Reservoir Water Quality Branch (RWQB), Hydraulic Structures Division (HSD), Hydraulics Laboratory (HL), U.S. Army Engineer Waterways Experiment Station (WES). Funding was provided by the U.S. Army Engineer District, Chicago.

Dr. Robert S. Bernard, RWQB, prepared this report under the general supervision of Messrs. Frank A. Herrmann, Jr., Director, HL; Richard A. Sager, Assistant Director, HL; and Glenn A. Pickering, Chief, HSD. Technical counsel was provided by Messrs. Mike Schneider, Stacy Howington, and Steve Wilhelms, RWQB; by Drs. Hartmut Kapitza and Dieter Eppel, GKSS Research Centre, Geesthacht, Germany; and by Drs. Abi Arabshahi, Lafe Taylor, Mike Stokes, Steve Davis, Boyd Gatlin, Dave Whitfield, Joe Thompson, Roger Briley, Pasquale Cinnella, Dave Huddleston, Bharat Soni, and Tim Swafford, and Mr. Mike Remotigue, Engineering Research Center for Computational Field Simulation, Mississippi State University. Dr. Kapitza provided the conjugate-gradient solver used for the pressure Poisson equation.

Technical monitors for the Chicago District were Mr. Tom Fogarty and Mrs. Linda Sorn.

At the time of preparation of this report, Dr. Robert W. Whalin was Director of WES, and COL Bruce K. Howard, EN, was Commander.

Conversion Factors, Non-SI to SI Units of Measurement

Non-SI units of measurement used in this report can be converted to SI units as follows:

Multiply	By	To Obtain
cubic feet	0.02831685	cubic meters
degrees (angle)	0.01745329	radians
feet	0.3048	meters
square feet	0.09290304	square meters

1   Introduction

Background

Computational fluid dynamics (CFD) is now used routinely by researchers and design engineers alike. New CFD codes (numerical flow models) appear every year. Although some of these are applicable for broad classes of flow problems, no single model is likely to gain universal acceptance in the foreseeable future. No one has yet written a general-purpose CFD code that works reliably and efficiently at all Reynolds numbers, Froude numbers, and Mach numbers. In spite of monumental gains in computer power, numerical flow modeling remains a problem-specific art.

Buoyant flow in reservoirs falls in a class of problems for which the Mach number is very small. Thus, the density can be assumed to vary only slightly with temperature and not at all with pressure. The resulting density gradients are so small that the governing equations reduce to the incompressible Navier-Stokes equations with a vertical perturbation added for buoyancy. The Froude number is generally small enough in reservoirs to justify neglect of surface waves, and the free surface can be assigned a uniform vertical velocity. In contrast, the Reynolds number may exceed 10^8, and empirical corrections are needed to model the small-scale influence of turbulence.

Some buoyant flow models assume the pressure in a water column to be hydrostatic, i.e., proportional to the weight of the water itself. This eliminates the vertical component of the momentum equation and guarantees that the remaining equations will all be of the same mathematical type, but it is acceptable only when the vertical acceleration is negligible. Deep reservoirs with submerged structures and sharply varying topography generally render the hydrostatic assumption invalid.

MAC3D is a numerical model for buoyant incompressible flow, with emphasis on reservoir hydrodynamics. In general, the model is intended for hydraulic applications in deep water where vertical motion and vertical acceleration are both important. It uses a variant of MacCormack's method (MacCormack 1969; Bernard 1992) to solve the Reynolds-averaged Navier-Stokes equations for three-dimensional (3-D) incompressible flow, which are discretized with six-sided finite-volume cells. The grid cells can be

nonrectangular in cartesian (x,y,z) space, but they are uniformly rectangular in the computational (i,j,k) space where they are indexed by the integer coordinates (i,j,k). This sequential ordering of grid cells in an ijk-array is commonly called a structured grid.

To improve local resolution and reduce computer memory requirements, MAC3D uses composite (multiblock) structured grids, i.e., structured grids composed of one or more subdomains (also known as blocks). The individual subdomains are rectangular in the computational (i,j,k) space, but they can have any shape and orientation in cartesian (x,y,z) space as long as their grid nodes match along the shared boundaries between the subdomains. The discrete flow variables are staggered, with contravariant (normal) velocity components defined at the centroids of the cell faces, and scalar quantities (pressure, temperature, etc.) defined at the cell centers.

MAC3D accounts for turbulence by using a k-ϵ turbulence model (Launder and Spalding 1974), which consists of two semiempirical equations for the production and transport of the turbulence energy k and the turbulence dissipation rate ϵ. Buoyancy arises from temperature-dependent density variations that add a perturbing force to the vertical momentum equation in the presence of gravity. The transport of heat (temperature) and other passive constituents is governed by advection-diffusion equations, in which the diffusion coefficients are proportional to the eddy viscosity obtained from the turbulence model.

The normal velocity along inflow/outflow boundaries can be imposed either as an unchanging, user-specified distribution or as a time-varying distribution extrapolated from the flow just inside the grid. In the latter case, the extrapolated velocities are obtained from a discrete radiation condition proposed by Orlanski (1976), which transmits internal disturbances out of the grid with negligible reflection. Solid boundaries can be designated as either no-slip (frictional) or slip (frictionless). The shear stress along no-slip boundaries is obtained either from Manning's equation or from an empirical wall function that defines the relation between velocity and distance from the boundary. Free surfaces are idealized as (rigid) slip boundaries.

MAC3D tentatively assumes all solid boundaries and free surfaces to be impermeable and adiabatic (thermally insulated), so that heat and other passive constituents can enter or leave the flow field only through the inflow/outflow boundaries. The actual rate of heat transfer through a free surface depends on external factors such as radiation and wind (which also creates momentum transfer), and these will be dealt with in future work. For the time being, however, the model allows the adiabatic constraint to be relaxed in the following manner.

Suppose that a reservoir is initially stratified with cold water at the bottom and warm water at the surface. If all the boundaries are adiabatic (no heat transfer) and impermeable (no inflow or outflow), then diffusion (heat conduction) will gradually eliminate the initial stratification, leaving the reservoir

with a single uniform temperature. In some cases, however, one may wish to know only the manner in which a particular flow alters the initial stratification, and not the rate at which the insulated reservoir otherwise comes to equilibrium. Accordingly, if the user so chooses, MAC3D will ignore any change in temperature not produced by the flow itself. In other words, it will ignore background heat conduction. This allows the user to isolate the effect of the flow upon the stratification. Otherwise, the model will allow the temperature to evolve toward an equilibrium state dictated by the imposed flow, the full heat conduction, and the adiabatic boundaries.

Purpose and Scope

The planned McCook Reservoir near Chicago, IL, will serve as a holding tank for runoff and sewage (prior to treatment) through the middle of the twenty-first century. Its design and construction pose major engineering challenges because of its size—roughly 4,700 ft[1] long, 3,300 ft wide, and 110 to 150 ft deep. Safe operation of the reservoir demands an intimate understanding of its hydrodynamics, and this warrants the development of a nonhydrostatic, 3-D numerical model as a means to that end. A model of this kind would be useful not only for McCook Reservoir, but for other applications as well.

This report documents the preliminary development of the MAC3D numerical model and offers qualitative demonstrations of MAC3D's capabilities using a provisional 10-block grid for McCook Reservoir. Quantitative testing and empirical validation of the model are already underway, but these are lengthy efforts that will be documented in future reports.

Chapter 2 outlines the governing equations for the major flow variables, while Chapter 3 describes the discrete methods used for their numerical solution. Chapter 4 summarizes briefly the operation of the model as a whole, and Chapter 5 presents the results of preliminary flow calculations for McCook Reservoir. Chapter 6 offers conclusions and recommendations with regard to further model development.

---

[1] A table of factors for converting non-SI units of measurement to SI units is found on page vi.

2   Governing Equations

Incompressible Flow

The speed of sound in fresh water is about 4,700 ft/sec. With Mach number defined as the ratio of flow speed to sound speed, water flowing at 47 ft/sec has a Mach number of 0.01. At Mach numbers on the order of 10^{-2}, water behaves as though it were truly incompressible (except for questions related to acoustics). In this context, an incompressible fluid is defined as one whose density varies with temperature but not with pressure.

The density of liquid water is greatest at 4° C, above which it falls monotonically with temperature up to 100° C. This behavior of the density ρ is conveniently expressed as

$$\rho = \rho_0 \left[1 - \theta(T) \right] \tag{1}$$

where[1]

ρ_0 = reference (maximum) density

θ = relative deviation from the reference value

T = temperature

For temperatures in the range 0-30° C, θ can be approximated with

$$\theta = A \left| T - T_0 \right| + B \left(T - T_0 \right)^2 \tag{2}$$

where

$A = 5.6250 \times 10^{-6}$

---

[1]   For convenience, symbols and abbreviations are listed in the notation (Appendix A).

$$B = 6.5625 \times 10^{-6}$$

$$T_0 = 4^{\circ} C$$

At 30 °C, Equation 2 gives $\theta = 0.00458$, indicating that the density deviates only slightly from its reference value. Dissolved constituents such as salt can also produce comparable density variations, and salinity may be included in future versions of MAC3D. In any case, except for the vertical buoyant force in the presence of gravity, one can ignore small variations of the density and impose the fully incompressible constraint for conservation of mass,

$$div \, \underline{u} = 0 \qquad (3)$$

where the symbol *div* denotes the divergence operator, $\underline{u}$ represents the velocity, and a single underbar henceforth indicates a vector. Applying the same arguments to the equation for conservation of momentum, one obtains

$$\rho_0 \frac{D\underline{u}}{Dt} = div \, \underline{\underline{\tau}} - grad \, p + \rho \, \underline{g} \qquad (4)$$

where

t = time

τ = shear stress

p = pressure

g = acceleration due to gravity

and a double underbar henceforth indicates a tensor. The symbol *grad* represents the gradient operator, and *D/Dt* denotes the substantive (total) time-derivative operator,

$$\frac{D}{Dt} = \frac{\partial}{\partial t} + \underline{u} \cdot grad \qquad (5)$$

The *grad* and *div* operators are standard vector notation. In cartesian (x, y, z) coordinates they take the following form:

$$div \, \underline{u} \;=\; \frac{\partial u}{\partial x} \;+\; \frac{\partial v}{\partial y} \;+\; \frac{\partial w}{\partial z} \tag{6}$$

$$grad \, \psi \;=\; \left[\frac{\partial \psi}{\partial x}, \frac{\partial \psi}{\partial y}, \frac{\partial \psi}{\partial z} \right] \tag{7}$$

The triad (u, v, w) gives the cartesian components of the vector $\underline{u}$, and the symbol ψ here denotes any scalar function or vector component. For the latter, the operator $\underline{u} \cdot grad$ yields

$$\underline{u} \cdot grad \, \psi \;=\; u \frac{\partial \psi}{\partial x} \;+\; v \frac{\partial \psi}{\partial y} \;+\; w \frac{\partial \psi}{\partial z} \tag{8}$$

For turbulent flow, the velocity in Equations 3 and 4 is the Reynolds-averaged velocity, and the shear stress includes the viscous stress and the turbulent Reynolds stress. Invoking the Boussinesq hypothesis for turbulence, the two stresses are combined in a single expression,

$$\tau_{ij} \;=\; \mu \left[\frac{\partial u_i}{\partial x_j} \;+\; \frac{\partial u_j}{\partial x_i} \right] \tag{9}$$

The dynamic viscosity μ is the sum of the molecular viscosity μ_M and the eddy viscosity μ_T. Since $\mu_T >> \mu_M$ one assumes in practice that $\mu \approx \mu_T$. In Equation 9, the subscripts i and j take integer values 1, 2, and 3. Thus, the vector (u_1, u_2, u_3) represents velocity (u, v, w), and the vector (x_1, x_2, x_3) represents position (x, y, z) in a cartesian coordinate system. The tensor stress component τ_{ij} is the shear stress in the x_i^{th} direction on a plane normal to the x_j^{th} direction (and vice versa, because of symmetry). For example, τ_{12} is the shear stress in the x-direction on a plane normal to the y-direction, given by

$$\tau_{12} \;=\; \tau_{21} \;=\; \mu \left[\frac{\partial u_1}{\partial x_2} \;+\; \frac{\partial u_2}{\partial x_1} \right] \;=\; \mu \left[\frac{\partial u}{\partial y} \;+\; \frac{\partial v}{\partial x} \right] \tag{10}$$

Assuming that the temperature, viscosity, and pressure are known at each instant, then Equations 3 and 4 uniquely determine the evolution of the flow with time. Temperature can be obtained from a transport equation for heat, and eddy viscosity from a suitable turbulence model, but there is no equation of state from which to derive the pressure. The correct pressure gradient for

incompressible flow is that which ensures conservation of mass as expressed by Equation 3. To obtain a governing equation of convenient form for pressure, one takes the divergence of Equation 4. This produces a Poisson equation, i.e.,

$$\frac{\partial^2 p}{\partial x^2} + \frac{\partial^2 p}{\partial y^2} + \frac{\partial^2 p}{\partial z^2} = -div \left[\rho_0 \frac{D\underline{u}}{Dt} - div\, \underline{\underline{\tau}} - \rho\, \underline{g} \right] \tag{11}$$

In practice, the right-hand side of Equation 11 is obtained in the following manner. Suppose that the flow is to be advanced from time t to $t + \Delta t$. Let u be the mass-conserving velocity at time t, and let $\underline{u}'$ be a non-mass-conserving velocity computed for time $t + \Delta t$ by <u>omitting</u> *grad p* from Equation 4. Thus, $div\, \underline{u}' \neq 0$, where

$$\underline{u}' = \underline{u} - \frac{\Delta t}{\rho_0} \left(\rho_0\, \underline{u} \cdot grad\, \underline{u} - div\, \underline{\underline{\tau}} - \rho\, \underline{g} \right) \tag{12}$$

If *grad p* is the (unknown) pressure gradient that has to be imposed at time t to guarantee conservation of mass at time $t + \Delta t$, then Equation 11 reduces to

$$\frac{\partial^2 p}{\partial x^2} + \frac{\partial^2 p}{\partial y^2} + \frac{\partial^2 p}{\partial z^2} = \frac{\rho_0}{\Delta t}\, div\, \underline{u}' \tag{13}$$

In other words, even if the velocity $\underline{u}$ is known at a given time, the pressure for that time is <u>not</u> necessarily known. To find the correct pressure, the momentum equation (4) must first be advanced (integrated) provisionally over a small time increment Δt <u>without</u> including a pressure gradient. The resulting mass-conservation error $div\, \underline{u}' \neq 0$ then provides the right side of the Poisson equation (11, 13) whose solution yields the unknown pressure gradient.

Passive Transport

The transport equations for quantities other than momentum all have the general form of an advection-diffusion equation with a source/sink term on the right side, i.e.,

$$\frac{D\psi}{Dt} = div\, (\nu_\psi\, grad\, \psi) + S_\psi \tag{14}$$

where ν_ψ is the diffusivity and S_ψ is the source/sink term for the transported quantity ψ. One ordinarily assumes ν_ψ to be proportional to the kinematic fluid viscosity ν, i.e.,

$$\nu_\psi \approx P_\psi \, \nu \tag{15}$$

where

$$\nu = \frac{\mu}{\rho} \approx \frac{\mu_T}{\rho_0} \tag{16}$$

where P_ψ is the ratio of diffusivity to kinematic viscosity for the particular quantity ψ.

Heat Transfer

For incompressible flow, thermal energy (heat) is uncoupled from kinetic energy and is directly proportional to temperature. Thus, the equation for passive transport of heat reduces to an equation for temperature, i.e.,

$$\frac{DT}{Dt} = div\,(P_T \nu \; grad \; T) \; + \; S_T \tag{17}$$

where the coefficient P_T is the ratio of thermal diffusivity to kinematic viscosity, also known as the Prandtl number. The thermal source/sink term S_T is zero in the absence of chemical, biological, or radiative processes that generate or absorb heat.

Equation 17 determines the rate of internal heat transfer through the fluid itself, but not through the boundaries. In practice, solid boundaries can be regarded as adiabatic walls that insulate the flow from its surroundings. The adiabatic boundary condition for temperature is

$$\underline{n} \cdot grad \, T \; = \; 0 \tag{18}$$

where $\underline{n}$ is a unit vector normal to the boundary. Equation 18 is an acceptable approximation on the bottom and sides of a reservoir, but generally not on a free surface. Heat transfer across a free surface entails radiation, convection, and conduction, which depend on sunlight, wind, and ambient air temperature. When the influence of these external factors is unknown or poorly

defined, the following procedure offers a means of avoiding some of the difficulties arising from uncertainty.

Suppose a reservoir is stably stratified initially with a vertical (z-dependent) temperature distribution $T_S(z)$ that is constant (or very slowly changing) with time. One may think of $T_S(z)$ as a static (background) distribution sustained by unknown conditions outside the reservoir. In designing artificial measures to overcome or eliminate the stratification, it is expedient to compute immediate response to a perturbing flow and to ignore slow response to external conditions. To this end, Equations 17 and 18 are replaced by

$$\frac{DT}{Dt} = div\left[P_T \nu \; grad \; (T - T_S)\right] \tag{19}$$

and

$$\underline{n} \cdot grad\left(T - T_S\right) = 0 \tag{20}$$

Equations 19 and 20 ensure that there will be no departure from the static temperature $T_S(z)$ if there is no flow ($\underline{u} \equiv 0$) in the reservoir. This reformulation of the equations ignores background heat conduction (diffusion) and seeks to isolate the influence of the flow in particular upon stratification.

External influences obviously do have to be included in long-term reservoir simulations, but these have been deferred for later work. In the preliminary version of MAC3D, Equation 19 is used by default, with Equation 20 imposed on all boundaries except inflow/outflow boundaries. Background heat conduction (Equations 17 and 18) is optional.

Turbulence

Turbulence arises whenever there is too little molecular viscosity to prevent small disturbances from growing and disrupting a laminar flow. The process is self-limiting, so that a turbulent flow can be thought of as having a slowly varying mean-flow component and a smaller, rapidly varying turbulence component. The coupling between mean flow and turbulence is so strong that one cannot be calculated independently of the other, but the resulting range of eddy sizes is so great that conventional numerical methods cannot resolve them all. Thus, one must introduce empirical or semiempirical equations to model the influence of turbulence on mean flow, and vice versa. Henceforth, except for k and ϵ, all reference to the flow variables will tacitly imply the mean flow. The influence of buoyancy in the production and dissipation of turbulence is omitted in the preliminary version of MAC3D, but it will be incorporated in future work.

One of the most widely used turbulence models is the k-ϵ model of Launder and Spalding (1974). Here k is the turbulence energy (per unit mass), and ϵ is its dissipation rate. The kinematic eddy viscosity ν is related to k and ϵ by

$$\nu = C_\nu \frac{k^2}{\epsilon} \qquad (21)$$

where C_ν is an empirical coefficient. In the standard k-ϵ model, the governing equations for k and ϵ are, respectively,

$$\frac{Dk}{Dt} = \nu \Gamma - \epsilon + \frac{1}{\sigma_k} div\,(\nu\,grad\,k) \qquad (22)$$

$$\frac{D\epsilon}{Dt} = C_1 \nu \Gamma \frac{\epsilon}{k} - C_2 \frac{\epsilon^2}{k} + \frac{1}{\sigma_\epsilon} div\,(\nu\,grad\,\epsilon) \qquad (23)$$

The first term $\nu\Gamma$ on the right side of Equation 22 is the production rate for turbulence energy, in which

$$\Gamma = 2\left(u_x^2 + v_y^2 + w_z^2\right) + \left(u_y + v_x\right)^2 + \left(u_z + w_x\right)^2 + \left(v_z + w_y\right)^2 \qquad (24)$$

and the subscripts x, y, and z indicate partial derivatives. The standard set of nondimensional empirical coefficients is

$C_\nu = 0.09$

$C_1 = 1.44$

$C_2 = 1.92$

$\sigma_k = 1.0$

$\sigma_\epsilon = 1.3$

In regions of low velocity and high turbulence energy, the standard k-ϵ model overpredicts the eddy viscosity, which means that k is too large, or ϵ is too small, or both. There is no perfect remedy for this tendency, but ad hoc modifications that preferentially reduce k, enlarge ϵ, or damp production in low-velocity, high-turbulence regions can sometimes be *tuned* to improve flow

10

predictions in general (Bernard 1991, 1993). In MAC3D the quantity Γ is replaced in Equations 22 and 23 by Γ_*, where

$$\Gamma_* = \Gamma \tanh\left[\frac{u^2 + v^2 + w^2}{R_* \, \nu \sqrt{\Gamma}}\right] \qquad (25)$$

and $R_* \approx 5$ is a new empirical coefficient whose value has been chosen (by trial and error) to improve predictions for two-dimensional (2-D) recirculating flow.

The turbulence model provides equations for the production and transport of k and ϵ, but not for the necessary boundary conditions. These have to be deduced from other considerations. In one scenario used in previous work (Bernard 1993) and also in MAC3D, the condition $\underline{n} \cdot grad\, k = \underline{n} \cdot grad\, \epsilon = 0$ is imposed on all impermeable boundaries except no-slip walls, where tangential velocity and turbulence energy are both assumed proportional to the 1/7 power of distance from the wall. The tangential shear stress on no-slip walls is then taken to be

$$\tau_w = \frac{2}{7} C_w \mu_T \frac{u_w}{\delta} \qquad (26)$$

where u_w is the average tangential velocity over a distance δ normal to the wall. The quantity C_w is a wall coefficient whose default value (unity) applies only for hydraulically smooth walls, but this value can be changed at the user's discretion.

In an alternative scenario offered only in MAC3D, the condition $\partial k / \partial n = \partial \epsilon / \partial n = 0$ is imposed on all impermeable boundaries, and the shear stress on no-slip walls is taken to be

$$\tau_w = \rho_0 C_f u_w^2 \qquad (27)$$

where u_w is defined as before, and C_f is a nondimensional friction coefficient. The latter is obtained from the following relation derived from Manning's equation:

$$C_f = 14.5 \, \frac{n^2}{\delta^{1/3}} \tag{28}$$

where n is the Manning coefficient, and δ is defined as before. In this context n serves as a convenient (and familiar) parameter that characterizes the roughness of the wall. The factor 14.5 applies only when δ is given in <u>feet</u> in Equation 28. Otherwise, it becomes 9.8 when δ is given in <u>meters</u>.

In the first scenario, the energy production rate $\nu\Gamma_*$ is calculated everywhere using the definitions for Γ and Γ_* given by Equations 24 and 25. In the second scenario, however, the product $\nu\Gamma_*$ is replaced adjacent to no-slip boundaries by

$$\nu\Gamma_* \approx \frac{2}{\kappa} \, C_f^{3/2} \, \frac{u_w^3}{\delta} \tag{29}$$

where $\kappa \approx 0.418$ is von Karman's constant. This gives the production rate a value that it would otherwise have only at equilibrium (when production balances dissipation and diffusion).

Curvilinear Coordinates

For simplicity, all the governing equations have thus far been expressed in cartesian coordinates (x,y,z), but they are better expressed in curvilinear coordinates (ξ,η,ζ) for numerical solution on nonrectangular grids. Written in terms of the latter, the cartesian components of *grad* ψ are

$$\psi_x = \xi_x \psi_\xi + \eta_x \psi_\eta + \zeta_x \psi_\zeta \tag{30}$$

$$\psi_y = \xi_y \psi_\xi + \eta_y \psi_\eta + \zeta_y \psi_\zeta \tag{31}$$

$$\psi_z = \xi_z \psi_\xi + \eta_z \psi_\eta + \zeta_z \psi_\zeta \tag{32}$$

where the subscripts x,y,z and ξ,η,ζ indicate partial derivatives. Using the Gauss theorem, one finds that

$$div \, \underline{u} = \frac{1}{J} \left(U_\xi + V_\eta + W_\zeta \right) \tag{33}$$

and from Equations 30-32, it follows that

$$\underline{u} \cdot grad \, \psi = \frac{1}{J} \left(U \psi_\xi + V \psi_\eta + W \psi_\zeta \right) \tag{34}$$

where J is the Jacobian determinant,

$$J = \frac{\partial(x,y,z)}{\partial(\xi,\eta,\zeta)} = \begin{vmatrix} x_\xi & x_\eta & x_\zeta \\ y_\xi & y_\eta & y_\zeta \\ z_\xi & z_\eta & z_\zeta \end{vmatrix} \tag{35}$$

and U, V, and W are the volumetric fluxes in the ξ-, η-, and ζ-directions, respectively, given by

$$U = J \left(\xi_x u + \xi_y v + \xi_z w \right) \tag{36}$$

$$V = J \left(\eta_x u + \eta_y v + \eta_z w \right) \tag{37}$$

$$W = J \left(\zeta_x u + \zeta_y v + \zeta_z w \right) \tag{38}$$

Lastly, the derivatives of the curvilinear coordinates (ξ, η, ζ) with respect to the cartesian coordinates (x,y,z) are

$$\xi_x = \frac{1}{J} \left(y_\eta z_\zeta - y_\zeta z_\eta \right) \tag{39}$$

$$\xi_y = -\frac{1}{J} \left(x_\eta z_\zeta - x_\zeta z_\eta \right) \tag{40}$$

$$\xi_z = \frac{1}{J} \left(x_\eta y_\zeta - x_\zeta y_\eta \right) \tag{41}$$

$$\eta_x = -\frac{1}{J}\left(y_\xi z_\zeta - y_\zeta z_\xi\right) \tag{42}$$

$$\eta_y = \frac{1}{J}\left(x_\xi z_\zeta - x_\zeta z_\xi\right) \tag{43}$$

$$\eta_z = -\frac{1}{J}\left(x_\xi y_\zeta - x_\zeta y_\xi\right) \tag{44}$$

$$\zeta_x = \frac{1}{J}\left(y_\xi z_\eta - y_\eta z_\xi\right) \tag{45}$$

$$\zeta_y = -\frac{1}{J}\left(x_\xi z_\eta - x_\eta z_\xi\right) \tag{46}$$

$$\zeta_z = \frac{1}{J}\left(x_\xi y_\eta - x_\eta y_\xi\right) \tag{47}$$

3 Numerical Considerations

Finite-Volume Discretization

With the aid of Equations 30-47, all derivatives with respect to x, y, and z can be eliminated from the governing equations in Chapter 2, leaving only derivatives with respect to ξ, η, and ζ. For discretization, one then has to define the grid spacing $(\Delta\xi, \Delta\eta, \Delta\zeta)$ in the curvilinear (computational) coordinate system. The latter is arbitrary, and standard procedure is to impose unit spacing for convenience; i.e.,

$$\Delta\xi = \Delta\eta = \Delta\zeta = 1 \tag{48}$$

Since infinitesimal volumes in the two coordinate systems are related by

$$J \, d\xi \, d\eta \, d\zeta = dx \, dy \, dz \tag{49}$$

it then follows that the finite volume of a single discrete grid cell is given by

$$J = \int \int \int dx \, dy \, dz \tag{50}$$

In computational (ξ, η, ζ) space, all the grid cells are unit cubes; but in cartesian (x, y, z) space, they are hexahedrons of arbitrary shape, as shown in Figure 1. Thus, a triple integral appears on the right-hand side of Equation 50, with the limits of integration being the six faces of the grid cell. All discrete calculations are done in the computational (ξ, η, ζ) space for convenience.

MAC3D uses grids of the marker-and-cell (MAC) type for discretizing the governing equations discussed in Chapter 2. This means that scalar quantities such as pressure, temperature, density, etc., are defined at the centers of the

grid cells, while the volumetric fluxes (U, V, W) given by Equations 36-38 are defined at the centroids of the cell <u>faces</u>. Since the fluxes are proportional to the three cartesian components of velocity (u, v, w), the latter must also be defined on the cell faces. In practice, one needs definitions for u, v, and w at the cell centers as well, but more will be said about this later.

Discrete flow equations are obtained for each cell by integrating the governing equations over the cell volume and converting volume integrals to surface integrals via the Gauss theorem. The details of this procedure are given for two dimensions in Bernard (1993), which discusses the depth-averaged STREMR model. The extension to three dimensions is tedious but straightforward.

Computational Coordinates

Since the grid has unit spacing in the computational (ξ, η, ζ) space, it is convenient to replace the curvilinear coordinates (ξ, η, ζ) with the integer computational coordinates (i, j, k). Although the two sets of coordinates are identical, the integers (i, j, k) also serve as indices for entire grid cells and cell faces, in addition to defining the locations of the grid nodes in computational space.

In the MAC3D indexing scheme, cell (i, j, k) is the particular cell whose corners lie inclusively between nodes $(i-1, j-1, k-1)$ and (i, j, k), as shown in Figure 2. For example, <u>cell</u> $(1,1,1)$ has its eight corners at <u>nodes</u> $(0,0,0)$, $(0,0,1)$, $(0,1,0)$, $(1,0,0)$, $(0,1,1)$, $(1,0,1)$, $(1,1,0)$, and $(1,1,1)$.

In contrast to the cells themselves, there are <u>three</u> orientations of cell <u>faces</u>. Faces of constant i are called <u>i-faces</u>; faces of constant j are called <u>j-faces</u>; and faces of constant k are called <u>k-faces</u>. Face indices consist of <u>one node coordinate</u>, corresponding to the constant coordinate <u>on</u> that particular face, and <u>two cell indices</u>, corresponding to the remaining two indices for that particular cell.

Thus, the two i-faces for cell (i, j, k) are labelled as i-face (i, j, k) and i-face $(i-1, j, k)$. The four corners of i-face (i, j, k) lie at nodes (i, j, k), $(i, j-1, k)$, $(i, j, k-1)$, and $(i, j-1, k-1)$. The four corners of i-face $(i-1, j, k)$ lie at nodes $(i-1, j, k)$, $(i-1, j-1, k)$, $(i-1, j, k-1)$, and $(i-1, j-1, k-1)$.

For example, the two i-faces of cell $(1,1,1)$ are i-face $(1,1,1)$ and i-face $(0,1,1)$. I-face $(1,1,1)$ has its four corners at nodes $(1,1,1)$, $(1,1,0)$, $(1,0,1)$, and $(1,0,0)$. On the opposite side of the cell, i-face $(0,1,1)$ has its four corners at nodes $(0,1,1)$, $(0,1,0)$, $(0,0,1)$, and $(0,0,0)$.

16

Face-Centered Fluxes

Expressed in terms of the curvilinear coordinates, the incompressible constraint for conservation of mass (Equation 3) becomes

$$\frac{\partial U}{\partial \xi} + \frac{\partial V}{\partial \eta} + \frac{\partial W}{\partial \zeta} = 0 \tag{51}$$

where U, V, and W are the volumetric fluxes given by Equations 36-38. For a MAC grid cell in computational (i,j,k) space, U is defined for i-faces, V for j-faces, and W for k-faces. Using the <u>same</u> indices for the <u>fluxes</u> and the <u>faces</u> of cell (i,j,k), the discrete expressions for the partial derivatives in Equation 51 are

$$\frac{\partial U}{\partial \xi} = U(i,j,k) - U(i-1,j,k) \tag{52}$$

$$\frac{\partial V}{\partial \eta} = V(i,j,k) - V(i,j-1,k) \tag{53}$$

$$\frac{\partial W}{\partial \zeta} = W(i,j,k) - W(i,j,k-1) \tag{54}$$

In simpler terms, the volumetric flux through a cell face is just the area of the face multiplied by the velocity normal to the face. Thus, a mass-conserving flow can be established for cell (i,j,k) by correctly defining a single normal component, instead of three cartesian components, for the velocity on each of the six faces.

Cartesian Velocities

If all three velocity components (u, v, and w) <u>are</u> known for each cell face, then it is straightforward to calculate the appropriate volumetric flux (U, V, or W) through each face. When solving Equations 36-38 for u, v, and w, however, one finds that each of these velocity components requires three flux components (U, V, and W) that have to be taken from three distinct cell faces. Thus, if the flux <u>alone</u> is known for each face, there is not enough information to calculate all three velocity components at a single location. To compute u, v, and w on a given cell face, it is necessary to use flux information from <u>other</u> cell faces. This creates a dilemma concerning the

unambiguous definition of velocity components in the equations for conservation of mass (3 and 51) and momentum (4).

The problem is as follows. To maintain conservation of mass as required by Equation 51, the fluxes (U, V, W) and their time increments $(\Delta U, \Delta V, \Delta W)$ have to be uniquely defined on the cell faces. But the flux increments $(\Delta U, \Delta V, \Delta W)$ depend on the velocity increments $(\Delta u, \Delta v, \Delta w)$ via Equations 36-38, and these cannot be uniquely defined at a given location unless the velocity components themselves are uniquely defined. In the end, one has to choose between two alternatives: averaging flux components in space or averaging flux increments in time. MAC3D takes the latter approach, implemented in a predictor-corrector scheme.

Predictor-Corrector Scheme for Updating Fluxes

In the predictor phase, flux components (U, V, W) from three of the six faces are used to define the required velocity components (u, v, w), which are used in Equation 12 to calculate provisional velocity increments $(\Delta u', \Delta v', \Delta w')$. These are inserted into Equations 36 - 38 to obtain non-mass-conserving flux increments $(\Delta U', \Delta V', \Delta W')$, which are then added to the existing flux increments to obtain provisional flux components (U', V', W'). The latter are inserted in the curvilinear version of the Poisson equation for pressure, i.e.,

$$div \; grad \; p \; = \; \frac{\rho_0}{J \Delta t} \left[\frac{\partial U'}{\partial \xi} + \frac{\partial V'}{\partial \eta} + \frac{\partial W'}{\partial \zeta} \right] \tag{55}$$

After Equation 55 is solved iteratively for the pressure p, using a preconditioned conjugate scheme developed by Kapitza and Eppel (1987), the resulting pressure gradient is used to compute the correct, mass-conserving flux increments $(\Delta U^{(p)}, \Delta V^{(p)}, \Delta W^{(p)})$ for the predictor phase.

The corrector phase is similar to the predictor phase, except that the flux components (U, V, W) from the other three cell faces are used to define the required velocity components (u, v, w). The rest of the procedure for computing mass-conserving flux increments $(\Delta U^{(c)}, \Delta V^{(c)}, \Delta W^{(c)})$ for the corrector phase is the same as that for the predictor phase. At the end of the corrector phase, however, the flux increments obtained in both phases are averaged to give the net increments $(\Delta U, \Delta V, \Delta W)$ for one time-step; e.g.,

$$\Delta U = \frac{1}{2}\left(\Delta U^{(p)} + \Delta U^{(c)}\right) \tag{56}$$

Note that, given six faces to choose from, there are eight possible combinations of three, whose flux components can be used to define velocity components in the predictor phase. To avoid directional bias, MAC3D uses each of the eight possible combinations once in every eight time-steps.

Predictor-Corrector Scheme for Transport Equations

With the exception of the turbulence quantities k and ϵ (to be discussed later), a predictor-corrector scheme is used for updating all variables whose governing equations have the general form of Equation 14. Expressed in curvilinear coordinates, the latter becomes

$$J\frac{\partial \psi}{\partial t} + U\frac{\partial \psi}{\partial \xi} + V\frac{\partial \psi}{\partial \eta} + W\frac{\partial \psi}{\partial \zeta} = J\left[div\left(\nu_\psi\ grad\ \psi\right) + S_\psi\right] \tag{57}$$

The right-hand side of Equation 57 contains first- and second-order derivatives in space, while the left-hand side contains first-order derivatives in space and time. In both the predictor and corrector phases, the time derivative is approximated with

$$\frac{\partial \psi}{\partial t} = \frac{\psi^* - \psi}{\Delta t} \tag{58}$$

where ψ^* is the <u>new</u> value and ψ is the <u>old</u> value. In finite-difference jargon, this is called forward-time differencing.

For the first-order space derivatives, the predictor and corrector phases alternately use forward-space and backward-space differencing. For example, if the predictor phase uses

$$U\frac{\partial \psi}{\partial \xi} = U(i,j,k)\left[\psi(i+1,j,k) - \psi(i,j,k)\right] \tag{59}$$

then the corrector phase must follow with

$$U \frac{\partial \psi}{\partial \xi} = U(i-1,j,k) \left[\psi(i,j,k) - \psi(i-1,j,k) \right] \tag{60}$$

and vice versa. For all three coordinate directions there are eight possible combinations of forward- and backward-space differences that can be used in the predictor phase. MAC3D uses each of these combinations once in every eight time-steps to avoid accumulating directional bias.

The alternate use of forward and backward differencing for first-order space derivatives is called MacCormack's method (MacCormack 1969; Bernard 1993). In contrast, central differencing is used for second-order derivatives in space in both the predictor and corrector phases; e.g.,

$$\frac{\partial^2 \psi}{\partial \xi^2} = \psi(i+1,j,k) - 2 \psi(i,j,k) + \psi(i-1,j,k) \tag{61}$$

For a single time-step, the net increment $\Delta \psi$ is half the sum of the predictor increment $\Delta \psi^{(p)}$ and the corrector increment $\Delta \psi^{(c)}$, i.e.,

$$\Delta \psi = \frac{1}{2} \left(\Delta \psi^{(p)} + \Delta \psi^{(c)} \right) \tag{62}$$

MAC3D uses the foregoing differencing scheme not only for updating passive constituents, but also for computing provisional velocity increments $(\Delta u', \Delta v', \Delta w')$ via Equation 12. Expressed in its curvilinear form, the advective term in the x-component of the momentum equation becomes

$$\underline{u} \cdot grad \, u = \frac{1}{J} \left[U \frac{\partial u}{\partial \xi} + V \frac{\partial u}{\partial \eta} + W \frac{\partial u}{\partial \zeta} \right] \tag{63}$$

with similar expressions for $\underline{u} \cdot grad \, v$ and $\underline{u} \cdot grad \, w$ in the y- and z-components, respectively.

In Equation 12, the cartesian velocity components (u, v, w) are treated as though they were cell-centered quantities, even though they are computed from flux components (U, V, W) taken from three different faces. This artifice allows the provisional velocity increments $(\Delta u', \Delta v', \Delta w')$ to be computed in the same manner as the increments of truly cell-centered quantities. Directional bias is small (though not completely insignificant) after each full time-step, because the cartesian velocity components (u, v, w) are computed with

flux components (U, V, W) taken from opposing cell faces in the predictor and corrector phases.

As an alternative to the MacCormack scheme for discretizing $\underline{u} \cdot grad \; \psi$, MAC3D also offers two-point upwind differencing in both the predictor and corrector phases. For example, if $U(i-1,j,k) > 0$, then upwind differencing gives

$$U \frac{\partial \psi}{\partial \xi} = U(i-1,j,k) \left[\psi(i,j,k) - \psi(i-1,j,k) \right] \tag{64}$$

Otherwise, if $U(i,j,k) < 0$, then upwind differencing gives

$$U \frac{\partial \psi}{\partial \xi} = U(i,j,k) \left[\psi(i+1,j,k) - \psi(i,j,k) \right] \tag{65}$$

Although formally less accurate than the MacCormack scheme, the upwind scheme guarantees that changes in ψ propagate only in the direction of flow. It is intended for use mainly in situations where the MacCormack scheme proves numerically unstable or otherwise unsatisfactory.

Single-Step Upwind Scheme for Turbulence

The governing equations for turbulence (22 and 23) are very sensitive to the spatial discretization used for the total derivatives Dk/Dt and $D\epsilon/Dt$, and also to that used for the velocity derivatives in the rate coefficient Γ defined by Equation 24. After considerable experimentation with the turbulence equations, the MacCormack predictor-corrector scheme was abandoned in favor of a single-step upwind scheme for advancing k and ϵ in time. In the latter scheme, both $\underline{u} \cdot grad \; k$ and $\underline{u} \cdot grad \; \epsilon$ are discretized with upwind differencing, and their increments $(\Delta k, \Delta \epsilon)$ are computed in a single (predictor) step.

In contrast, the velocity derivatives appearing in Γ cannot be approximated with one-sided differencing, nor can the velocities themselves be calculated in the manner used in the predictor-corrector scheme for the momentum equation. In this case, the flux components (U, V, W) are averaged for opposing cell faces to obtain truly cell-centered approximations for the velocity components (u, v, w). The cell-centered velocities are then used in central-difference approximations for the velocity derivatives in Γ; e.g.,

$$\frac{\partial u}{\partial \xi} = \frac{1}{2}\left[u(i+1,j,k) - u(i-1,k,j) \right] \tag{66}$$

The foregoing measures are necessary to keep the variation of k, ϵ, and ν smooth and well-behaved. If the MacCormack scheme is used for k and ϵ, or if other approximations are imposed for the velocity derivatives in Γ, the computed flow may become unpredictably erratic.

Inflow/Outflow Boundaries

The bottom, sides, and free surface of a reservoir are true boundaries. That is, they are impermeable, and no fluid passes through them. In contrast, inflow/outflow boundaries are not true boundaries at all, but are mathematical conveniences that facilitate flow computation on a grid of limited extent.

MAC3D recognizes two types of inflow/outflow boundaries (FLUX and OPEN), both of which allow flow fluid to enter or leave the grid. The volumetric flux components (U, V, W) are fixed and unchanging (with time) on cell faces designated as FLUX faces. In addition, cell-centered quantities such as temperature, turbulence energy, etc., are assigned fixed values just outside the grid along FLUX boundaries.

OPEN boundaries are frontiers beyond which the flow is unknown and through which it passes as if no boundary were present at all. In principle, the only property of OPEN boundaries is transparency, and they should transmit outward-moving disturbances without producing any reflections. To obtain boundary values for velocity components normal to OPEN faces, as well as external values for cell-centered quantities just outside OPEN boundaries, MAC3D uses a discrete radiation condition proposed by Orlanski (1976). Subject to this boundary condition, normal velocities on OPEN faces are free to change in response to the flow just inside the grid, and cell-centered quantities just outside the grid are free to change in a similar manner.

Let ψ represent a face-centered (or cell-centered) quantity whose value is needed on (or just outside) an OPEN i-face. The discrete radiation condition imposes the following equation for the radiation of ψ through the i-face:

$$\psi_t + c\,\psi_\xi = 0 \tag{67}$$

Both the time derivative ψ_t and the space derivative ψ_ξ can be calculated from the existing flow in the previous time-step (or predictor phase). The one remaining unknown in Equation 67 is the propagation speed c, given by

$$c = -\frac{\psi_t}{\psi_\xi} \qquad (68)$$

The derivatives ψ_t and ψ_ξ are calculated via central-difference approximations using previous values for ψ and $\Delta\psi$ at locations just inside the grid.

If the sign of c is such that the direction of propagation would be inward rather than outward, the computed value of c is automatically replaced by zero. Now with the propagation speed completely defined, the new boundary value ψ' is given by

$$\psi' = \psi - c\,\Delta t\,\psi_\xi \qquad (69)$$

in which the derivative ψ_ξ is computed with a one-sided (forward or backward) difference approximation in the ξ-direction. For example, if i-face (i,j,k) is an OPEN face, and an external value is needed for ψ' in cell $(i+1,j,k)$, then

$$\psi'(i+1,j,k) = \psi(i+1,j,k)$$
$$- c\,\Delta t\,[\psi(i+1,j,k) - \psi(i,j,k)] \qquad (70)$$

4 Model Operation

Composite Grids

MAC3D uses composite grids (also known as multiblock grids) made up of one or more subdomains. These can have any shape and orientation in cartesian (x,y,z) space, and each subdomain occupies a distinct rectangular block of computational (i,j,k) space. The subdomains, or grid blocks, must be contiguous in cartesian space, but their placement in computational space is arbitrary as long as they are separated with buffer zones at least two (i,j,k) units thick. The buffer zones are needed to store updated values of flow variables for neighboring cells adjacent to the subdomain interfaces (in cartesian space).

For convenience, each grid block has its own local (i,j,k) coordinates. Once the position of a block has been specified in the global (i,j,k) coordinate system, all subsequent input for that block refers to its local (i,j,k) coordinates. Moreover, if a calculation is to be made for a limited portion of a reservoir, then only the grid blocks that encompass the region of interest need to be loaded into the calculation.

Composite grids facilitate calculations in which fine grid spacing is needed near a particular structure or boundary feature, but not elsewhere. For example, the wake created by a cylindrical pier in a rectangular channel is best computed with a fine cylindrical grid close to the pier, and a coarse rectangular grid far downstream.

Grid Generation

Grid generation can be accomplished with any of several 3-D numerical grid generators that are now commercially available. The main things to keep in mind are, first, that the grid nodes have to match perfectly (with no overlap) on the common boundaries of neighboring subdomains; second, that variations in grid spacing should be gradual rather than abrupt; and, third, that extreme skewness of intersecting grid lines should be avoided. As a rule of thumb, the grid spacing should change by no more than 30 percent from one

cell to the next, and the angle between intersecting grid lines should lie between 45 and 135 deg.

Inflow/Outflow Data

MAC3D accepts user-specified inflow/outflow data along FLUX boundaries and OPEN boundaries. Input velocity distributions may be uniform, linear, or parabolic. Temperature and other passive constituents may be assigned a single value along a particular boundary segment, or otherwise extrapolated from the initial vertical distribution in the reservoir. Uniform values are imposed for turbulence energy and dissipation rate (or eddy viscosity) along all inflow/outflow boundaries. As discussed in Chapter 3, initial values are held fixed for all time along FLUX boundaries, but they are allowed to change subject to the discrete radiation condition (e.g., Equation 67) along OPEN boundaries.

Initial Conditions

MAC3D uses the velocities specified along inflow/outflow boundaries to compute an irrotational, mass-conserving flow (potential flow) inside the grid, and this provides an initial condition for velocity. The net flow rate can be either computed directly from the inflow/outflow velocities or specified independently. In the latter case, MAC3D adjusts the magnitudes (but not the relative distributions) of the inflow/outflow velocities to match the specified flow rate. The initial temperature is a user-specified vertical distribution, which can be linear, cubic, or cubic spline.

Flow Development

Using the initial and boundary conditions previously discussed, MAC3D employs the numerical algorithms discussed in Chapter 3 to solve the governing equations outlined in Chapter 2. The discrete solution is advanced step by step through time to produce the developing flow. If a steady state is possible for the flow under consideration, the model should converge to that state and hover about it (with small deviations from one time-step to the next).

Because of the alternating directions used in the predictor-corrector scheme, small deviations from the steady state tend to repeat themselves over cycles of eight time-steps. Steady state is usually at hand when the maximum and minimum values of the flow variables remain unchanged for fifty or more of these cycles. In any case, when the real flow has no steady state, the computed flow likewise has no steady state.

The size of the time-step Δt has to be specified by the user, but MAC3D computes and prints two reference values that can be used for guidance. The first of these is the maximum allowable time increment Δt_{max} based on numerical stability considerations (Bernard 1993). The second is the period τ_N, which is the inverse of the Brunt-Väisälä frequency N. The quantity τ_N is the fundamental period of oscillation for a stratified fluid in the presence of gravity, given by

$$\tau_N = \sqrt{\frac{\rho_0}{g\frac{d\rho}{dz}}} \tag{71}$$

As a rule of thumb, the time-step should be slightly less than Δt_{max} and at least ten times smaller than τ_N.

If so directed by the input, MAC3D will compute and store the initial flow, and then stop. At this point, the user can examine the printed output, which includes quantities like Δt_{max} and τ_N, and set Δt to a suitable value. The computation can then be restarted and continued for a specified number of time-steps, after which Δt can be reset. This procedure can be repeated as many times as necessary.

Flow Visualization

At the end of each MAC3D run, all the major flow variables are stored in output files that can be used with appropriate flow-visualization software to create vectors, streamlines, color/contour maps, and other types of plots from the computed results. Output from MAC3D is generated in the well-known PLOT3D format, which is accepted by several different visualization packages that are now commercially available. Although the flow calculations them- selves can be executed on workstations or even personal computers (PC's), they are much more quickly done on supercomputers. In the latter case, the resulting output files usually have to be transferred back to a workstation or PC for flow visualization.

5 Flow Simulations

Provisional Grid for McCook Reservoir

Figures 3 and 4 show overhead views of the surface and bottom grids, respectively, for a provisional configuration of McCook Reservoir. The north arrow in Figure 3 is not true north; it is defined only for convenience of orientation. The cutout in the bottom (Figure 4) represents a sump. The grid as a whole is divided into ten subdomains (blocks), which together occupy a $129 \times 44 \times 5$ region in computational (i,j,k) space. Figure 5 shows an overhead view of the block edges (thin white lines) with the sump grid inset, and Figure 6 shows a perspective view with the sump walls and bottom shaded. Figure 7 offers a similar view of the reservoir bottom with the sump excluded.

The simulated reservoir has a maximum width of 3,260 ft (east to west in Figure 3) and a maximum length of 4,655 ft (north to south in Figure 3). When filled to capacity, it is 113 ft deep along the ridge of the central berm (Figure 7), 135 ft deep along the plateau immediately to the west of the berm, and 150 ft deep in the trough on the extreme west side of the grid. East of the berm, the reservoir is uniformly 130 ft deep except in the sump, where the total depth is 230 ft. The ramp at the north end of the berm (Figure 7) reduces the depth gradually to a minimum value of 20 ft.

Each grid block is five cells deep, including the block that represents the sump. Thus, the discrete flow field is five cells deep except for the region containing the sump (Figure 8). This region consists of two blocks stacked vertically, and it is ten cells deep altogether. In the MAC3D flow simulations, as discussed in the following section, flow was injected uniformly through a port consisting of the bottom two rows of cell faces on the right side of the sump (Figure 9), and withdrawn uniformly through the reservoir surface (Figure 3). The inflow port and the reservoir surface were designated as FLUX boundaries in the MAC3D input.

The computational grid is fine enough to capture the largest eddies in the flow, but not fine enough to achieve grid independence (i.e., negligible change in the computed flow with further grid refinement). For the latter purpose, ten to twenty additional grid spaces would be needed in the vertical

for each subdomain. In some regions of the reservoir, a comparable increase in the horizontal resolution might also be necessary. For qualitative model demonstrations, however, the grid used here is adequate.

Imposed Flow Conditions

The reservoir was assumed to be completely full. The velocity through the inflow port was fixed at 1 fps, which created an inflow of 10,870 cfs. This was balanced by an equal outflow with a uniform vertical velocity of 0.001 fps at the reservoir surface. The walls and bottom of the reservoir were given a Manning coefficient of 0.02, and the turbulence model was activated in all cases. The inflow turbulence energy was 2 percent of the total inflow energy, and the kinematic eddy viscosity was set at 2 ft^2/sec along the inflow port. The Prandtl number was set to unity, making the thermal diffusivity equal to the eddy viscosity. MAC3D flow simulations were then made for the following conditions:

a. Cold inflow (10 °C) into cold reservoir (10 °C)

b. Cold inflow (10 °C) into warm reservoir (20 °C)

c. Cold inflow (10 °C) into stratified reservoir (10 to 20 °C)

   (1) With background heat conduction

   (2) Without background heat conduction

For the stratified reservoir, the initial temperature profile (Figure 10) was 20 °C from the surface to a depth of 39 ft; linear with depth from 39 ft to 91 ft; and 10 °C below 91 ft.

The initial flow used for all cases was potential flow. This was computed automatically by MAC3D to establish an irrotational, mass-conserving velocity field throughout the entire reservoir. The governing equations were then marched through time for 7,200 sec (2 hours) in increments of 1 sec per timestep. By this time, the cold reservoir with cold inflow (neutrally buoyant flow) had essentially reached steady state. The other (buoyant) cases did not reach steady state, partly because cold water was continuously flowing into the reservoir and displacing warmer water. The stratified case was run with and without background heat conduction (as discussed in Chapter 2) to illustrate the extent to which the adiabatic boundary conditions and thermal diffusivity can affect the computed flow.

Presentation of Computed Results

To facilitate interpretation and qualitative comparison of the computed results, the same information is presented graphically for each set of imposed flow conditions. First comes a perspective view of selected velocity profiles over the entire reservoir (e.g., Figure 11). Next are shown close-ups of the velocities in and above the sump (e.g., Figures 12 and 13), followed by an overhead view of the surface velocities (e.g., Figure 14). Then comes a series of overhead views of flow patterns in five successive grid planes (e.g., Figures 15-19), beginning at the surface and ending at 80 percent of the total depth (to the top of the sump). These flow patterns were obtained by normalizing all the velocity vectors so that each has a magnitude of unity. Thus, the displayed vectors indicate only the local <u>direction</u> of the flow. In an overhead view for a single grid plane, however, the projected vector lengths will not all be the same unless the vertical velocity component is uniform.

Cold Reservoir with Cold Inflow

Most of the action for the cold reservoir (Figures 11-19) is confined to the region near the sump. Strong eddies are evident in both the elevation and horizontal planes of the sump itself. These are complemented by a strong eddy just to the south, and a weaker eddy (near the bottom) just to the north. Velocities in the southern half of the reservoir are very small in comparison with those in and around the sump.

Warm Reservoir with Cold Inflow

Results for the warm reservoir (Figures 20-28) are dramatically different from those for the cold (neutrally buoyant) reservoir. In this case, the downward buoyant force increases the energy required for the cold inflow to penetrate vertically the warmer (lighter) water in the reservoir. Thus, the colder the inflow, the greater the tendency for water leaving the sump to flow <u>under</u> the ambient water (as in Figure 21) instead of up and through it (as in Figure 12).

The underflow away from the sump along the bottom induces a return flow along the surface, as shown in Figures 21 and 22. At the elapsed time (2 hours) for which results are shown, the highest velocities are confined roughly to the northern third of the reservoir. Questions of magnitude aside, the overall flow patterns are more complex than those for the neutrally buoyant flow, with each grid plane exhibiting horizontal recirculation in different locations (Figures 24-28).

Stratified Reservoir with Cold Inflow

Distinct simulations were made for the stratified reservoir with and without background heat conduction (Figures 29-46). These should be regarded as bounding calculations rather than as realistic simulations. They are presented mainly to demonstrate the disparity of prediction that can arise because of uncertainty concerning the internal rate of heat transfer.

Near the sump, the velocities for the stratified reservoir with background heat conduction (Figures 29-32) loosely resemble those for the unstratified warm reservoir (Figures 20-23). In this case, however, there is a strong vertical recirculation west of the central berm, which was not evident for the unstratified reservoir. The flow in this region is generally east to west along the surface and west to east along the bottom.

The flow in the stratified reservoir without background heat conduction (Figures 38-46) is totally different from that for the reservoir with background heat conduction (Figures 29-37). Here the largest velocities are confined to the region near the sump (Figures 38-41), with multiple zones of horizontal recirculation occurring in different planes at various distances from the sump (Figures 42-46).

The difference between these two flows indicates the relative influence of the eddy diffusivity. If the initial diffusivity of 2 ft^2/sec were held constant, it would be sufficient to bring the entire reservoir to thermal equilibrium within 2 hours (in the absence of any flow). Thus, the flow simulation with background heat conduction combined the effects of cold inflow and rapid internal heat conduction. Although the reservoir was initially stratified, it gradually became unstratified far from the sump, with a temperature of about 15 °C.

In the flow simulation without background heat conduction, the local temperature changed only in response to the inflow, which was too weak to destratify the entire reservoir through fluid motion alone. In this case, the buoyant forces were strong enough to restrict the main action to the region near the sump, and the initial temperature distribution hardly changed at all.

Figure 47 shows a gray-scale map of the initial stratified temperature (in degrees centigrade) on vertical (elevation) surfaces inside the reservoir and along its sides. Figure 48 shows the temperature map for the flow without background heat conduction after 2 hours elapsed time, and Figure 49 shows the corresponding map for the flow with background heat conduction. For comparison, Figure 50 shows the temperature map for the previous case of the warm reservoir (20 °C) with cold inflow (10 °C) after 2 hours elapsed time. Note that vertical distances have been magnified by a factor of five in Figures 47-50.

6 Conclusions and Recommendations

In most respects, one can regard MAC3D as a three-dimensional extension of the depth-averaged STREMR model. MAC3D uses the same numerical algorithms and turbulence model as STREMR, but it also includes buoyancy and offers the added flexibility of composite (multiblock) grids. In any case, MAC3D draws heavily on the insight and experience previously gained in developing STREMR, which has been extensively tested and documented (Bernard 1992, 1993; Bernard and Schneider 1992; Maynord, in preparation).

This report offers no comparison of model predictions with physical test data, but MAC3D is not completely unverified. At each stage of development, the model has been run and checked against STREMR predictions for 2-D flow. Thus, in certain 3-D settings for which the flow should be 2-D, MAC3D actually produces a 2-D flow; and the predictions agree with those of STREMR. In future work, MAC3D predictions should be tested against pertinent experimental results for fully 3-D flow.

The existing model now seems ready for implementation as a supplementary aid in design studies of McCook Reservoir, although undiscovered deficiencies may still have to be dealt with. Given a specified inflow or outflow, MAC3D can predict reasonable bounds for the resulting circulation inside the reservoir. The major uncertainties are the rates of surface heat exchange and internal heat conduction, and these merit considerable further study. In particular, modules need to be developed to account for reflection and absorption of solar radiation, shear stress produced by surface winds, and surface heat flux produced by changes in ambient atmospheric temperature.

MAC3D is capable of predicting the hydrodynamic response to inflow, outflow, and hydraulic mixers, but it also needs to predict the response to bubble diffusers. The latter represents a special problem, because rising bubbles generally move with a different velocity from that of the flow. Thus, future work should include the development of adequate models for localized bubble plumes and their influence on the flow. These might include special buoyant forces added along the vertical planes or axes of diffusers, along with empirical rules for the spreading of the plumes themselves.

At present MAC3D deals with hydrodynamics, but not with water quality. To make the model more generally useful as an aid for reservoir design, operation, and modification, future work should include the addition of modules to account for oxygen transport and degradation, as well as pertinent chemical and biological processes.

References

Bernard, R. S. (1991). "A turbulence model for recirculating flow," Technical Report HL-91-14, U.S. Army Engineer Waterways Experiment Station, Vicksburg, MS.

Bernard, R. S. (1992). "A MacCormack scheme for incompressible flow," *Computers and Mathematics with Applications* 24(5/6), 151-168.

Bernard, R. S. (1993). "STREMR: Numerical model for depth-averaged incompressible flow," Technical Report REMR-HY-11, U.S. Army Engineer Waterways Experiment Station, Vicksburg, MS.

Bernard, R. S., and Schneider, M. L. (1992). "Depth-averaged numerical modeling for curved channels," Technical Report HL-92-9, U.S. Army Engineer Waterways Experiment Station, Vicksburg, MS.

Kapitza, H., and Eppel, D. (1987). "A 3-D Poisson solver based on conjugate gradients compared to standard iterative methods and its performance on vector computers," *Journal of Computational Physics* 68, 474-484.

Launder, B. E., and Spalding, D. B. (1974). "The numerical calculation of turbulent flows," *Computer Methods in Applied Mechanics and Engineering* 3, 269-289.

MacCormack, R. W. (1969). "The effect of viscosity in hypervelocity impact cratering," AIAA Paper 69-354, American Institute of Aeronautics and Astronautics, Cincinnati, OH.

Maynord, S. T. "Open channel velocity prediction with STREMR Model" (in preparation), U.S. Army Engineer Waterways Experiment Station, Vicksburg, MS.

Orlanski, I. (1976). "A simple boundary condition for unbounded hyperbolic flows," *Journal of Computational Physics* 21, 251-269.
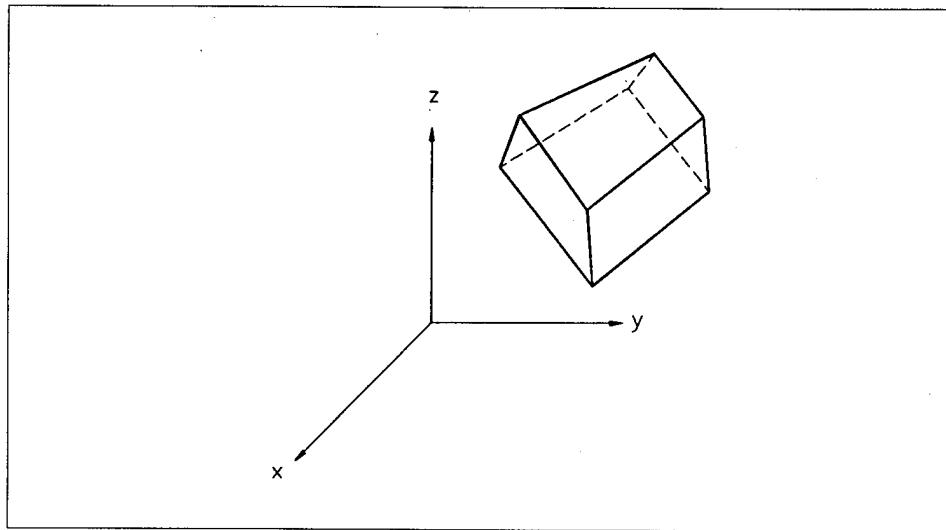
a. Cartesian coordinates
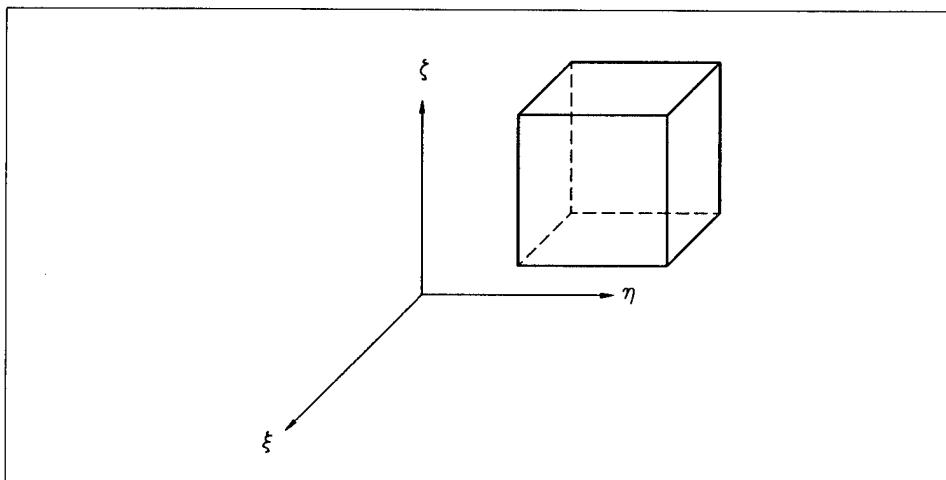
b. Curvilinear coordinates

Figure 1. Grid cells as they appear in cartesian space and computational
(curvilinear) space
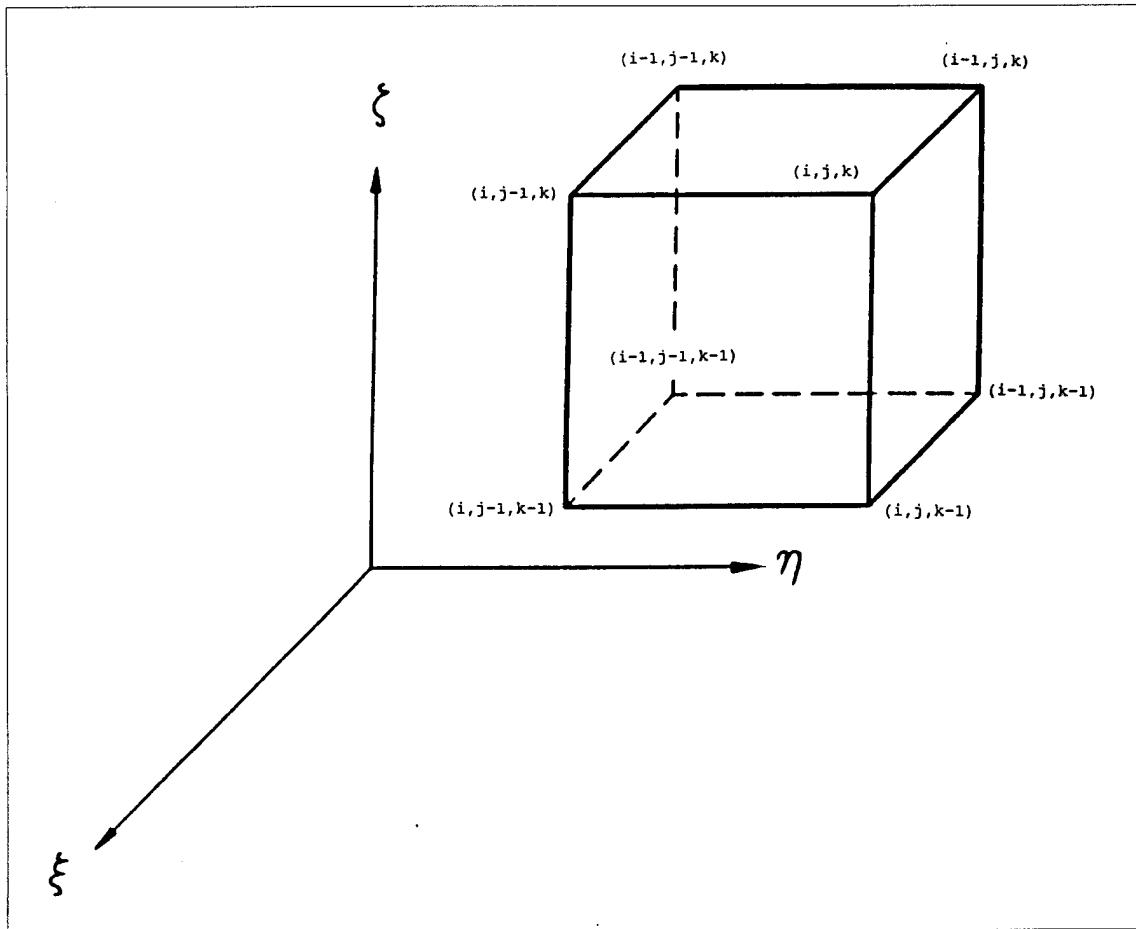
Figure 2. Nodal coordinates in computational space
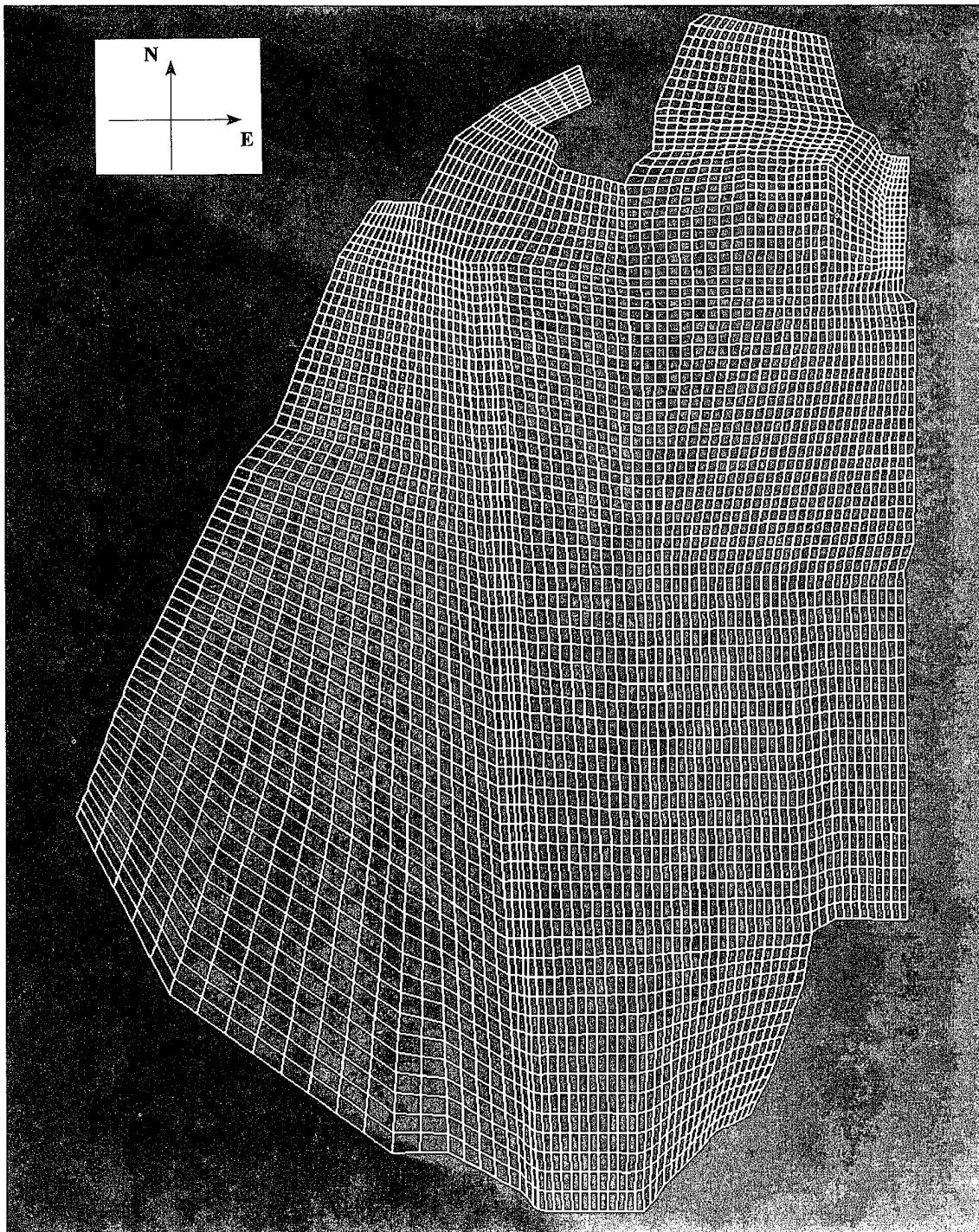
Figure 3. Surface grid for McCook Reservoir
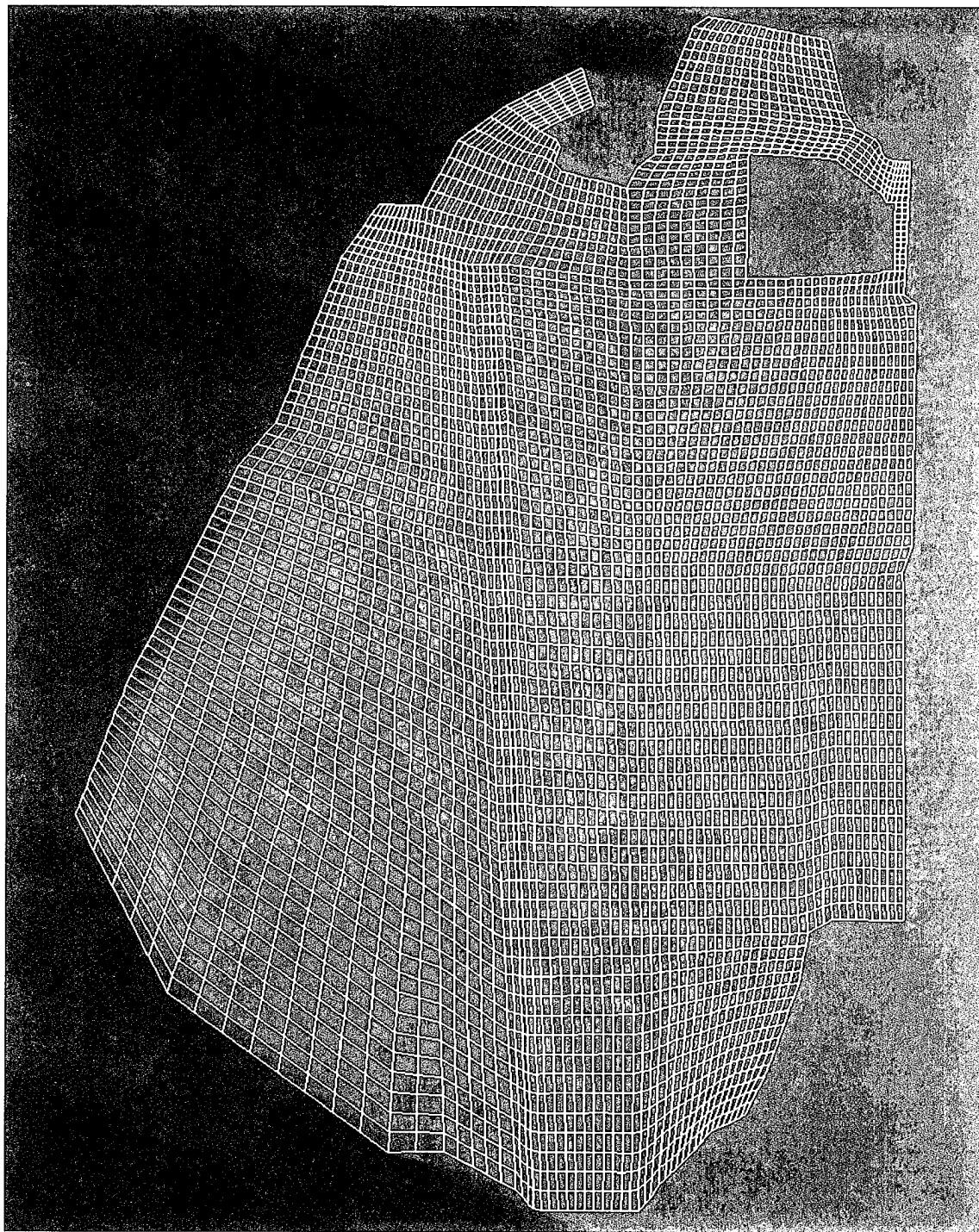
Figure 4. Bottom grid with sump excluded
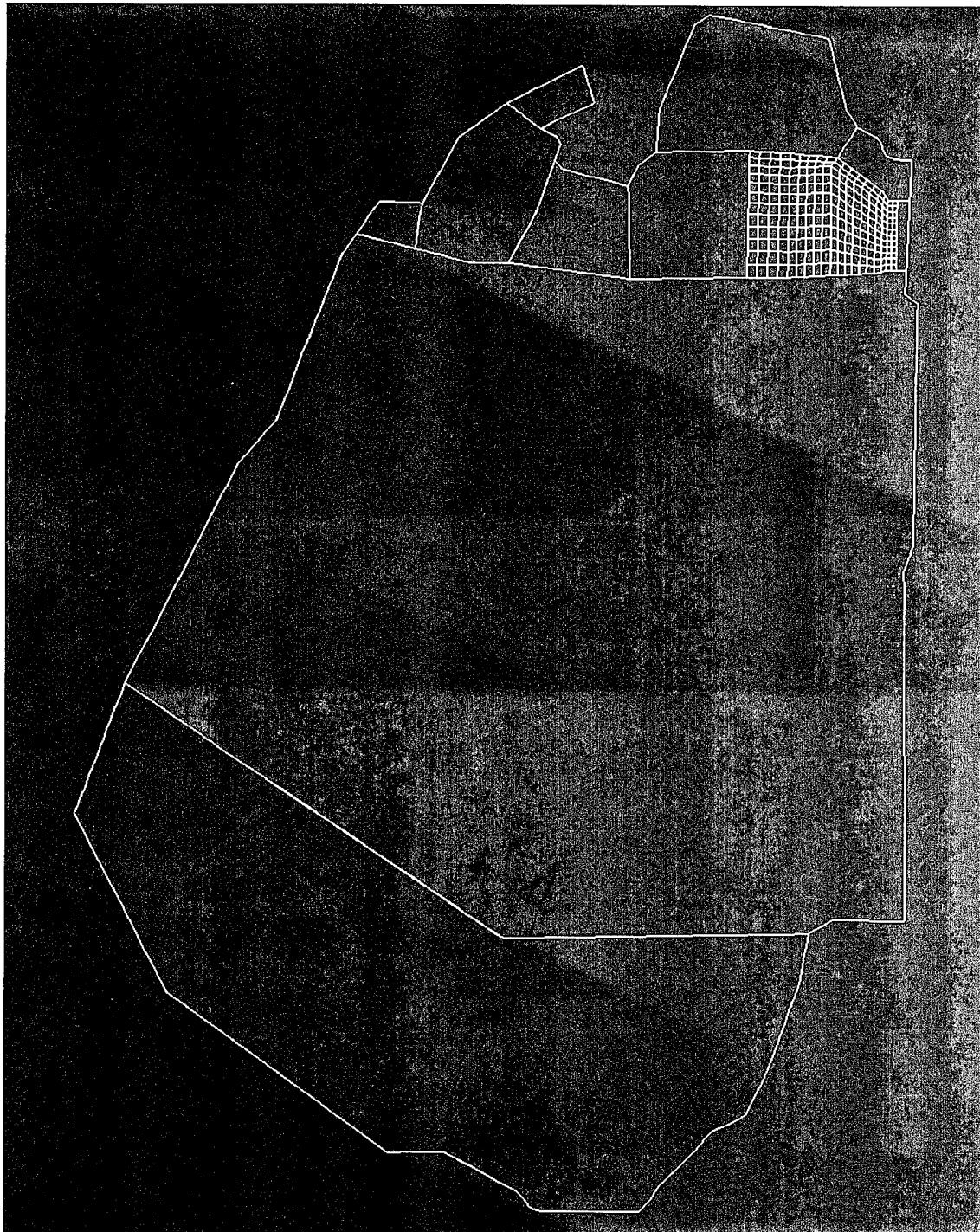
Figure 5. Overhead view of subdomain edges with sump grid inset
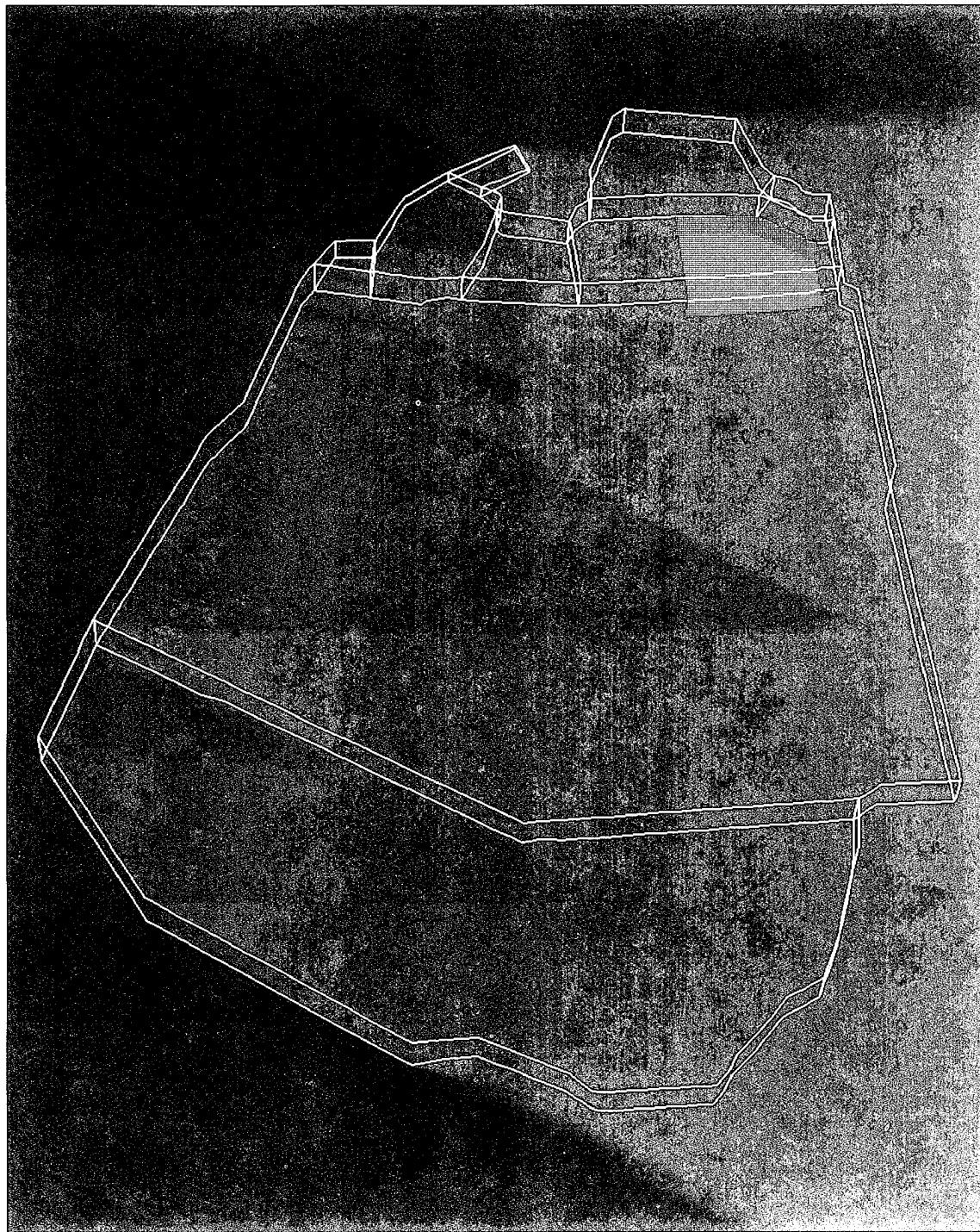
Figure 6. Perspective view of subdomain edges with sump inset
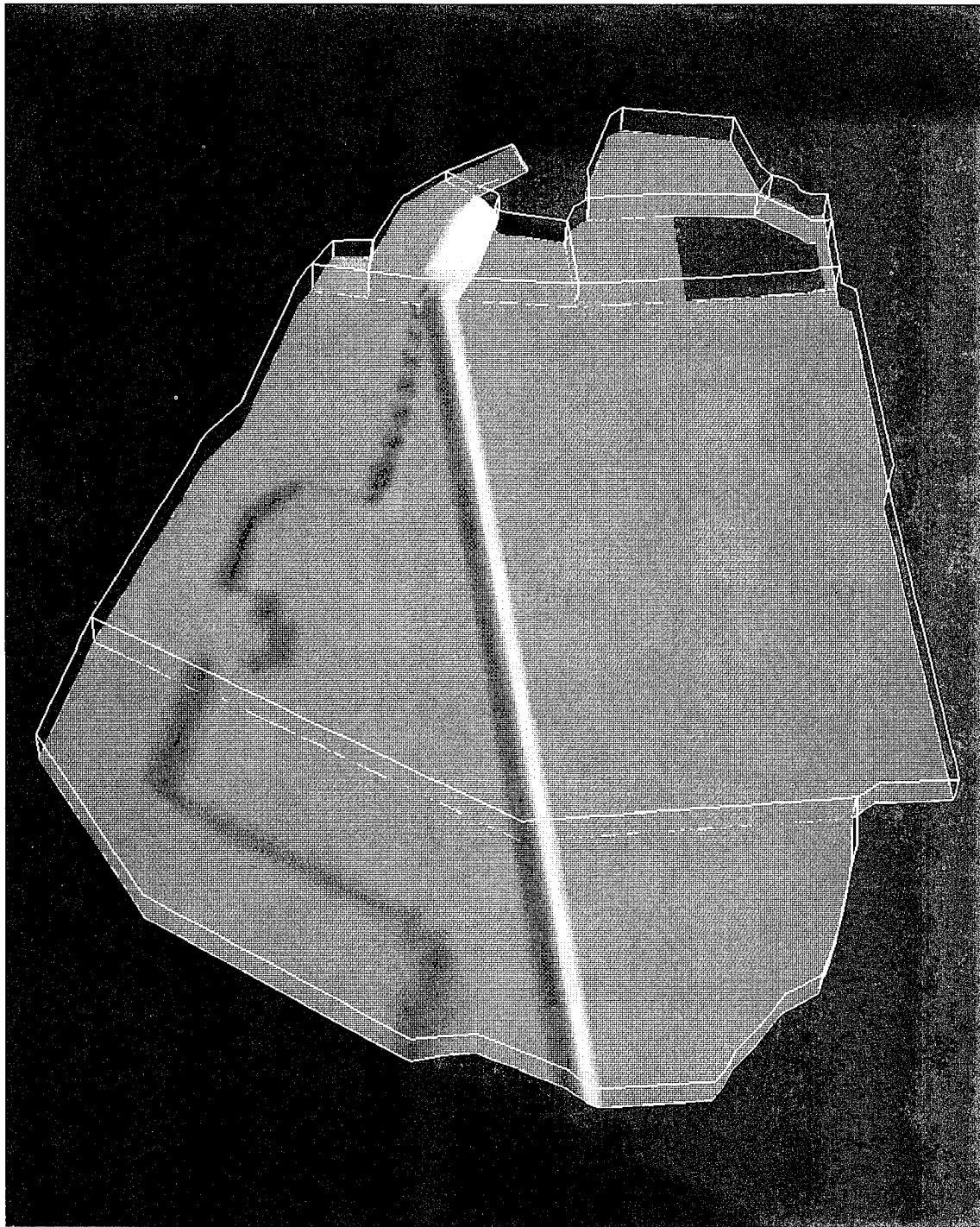
Figure 7. Perspective view of bottom with sump excluded
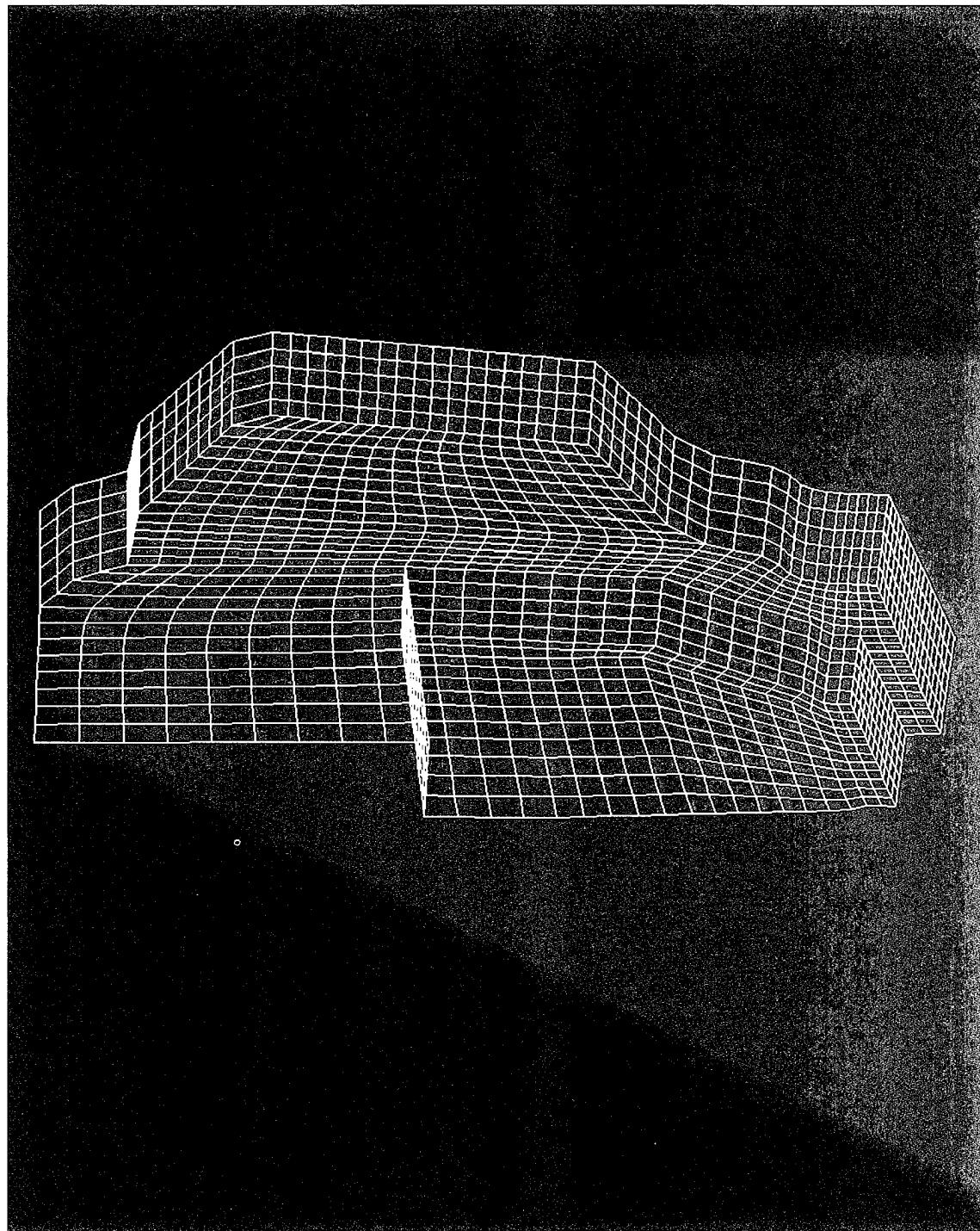
Figure 8. Cutaway of bottom and side grids in and around sump
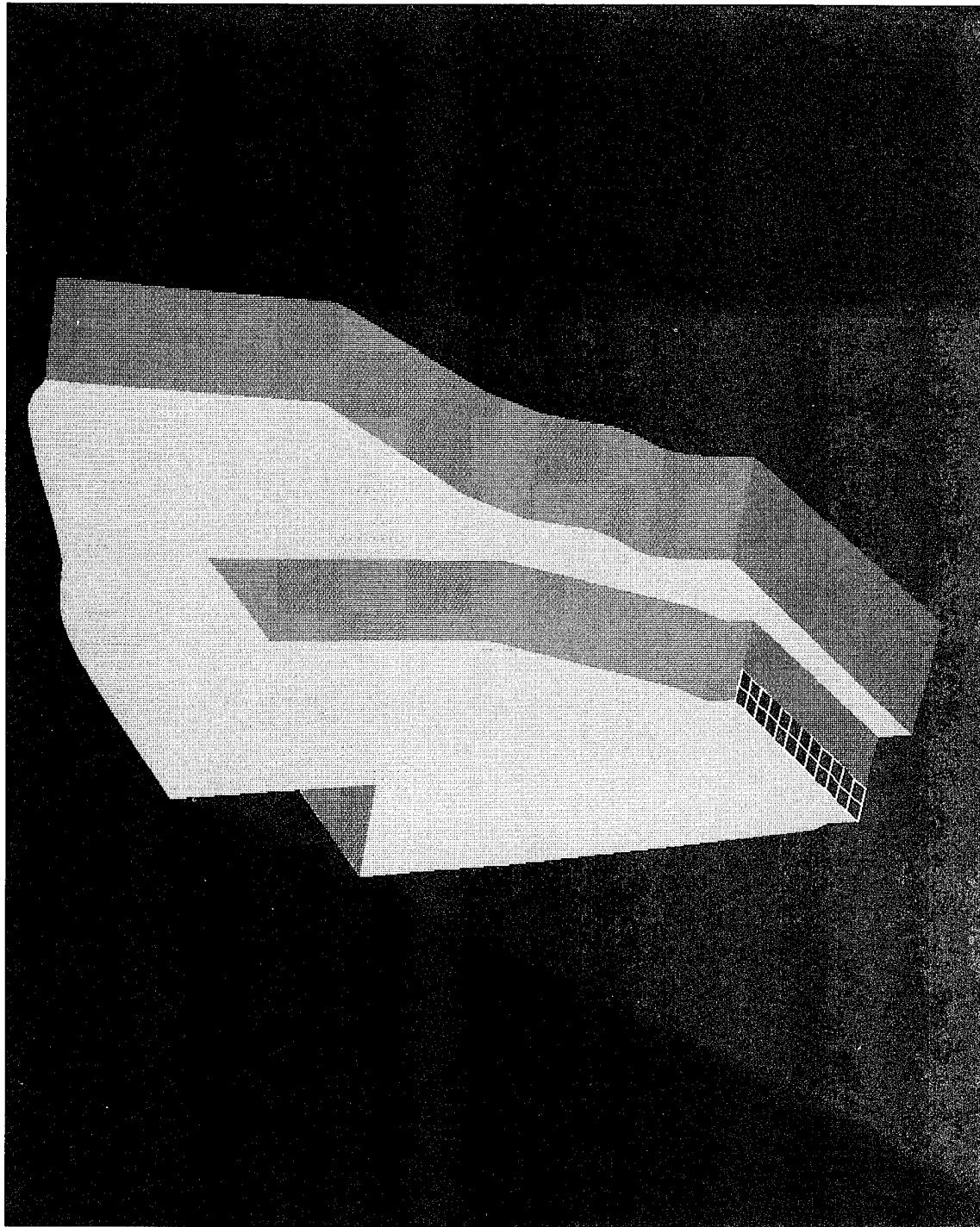
Figure 9. Solid walls (shaded) with inflow port for sump
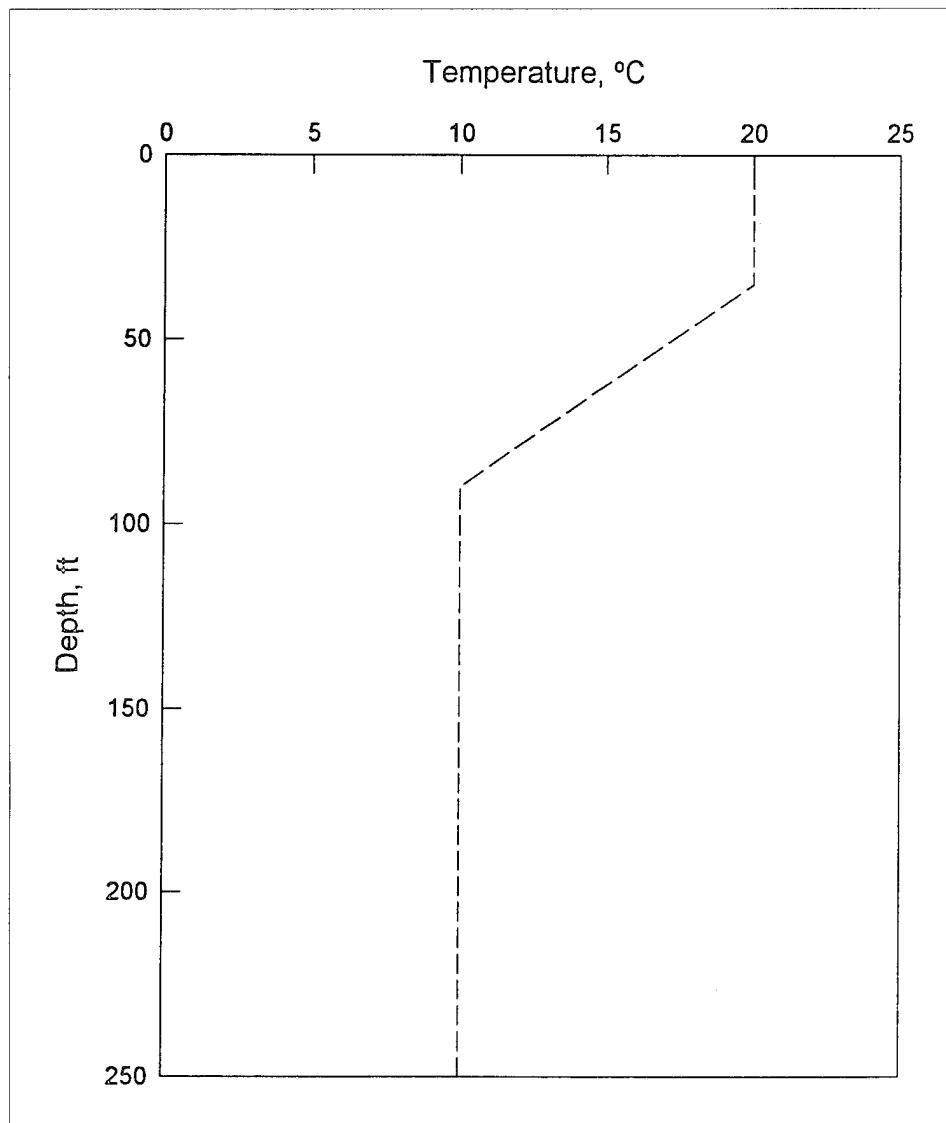
Figure 10. Initial temperature profile for stratified reservoir
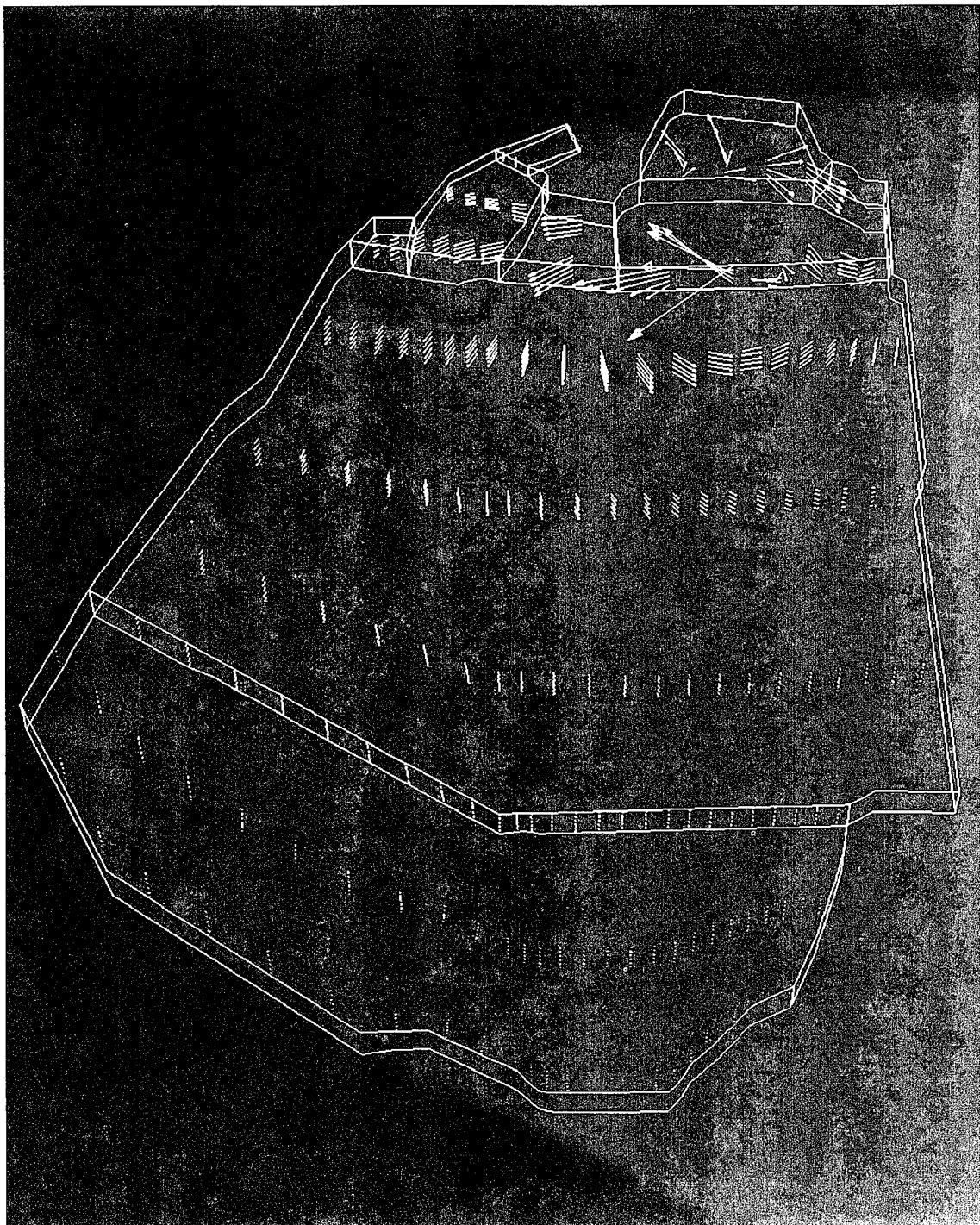
Figure 11. Velocity profiles for cold reservoir with cold inflow
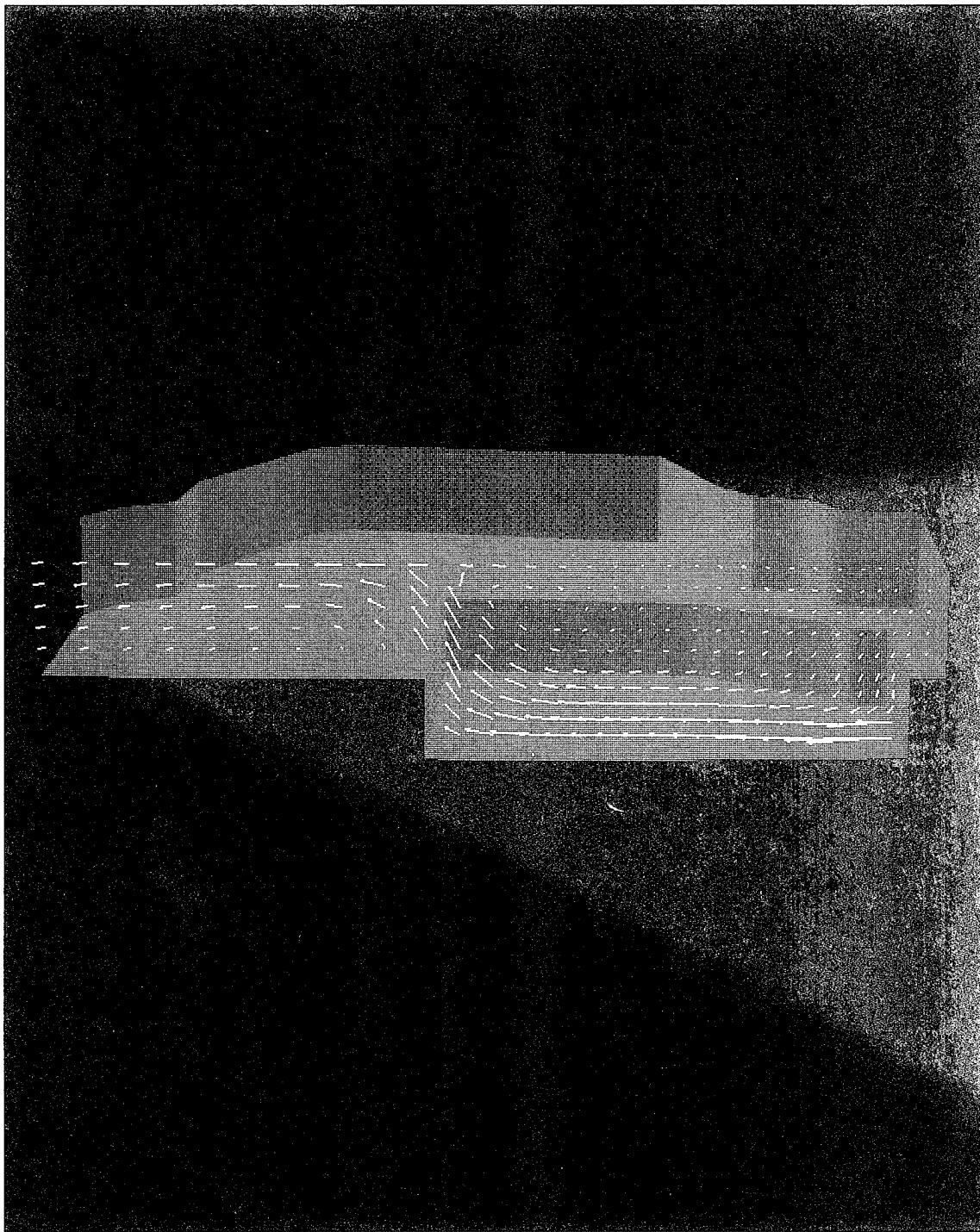
Figure 12. Velocities in elevation plane of sump for cold reservoir with cold inflow
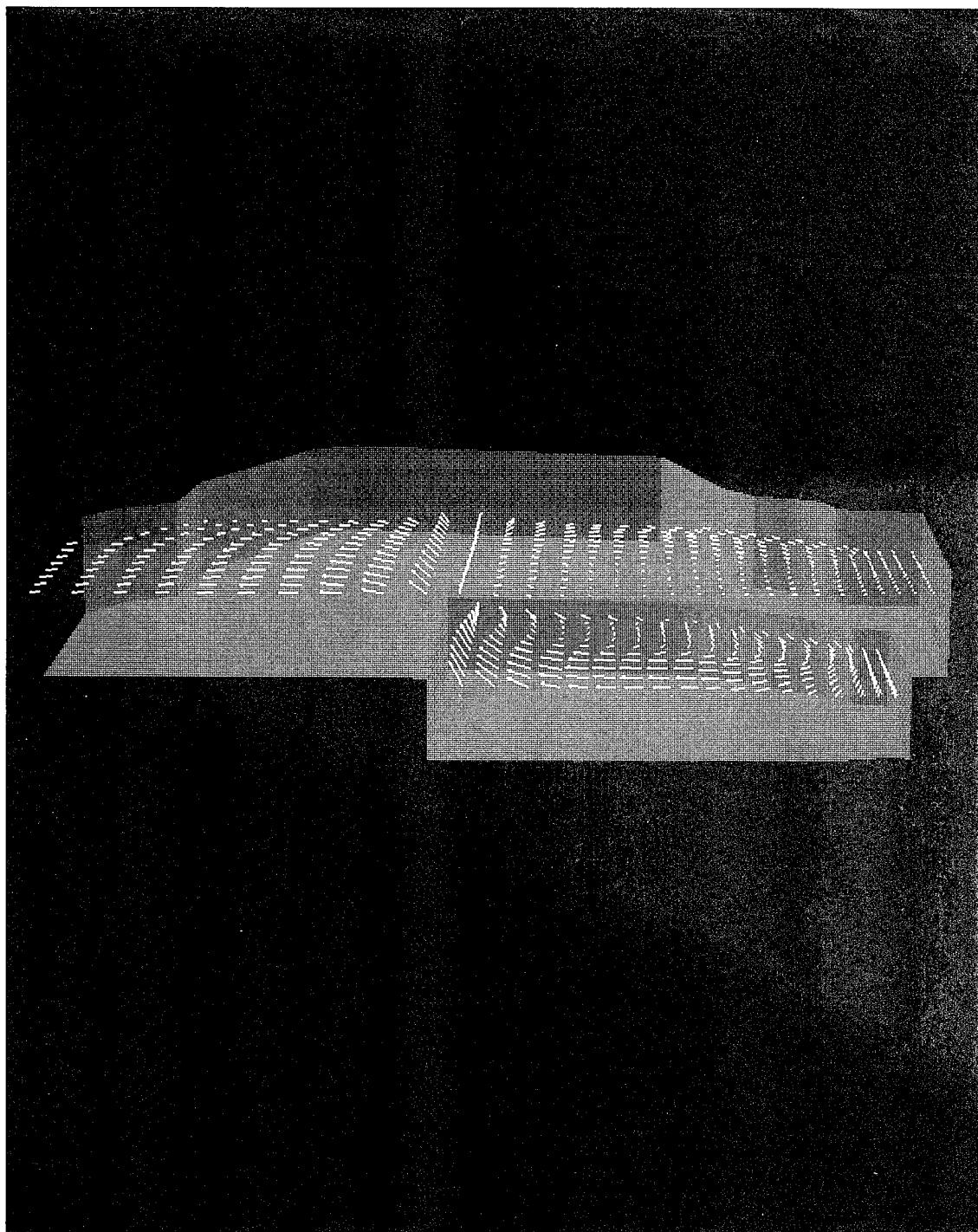
Figure 13. Velocities for horizontal planes in and above sump for cold reservoir with cold inflow
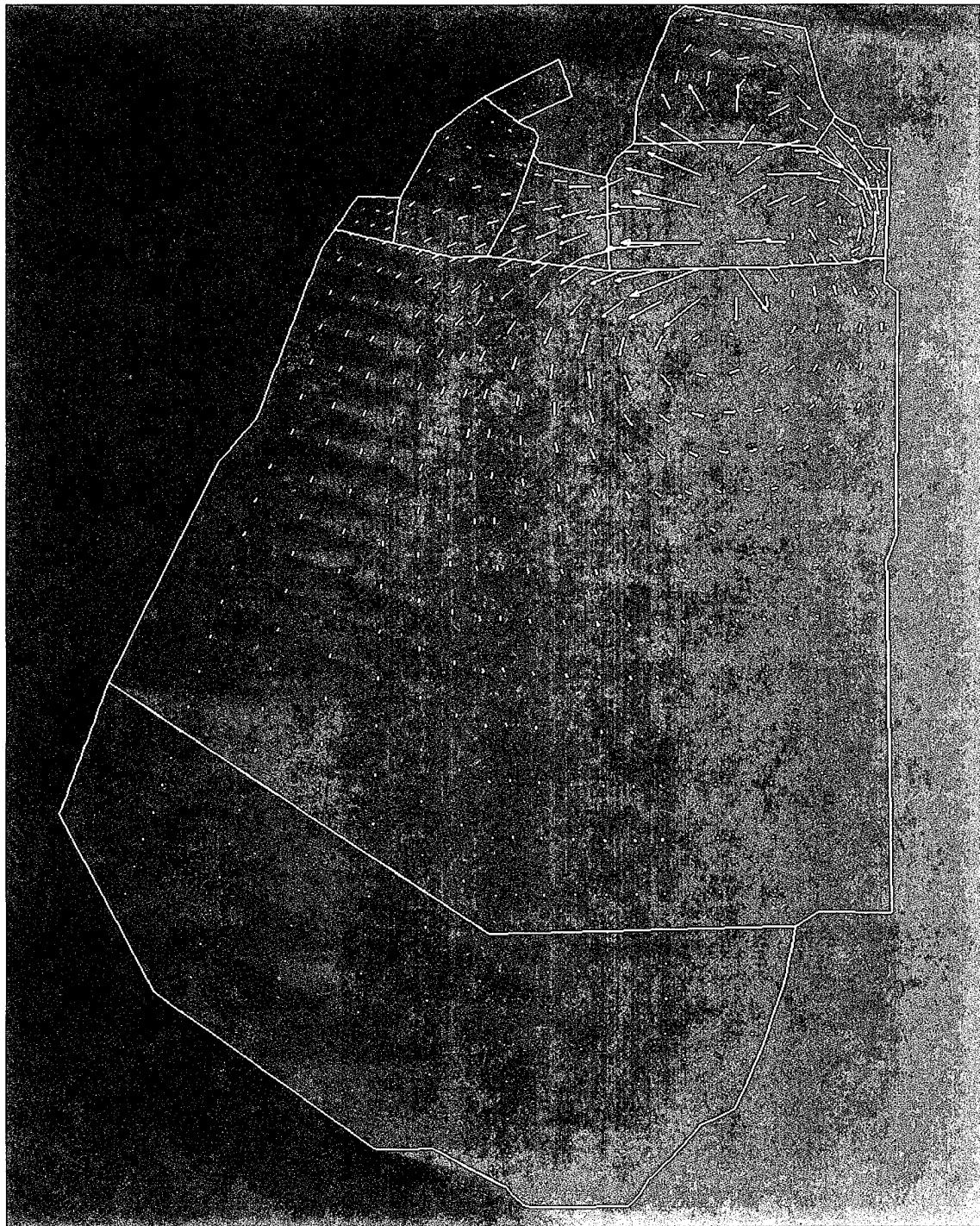
Figure 14. Surface velocities for cold reservoir with cold inflow
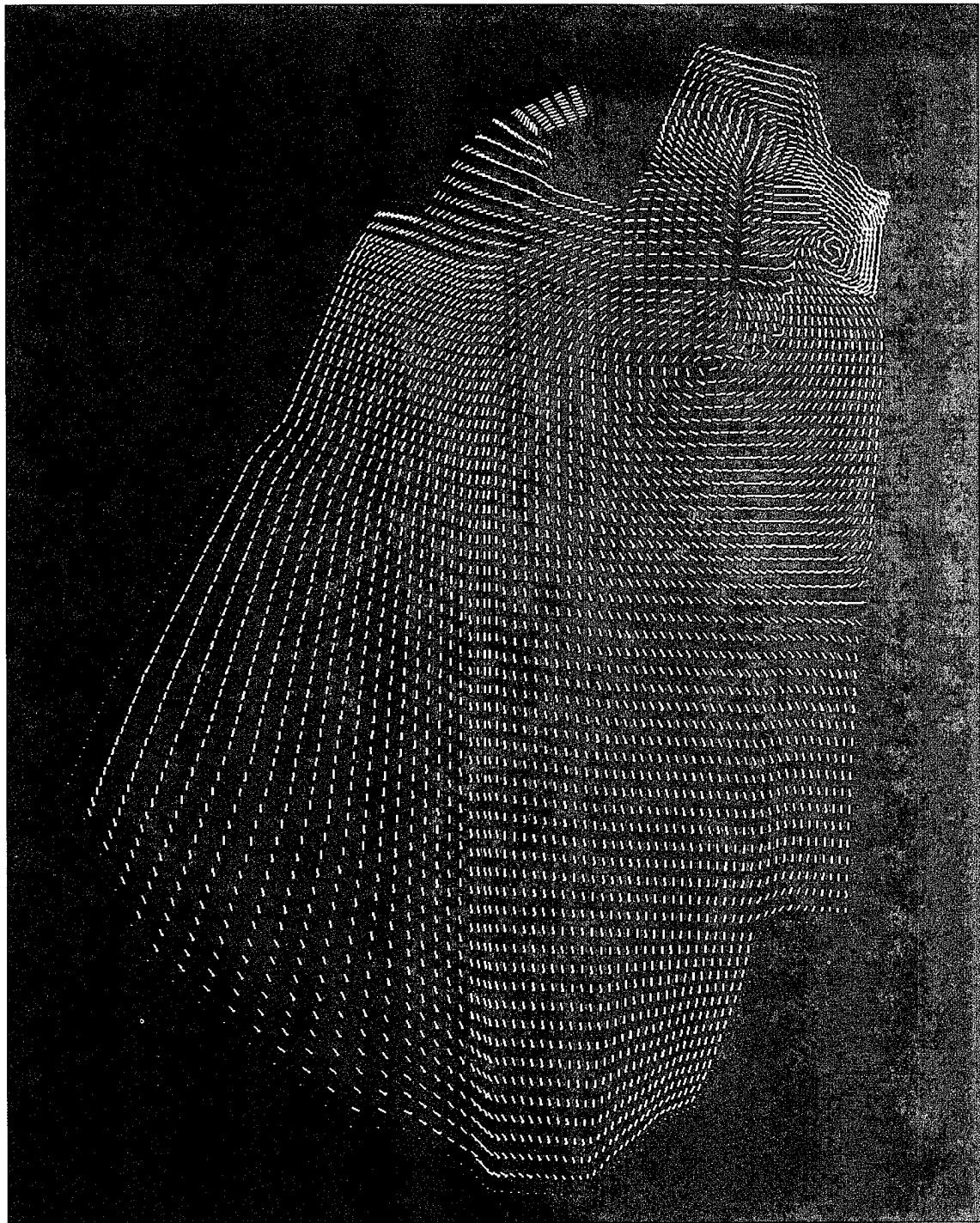
Figure 15. Surface flow patterns for cold reservoir with cold inflow
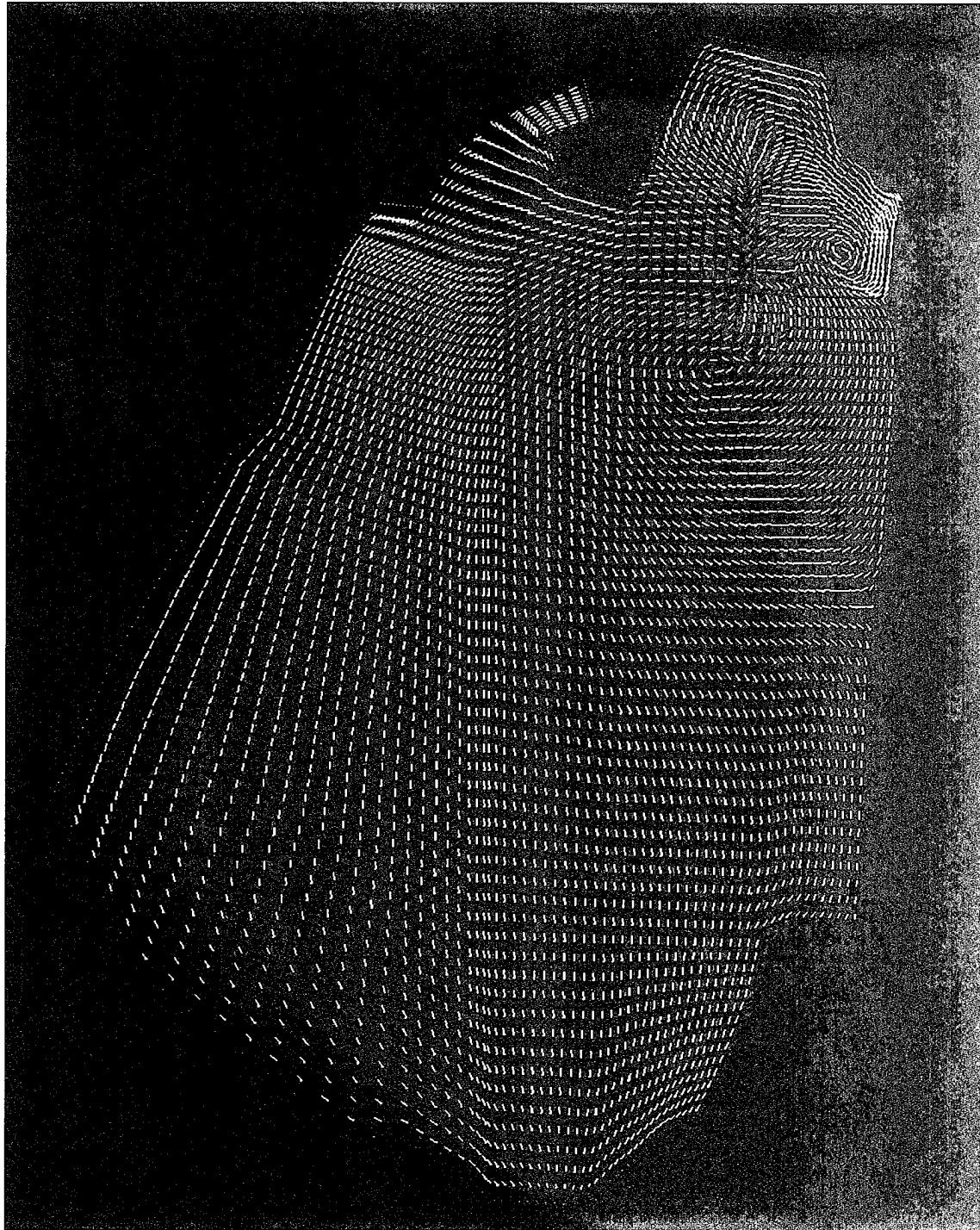
Figure 16. Flow patterns at 20 percent of total depth for cold reservoir with cold inflow
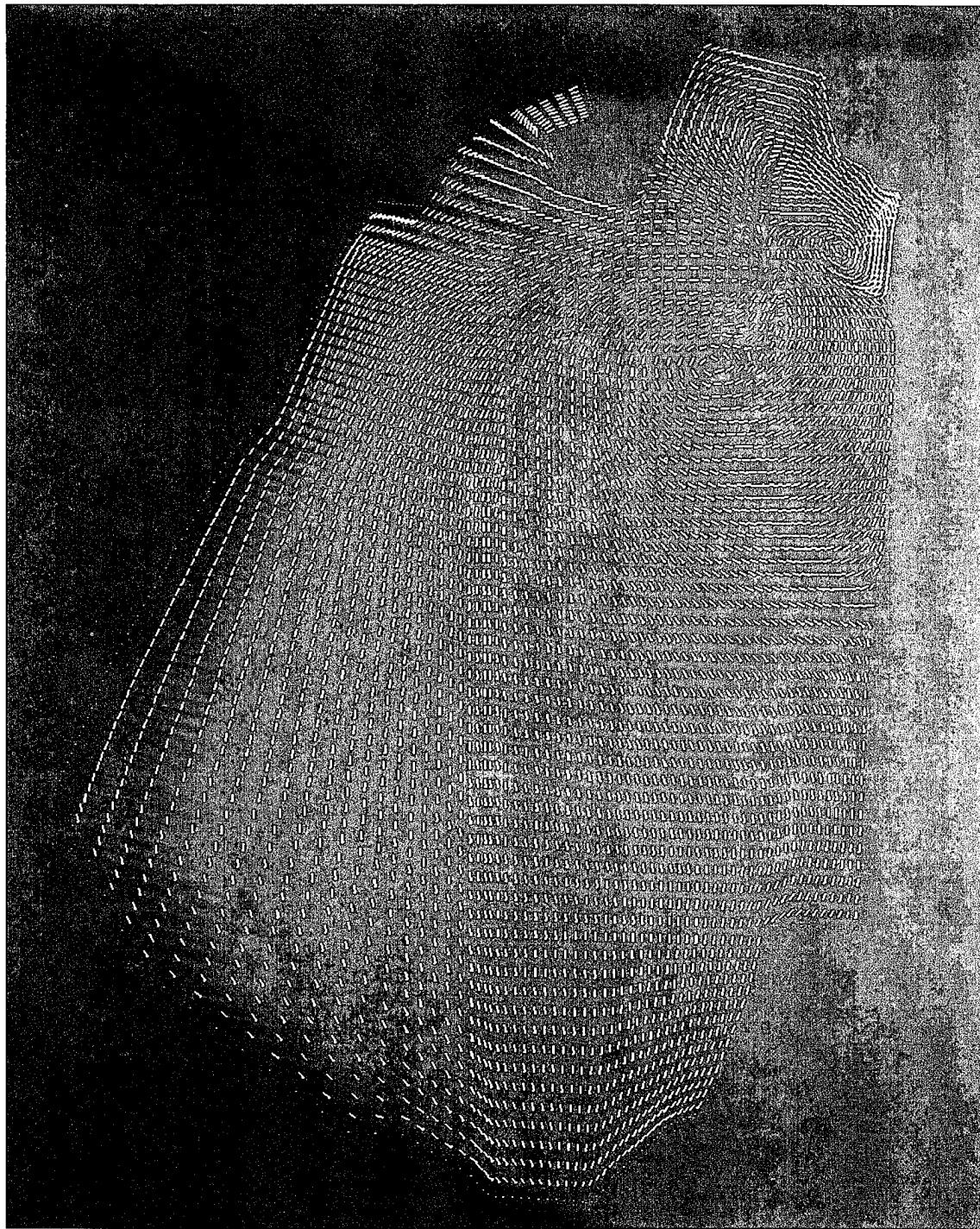
Figure 17. Flow patterns at 40 percent of total depth for cold reservoir with cold inflow
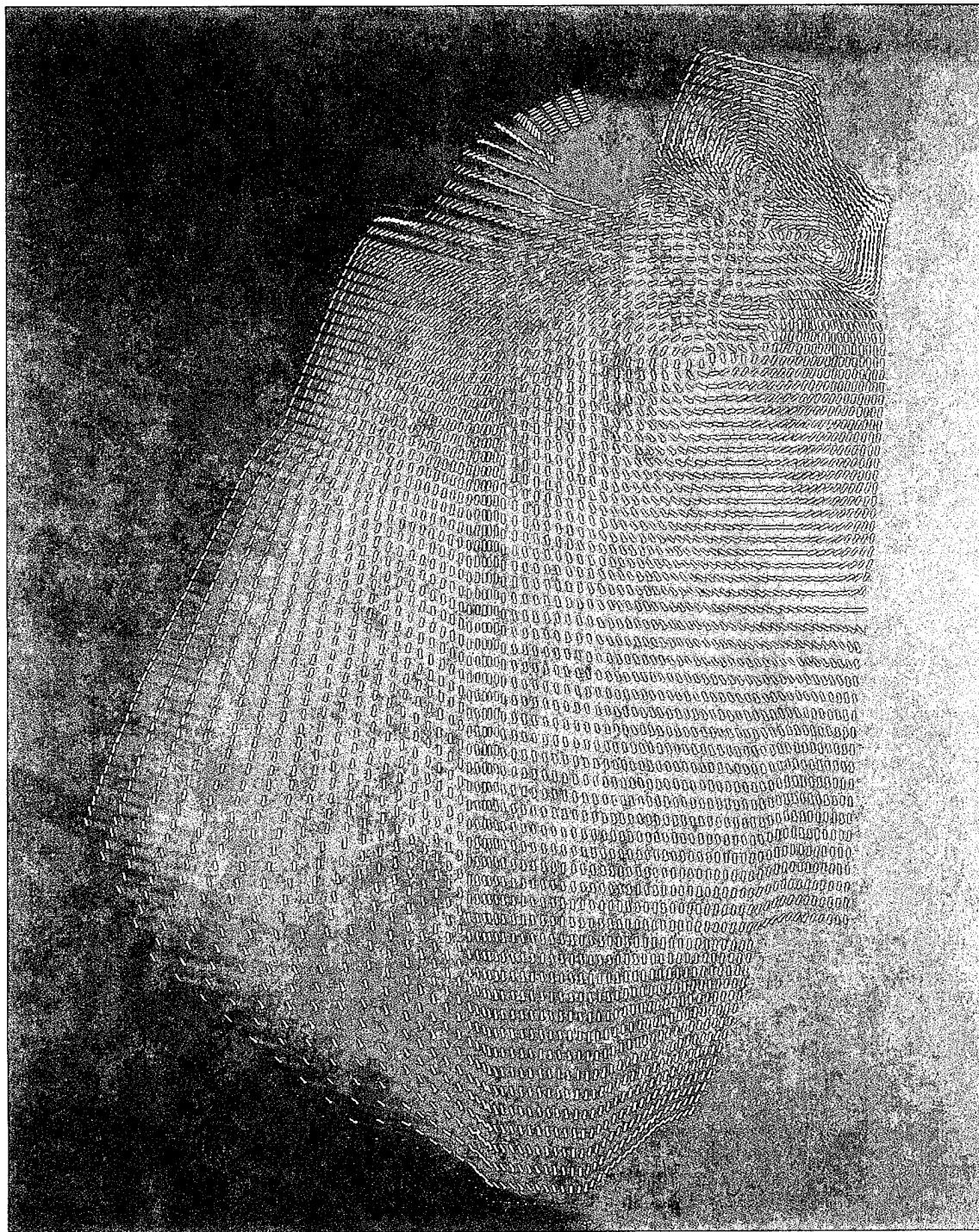
Figure 18. Flow patterns at 60 percent of total depth for cold reservoir with cold inflow
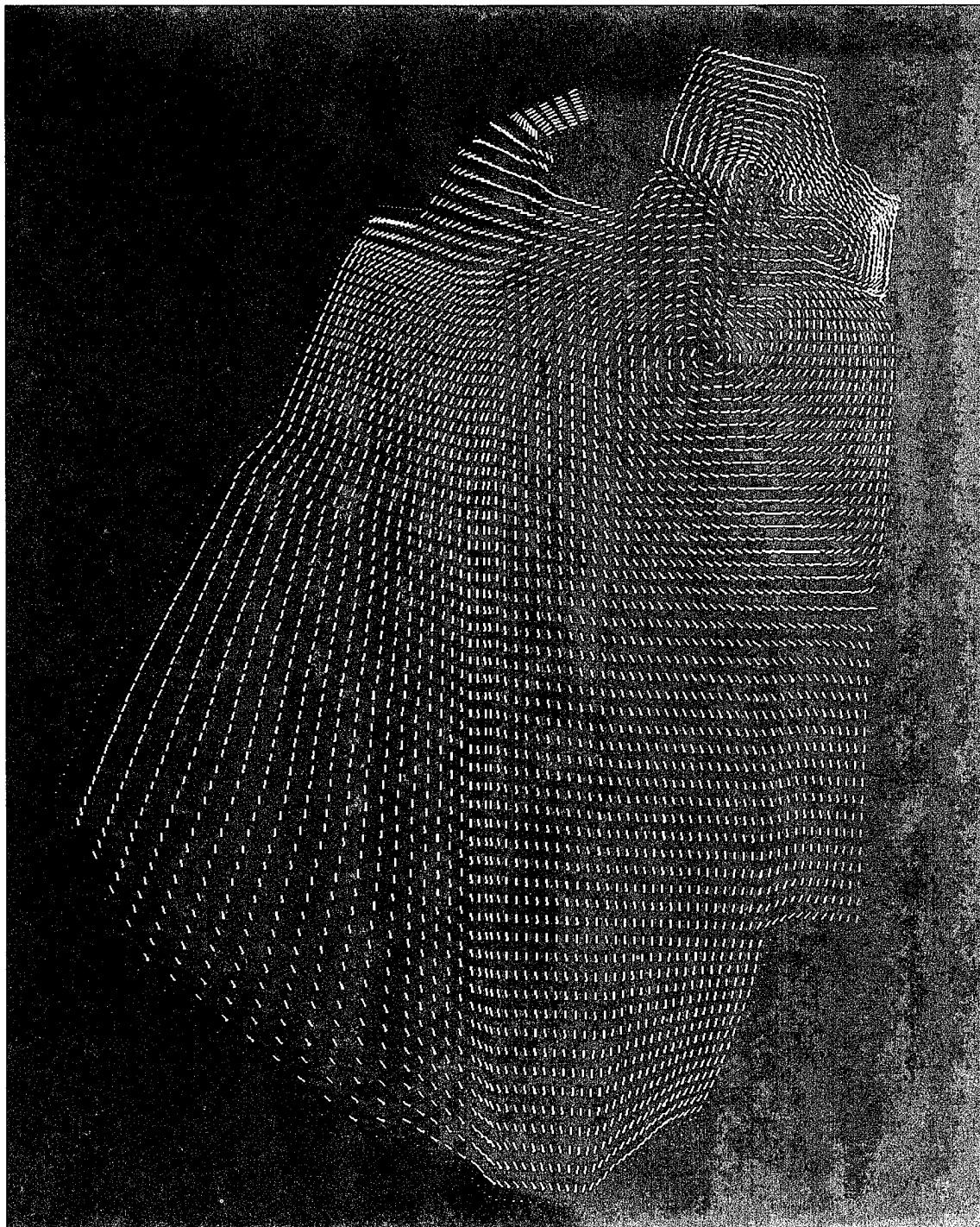
Figure 19. Flow patterns at 80 percent of total depth for cold reservoir with cold inflow
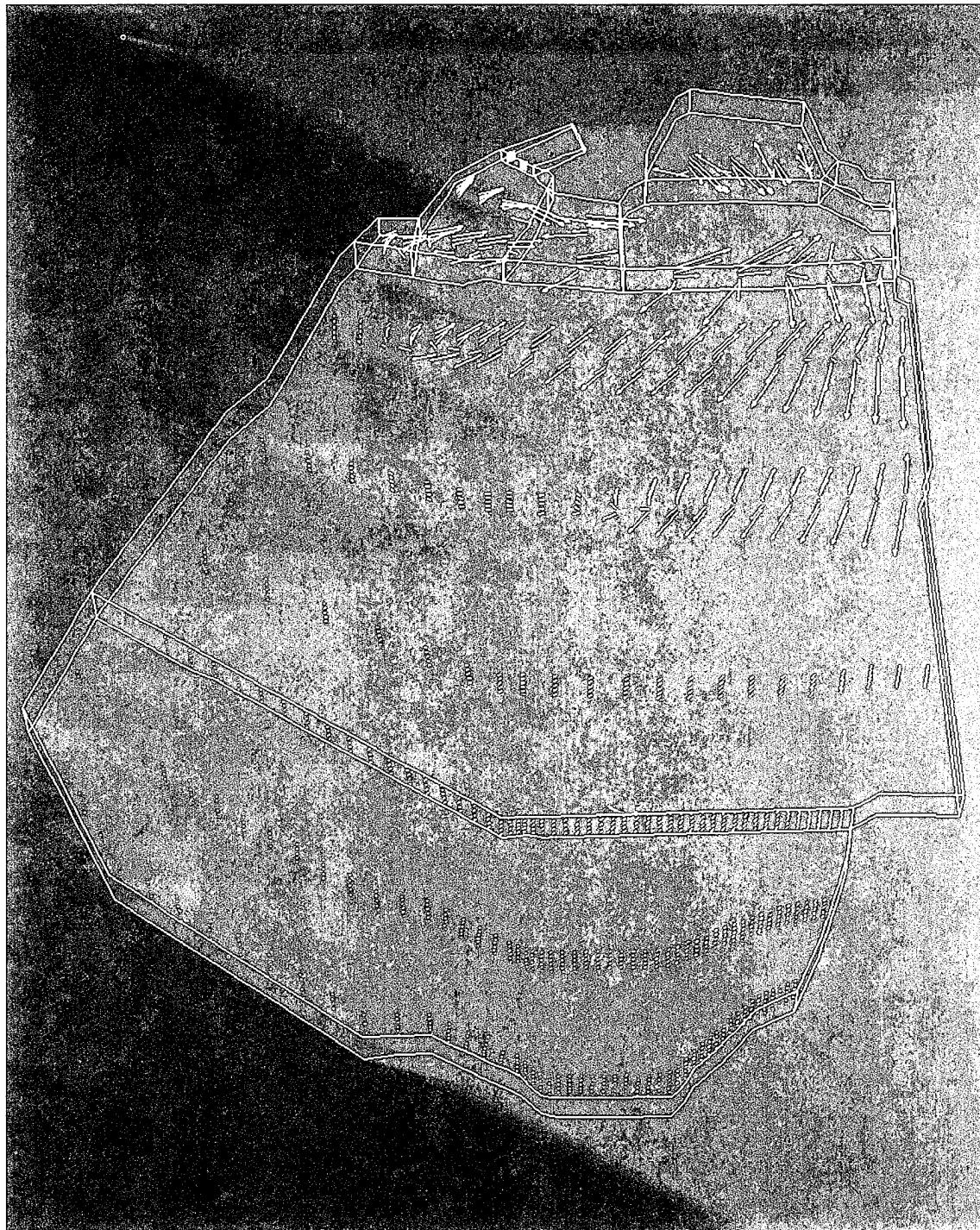
Figure 20. Velocity profiles for warm reservoir with cold inflow
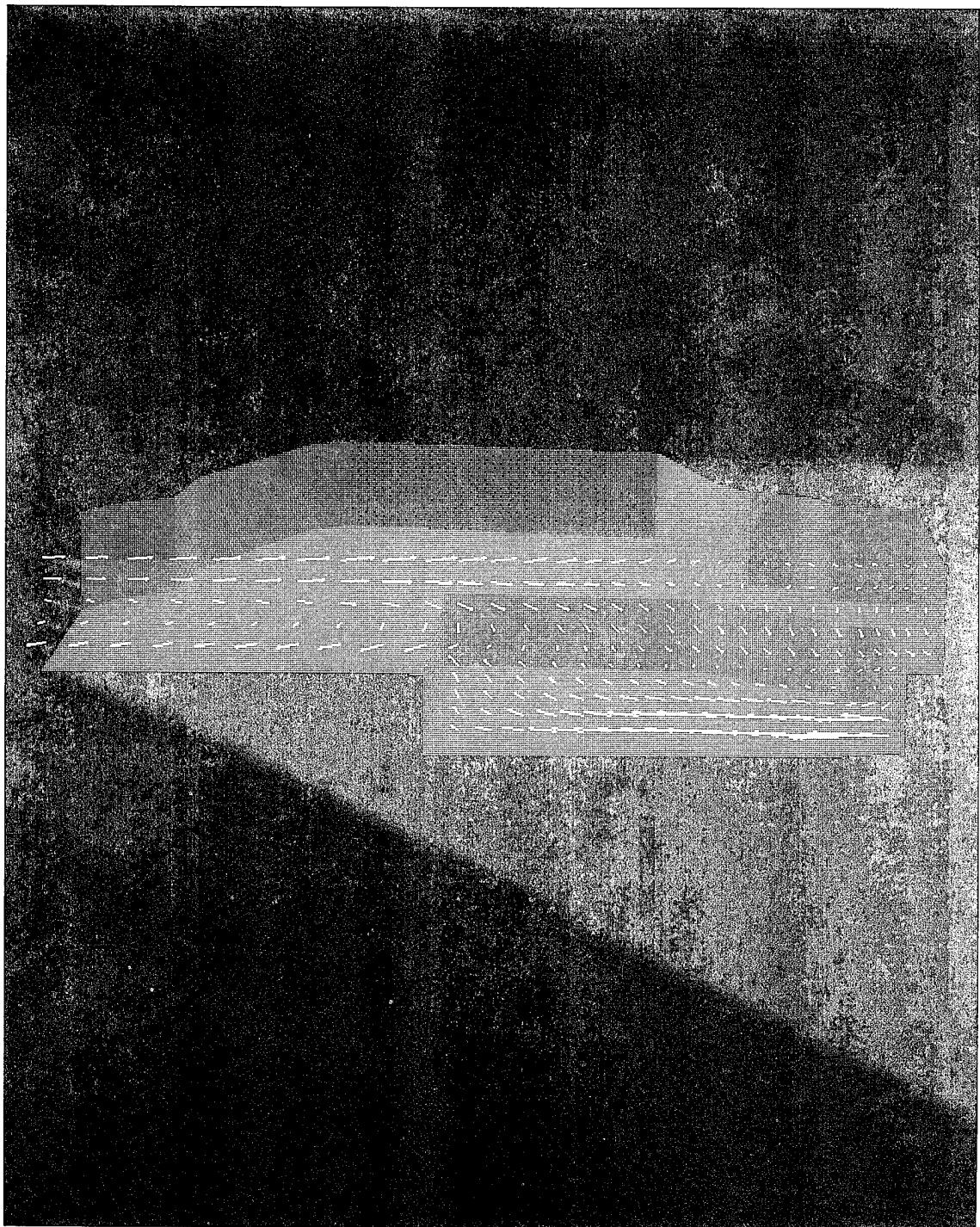
Figure 21. Velocities in elevation plane of sump for warm reservoir with cold inflow
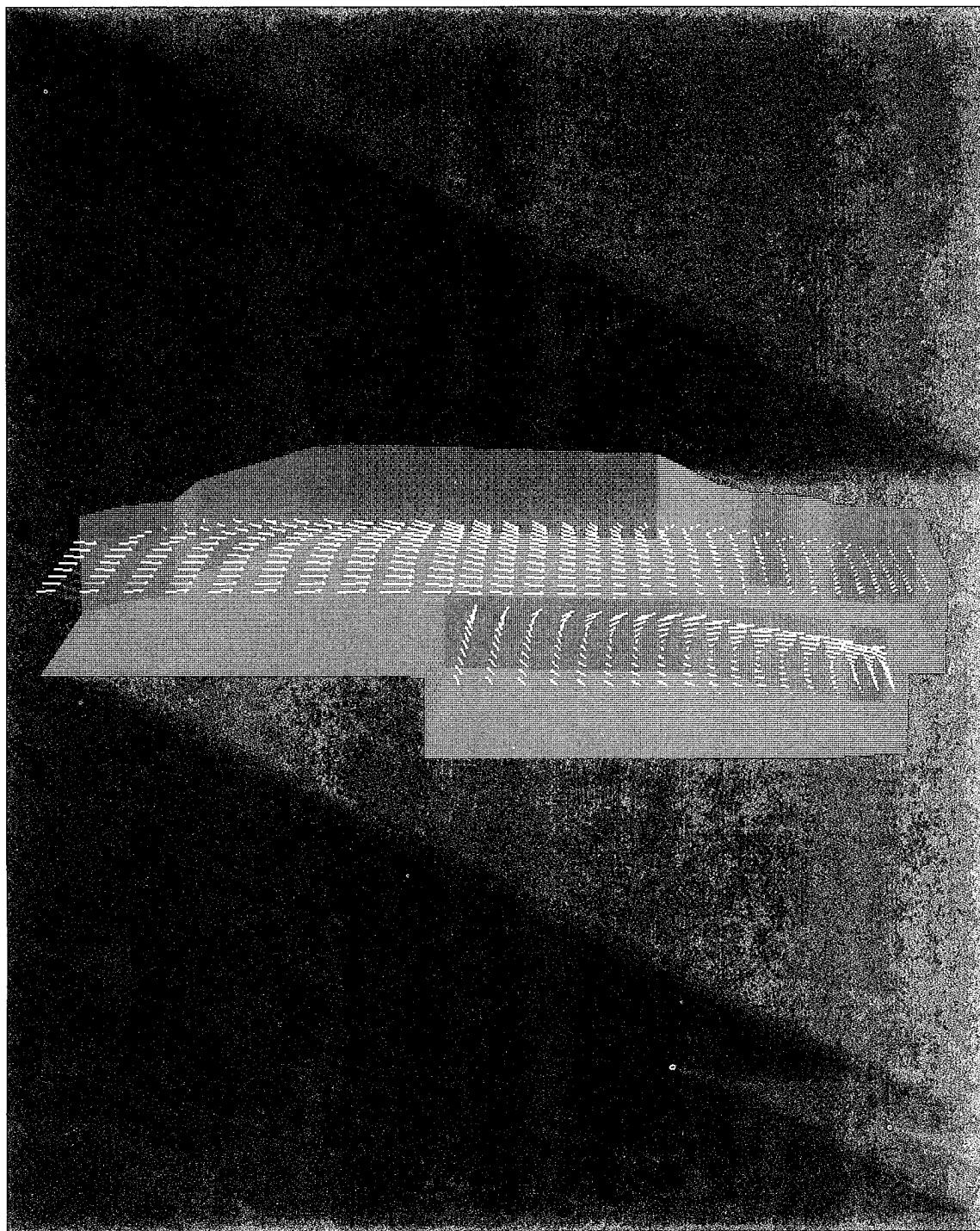
Figure 22. Velocities for horizontal planes in and above sump for warm reservoir with cold
              inflow
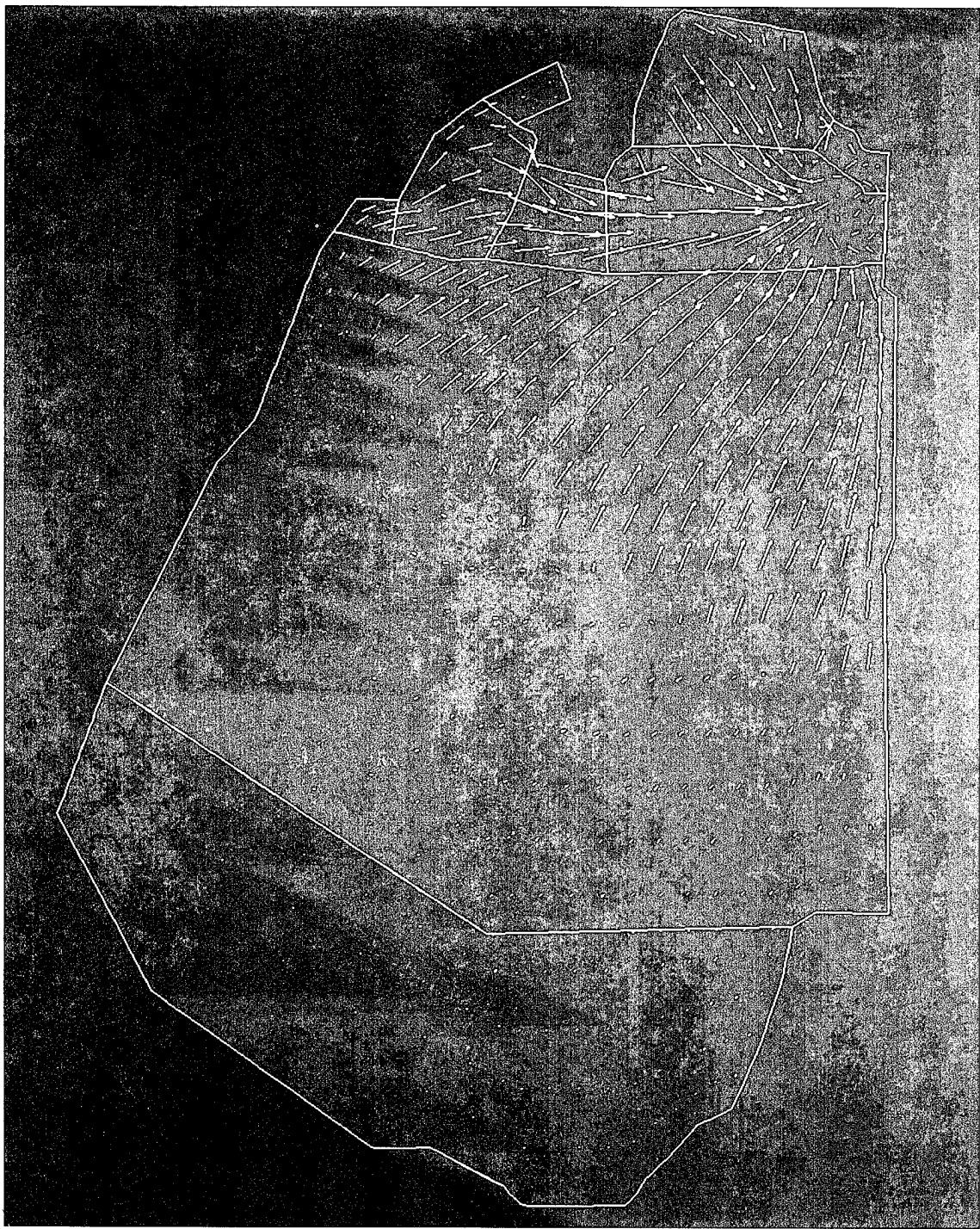
Figure 23. Surface velocities for warm reservoir with cold inflow
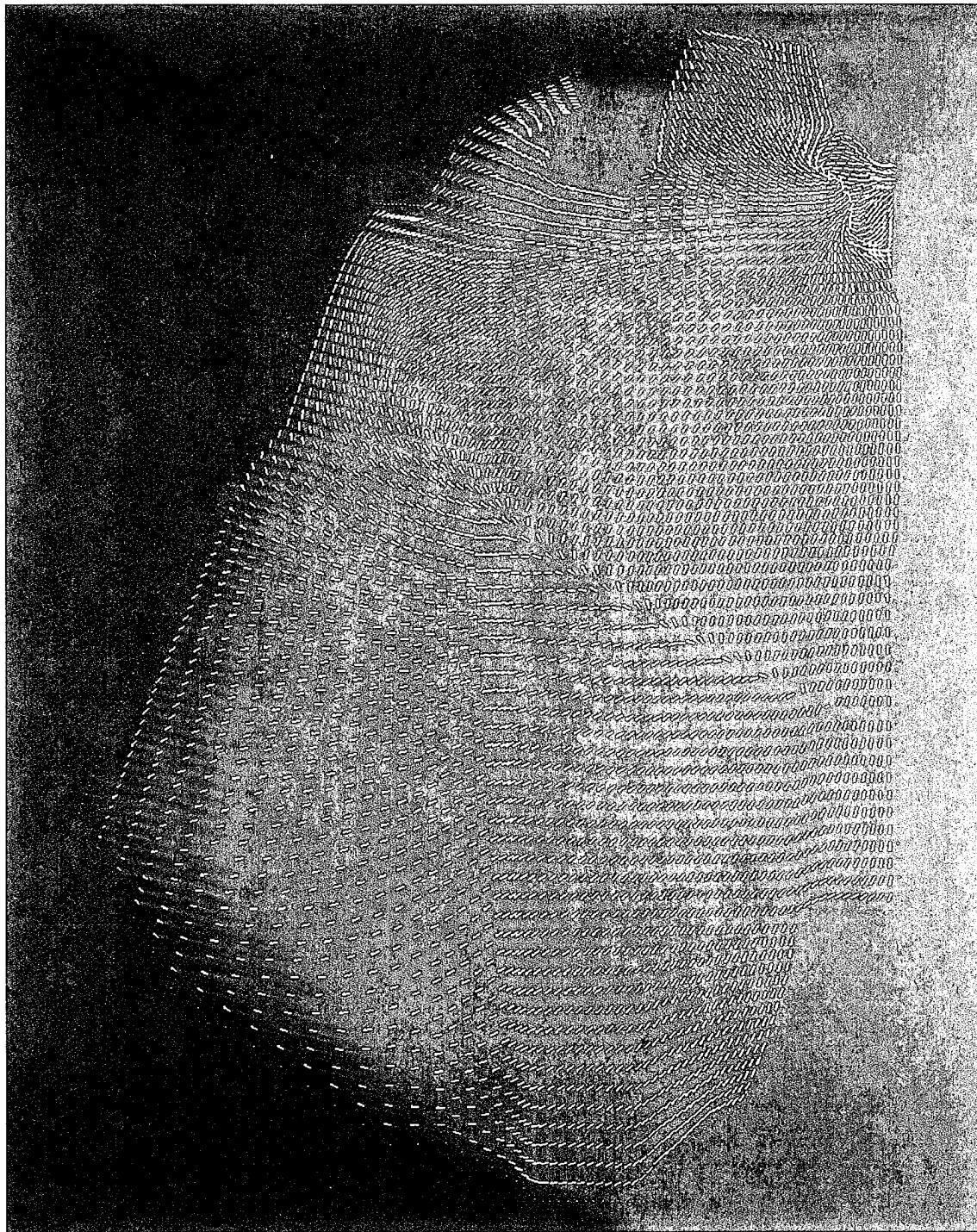
Figure 24. Surface flow patterns for warm reservoir with cold inflow
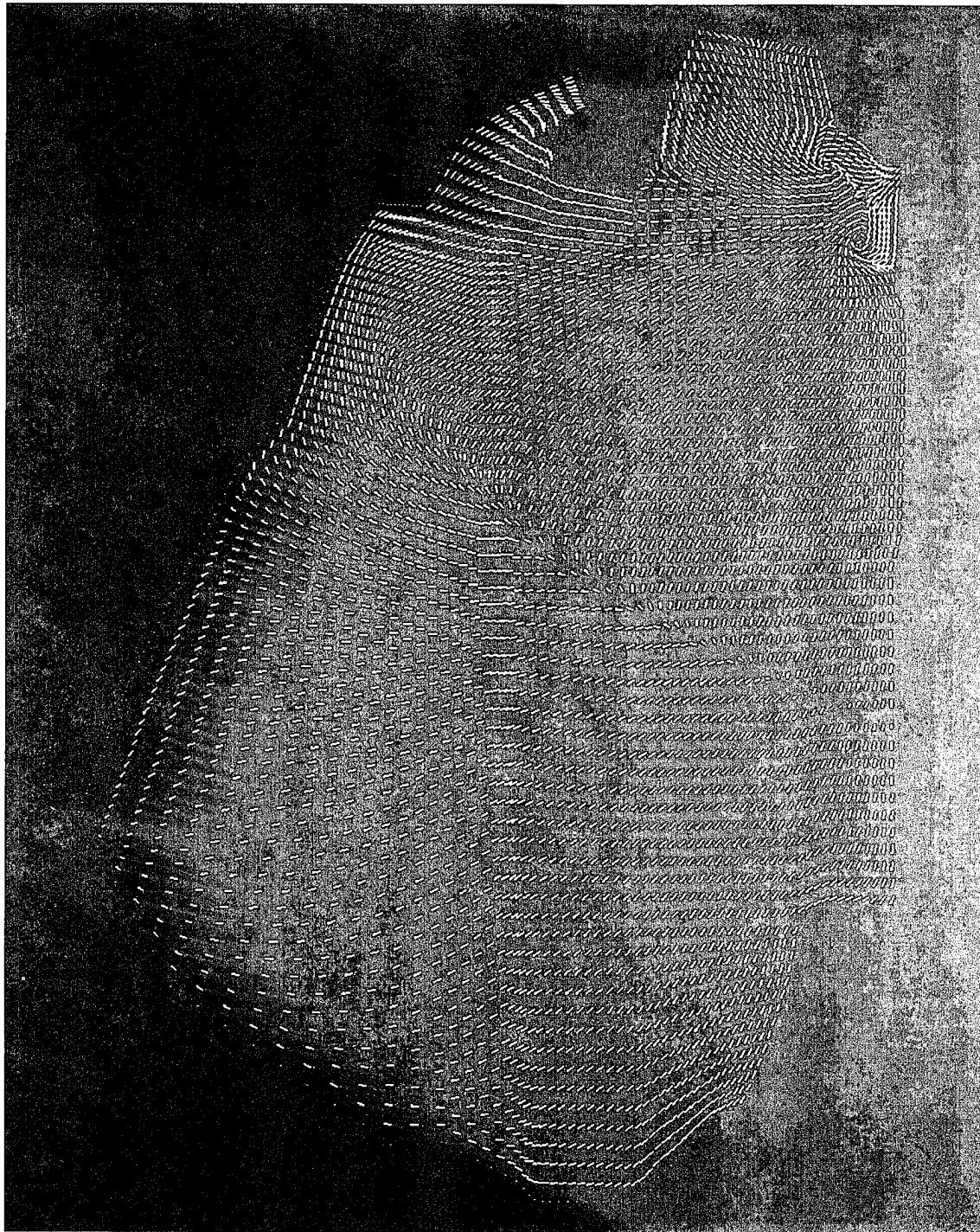
Figure 25. Flow patterns at 20 percent of total depth for warm reservoir with cold inflow
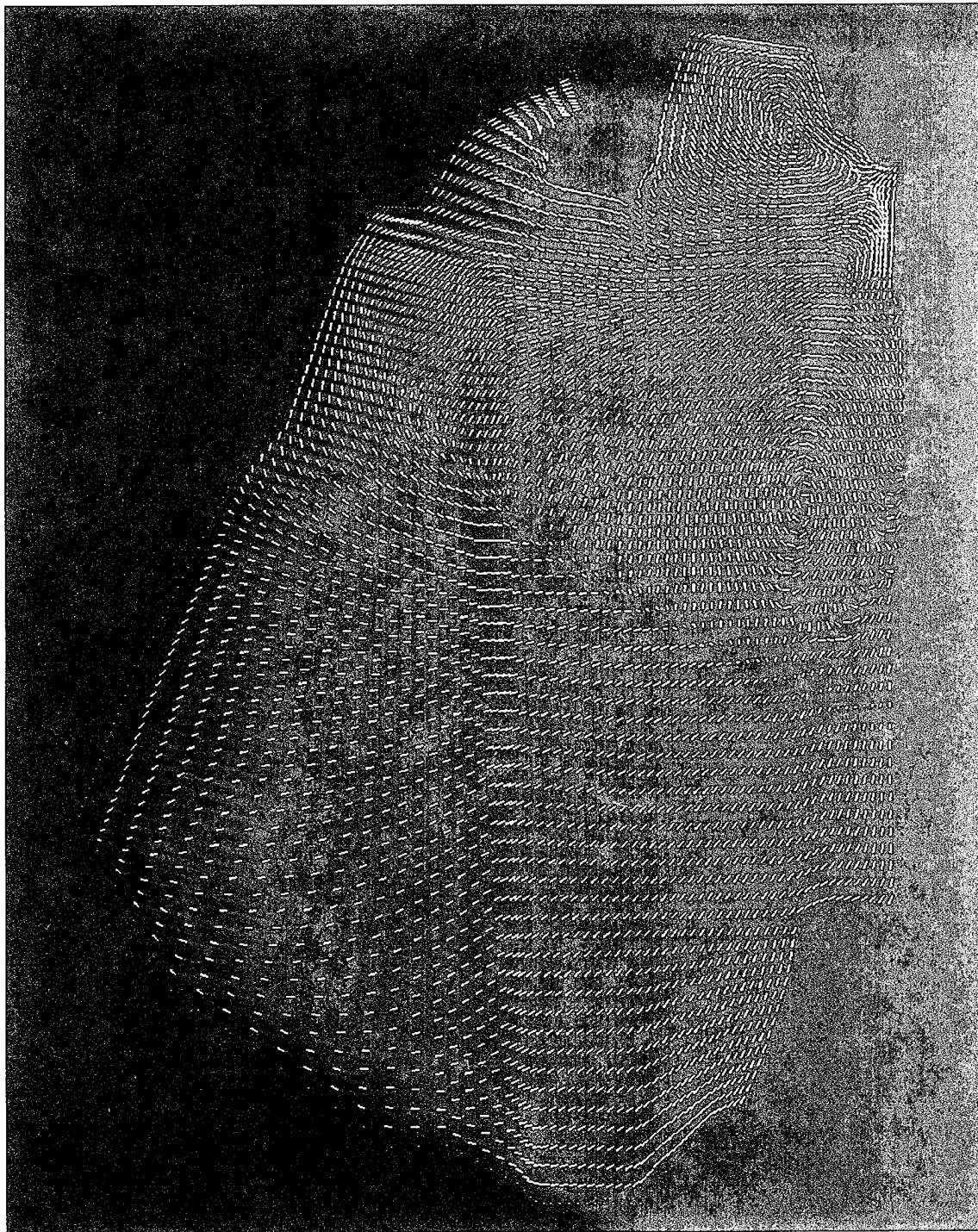
Figure 26. Flow patterns at 40 percent of total depth for warm reservoir with cold inflow
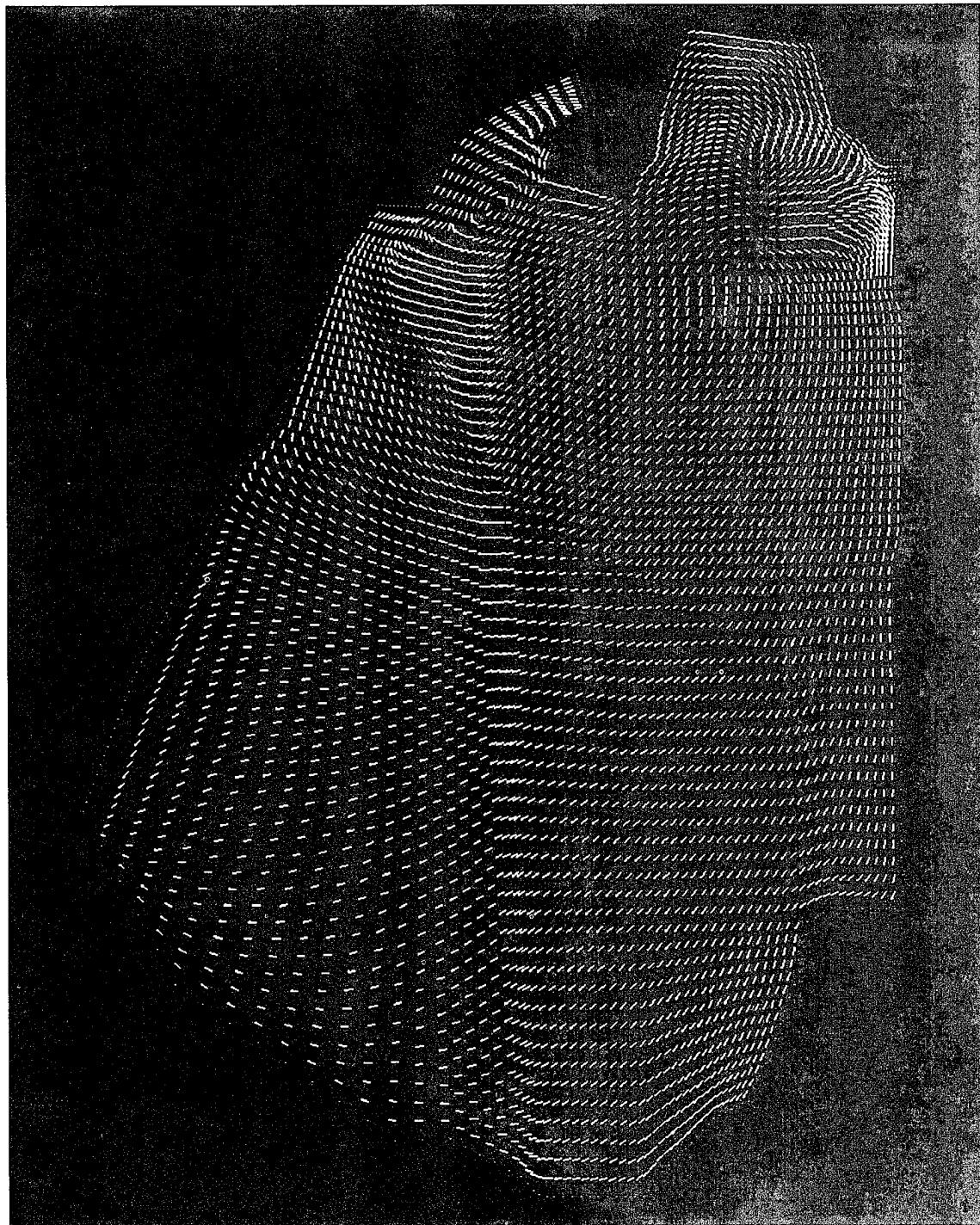
Figure 27. Flow patterns at 60 percent of total depth for warm reservoir with cold inflow
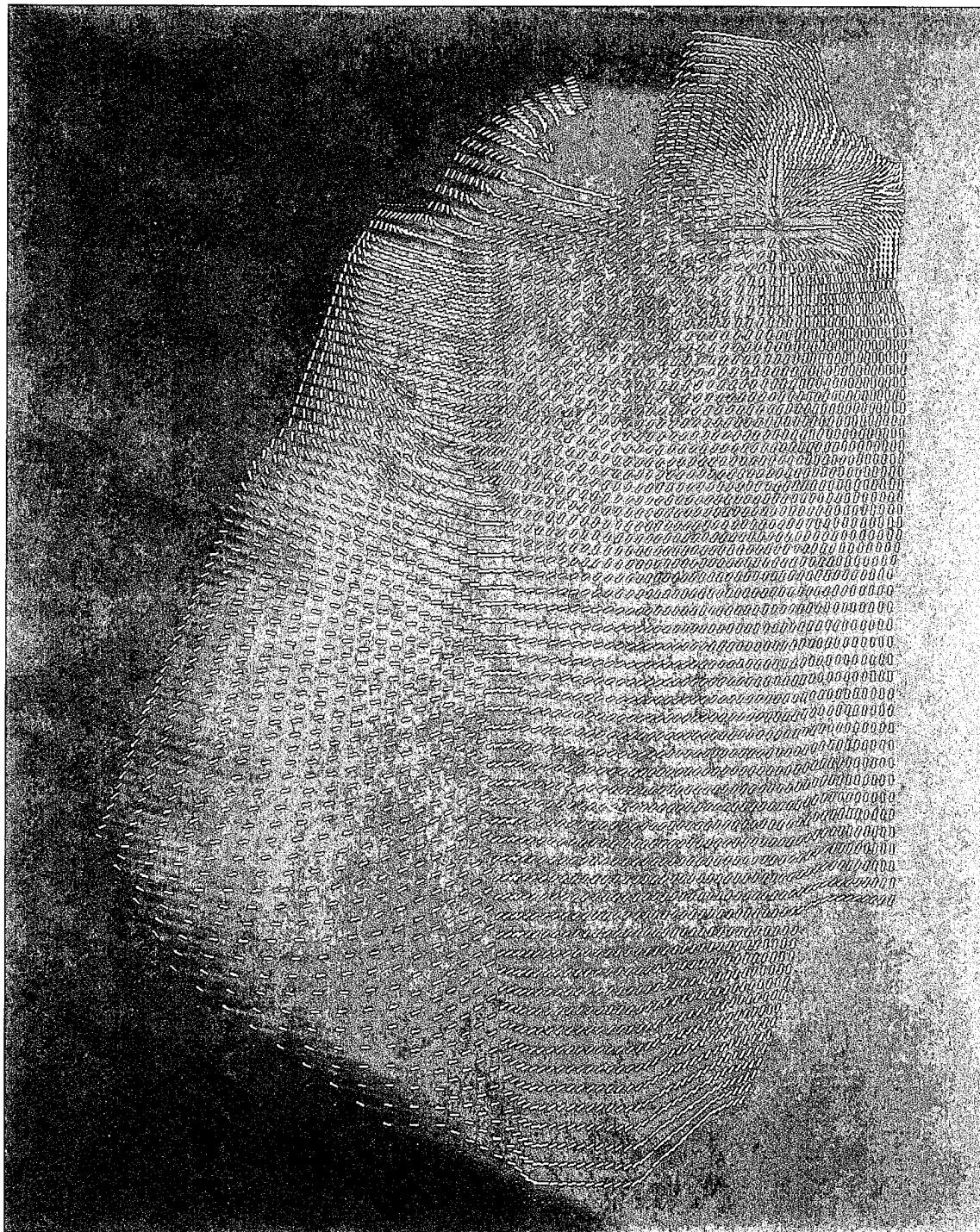
Figure 28. Flow patterns at 80 percent of total depth for warm reservoir with cold inflow

Figure 29. Velocity profiles for stratified reservoir with cold inflow
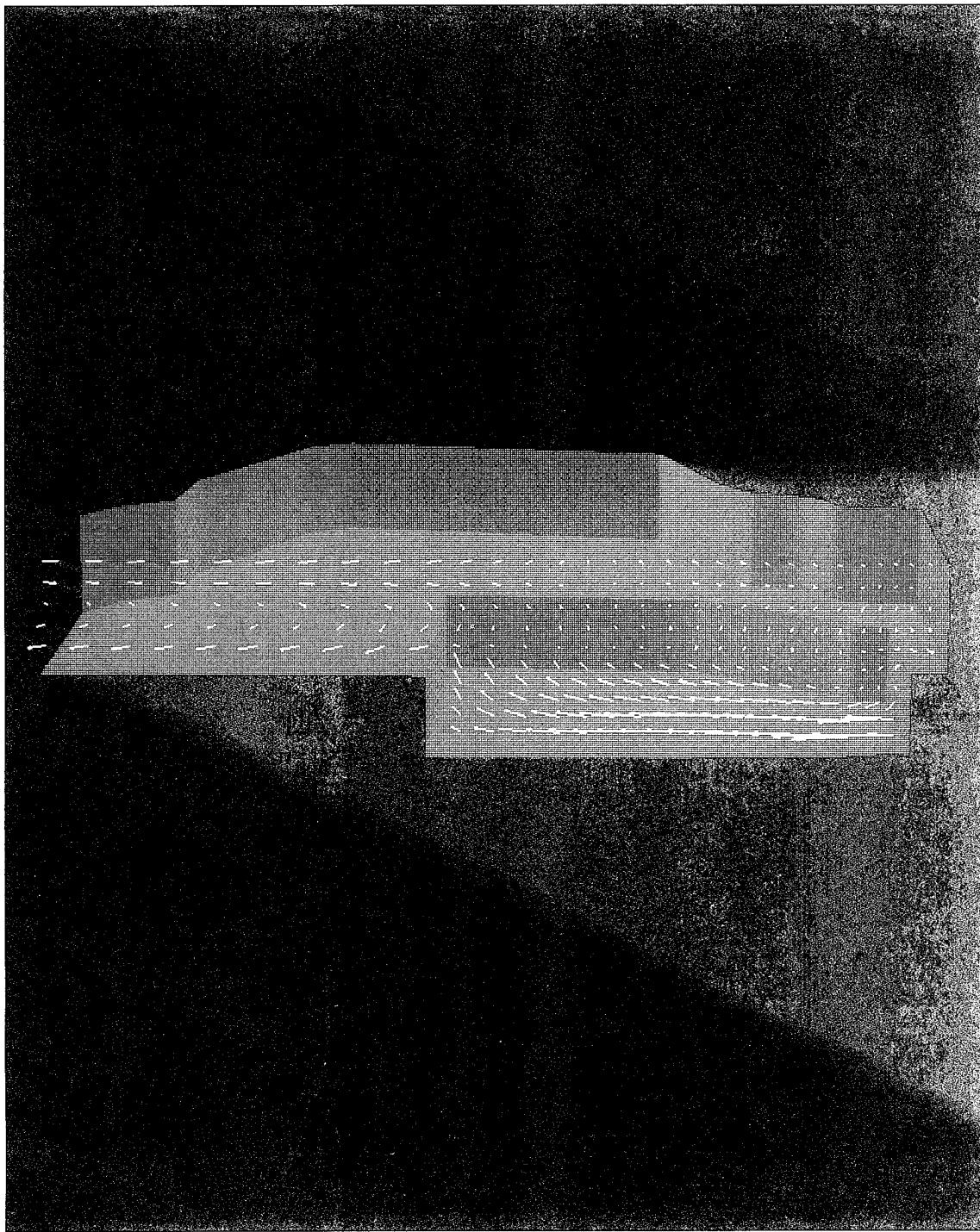
Figure 30. Velocities in elevation plane of sump for stratified reservoir with cold inflow
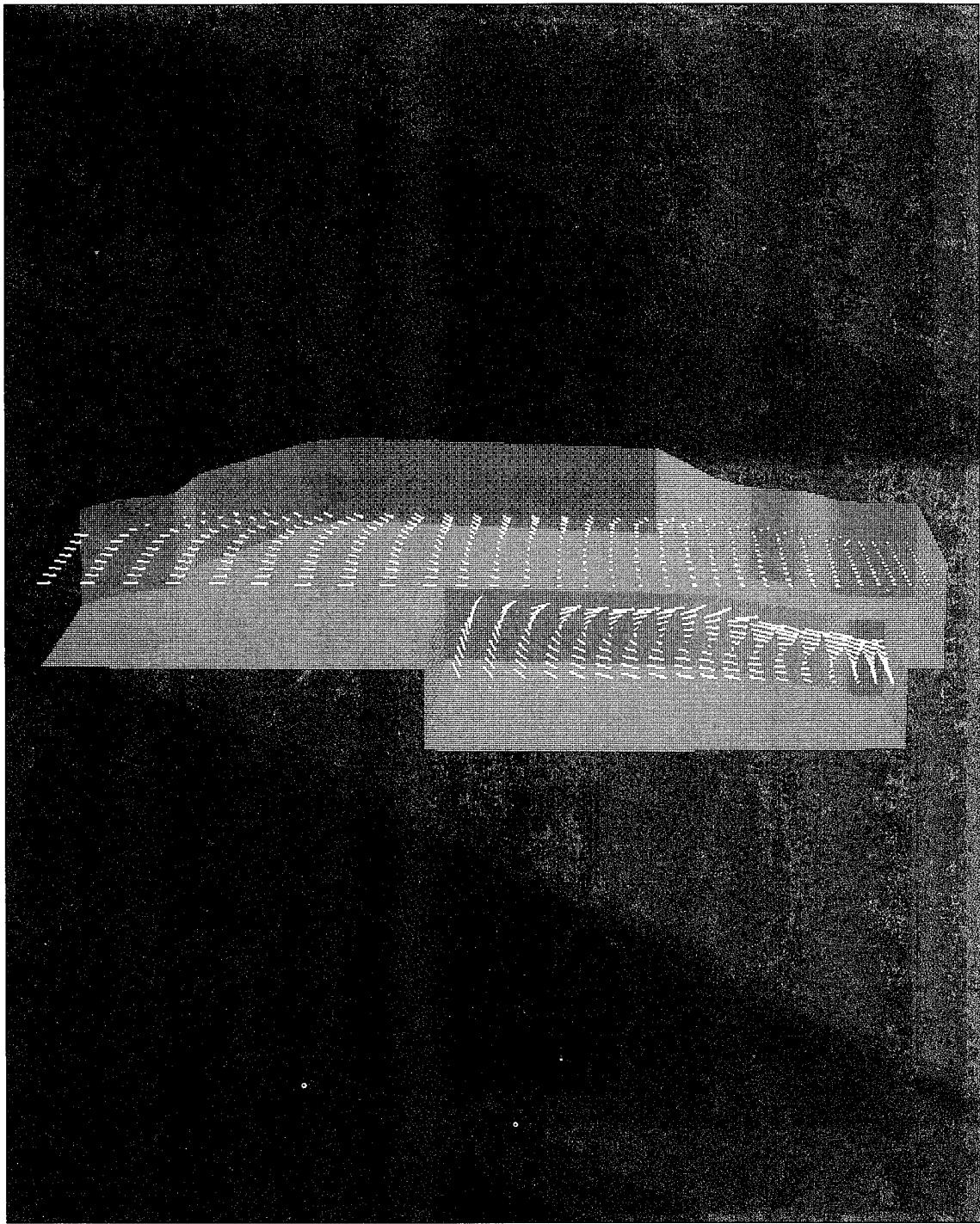
Figure 31. Velocities for horizontal planes in and above sump for stratified reservoir with cold inflow
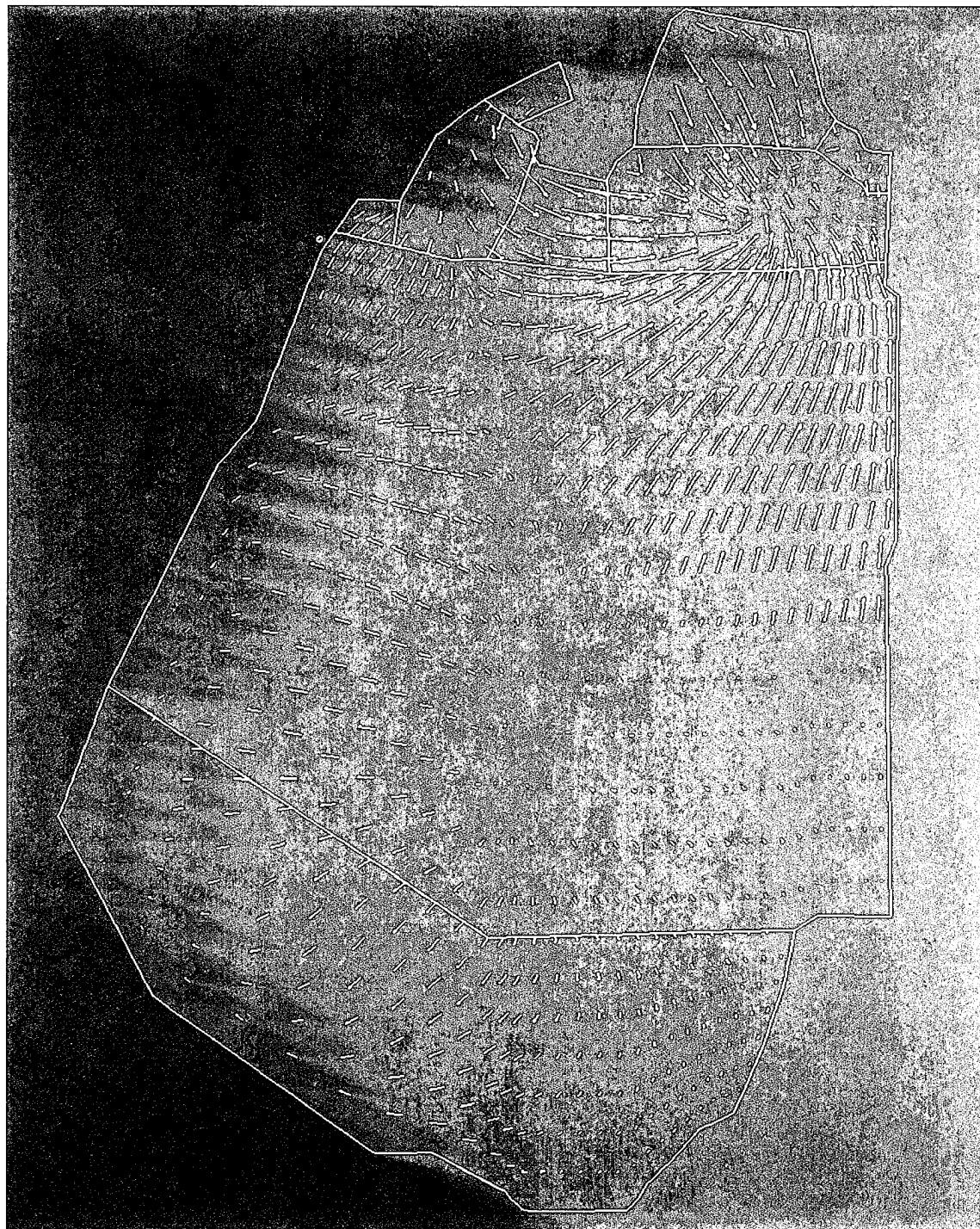
Figure 32. Surface velocities for stratified reservoir with cold inflow
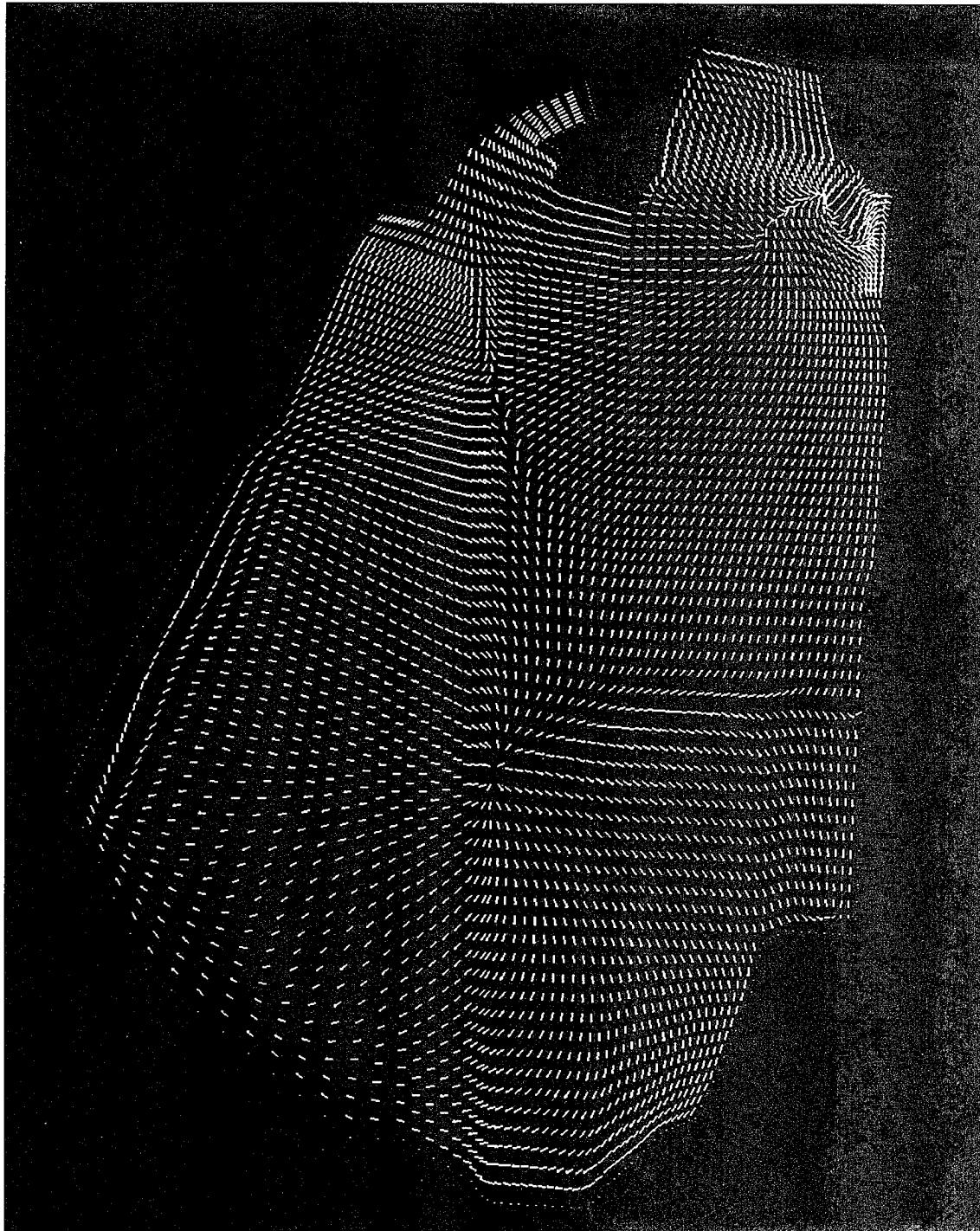
Figure 33. Surface flow patterns for stratified reservoir with cold inflow
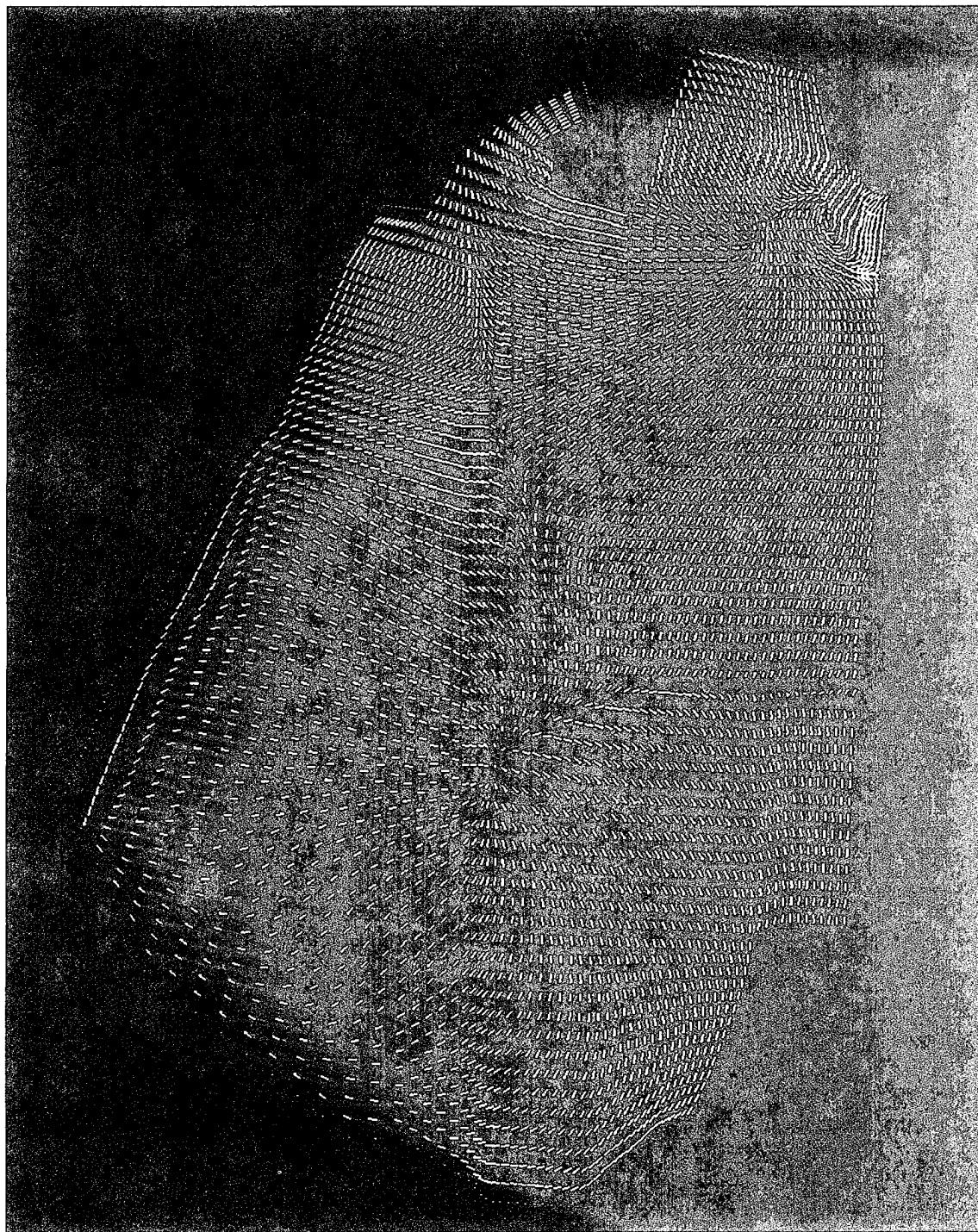
Figure 34. Flow patterns at 20 percent of total depth for stratified reservoir with cold inflow
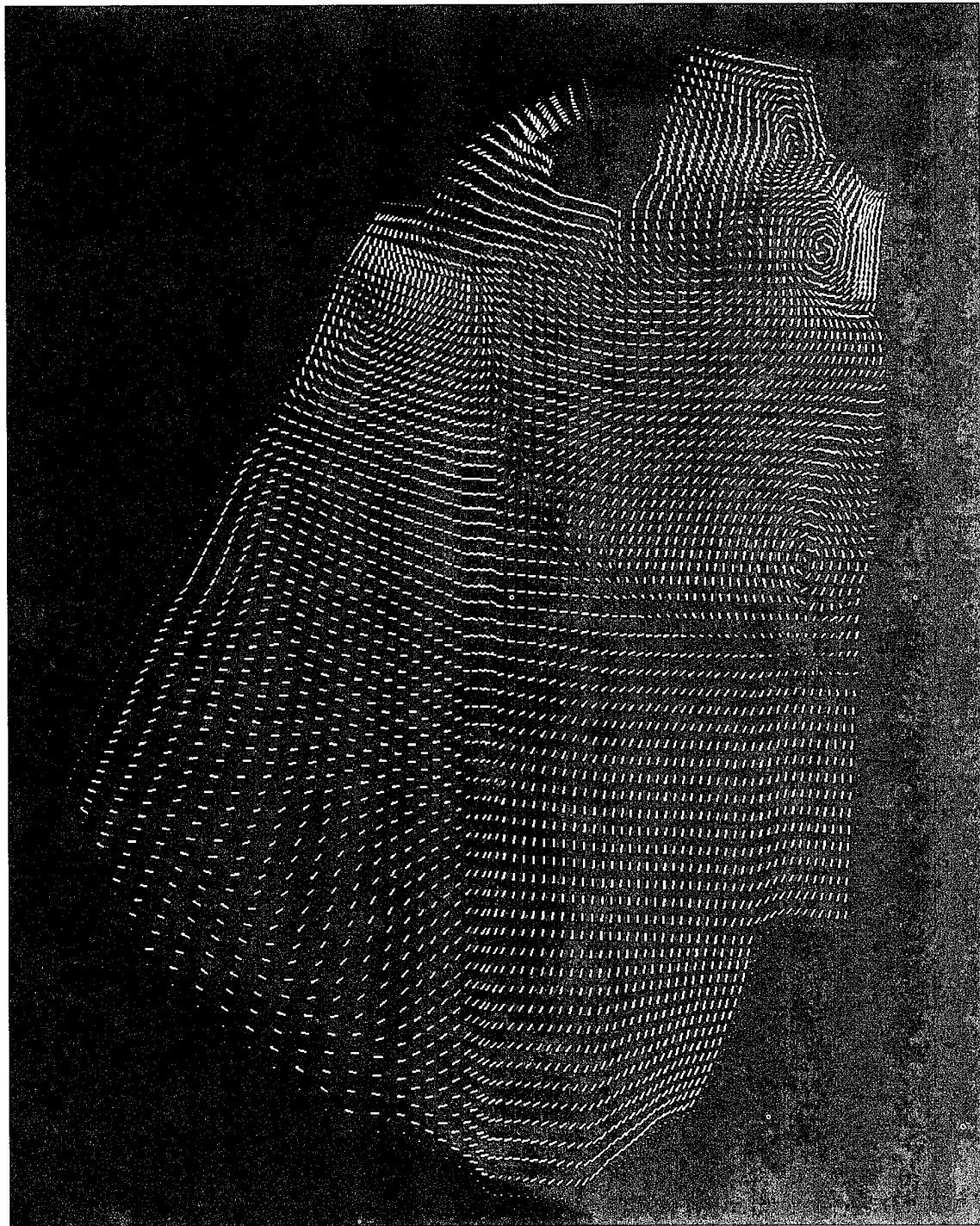
Figure 35. Flow patterns at 40 percent of total depth for stratified reservoir with cold inflow
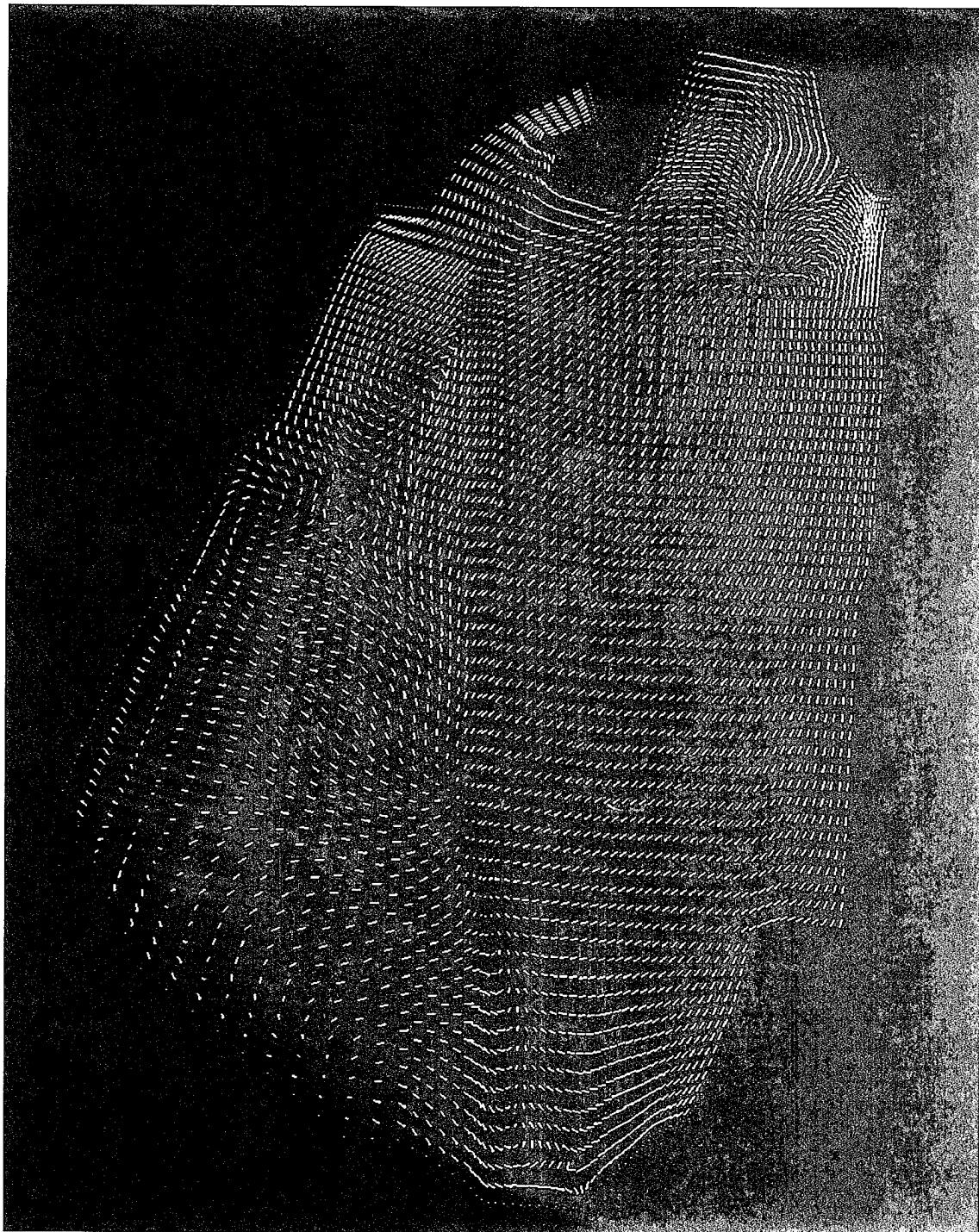
Figure 36. Flow patterns at 60 percent of total depth for stratified reservoir with cold
inflow
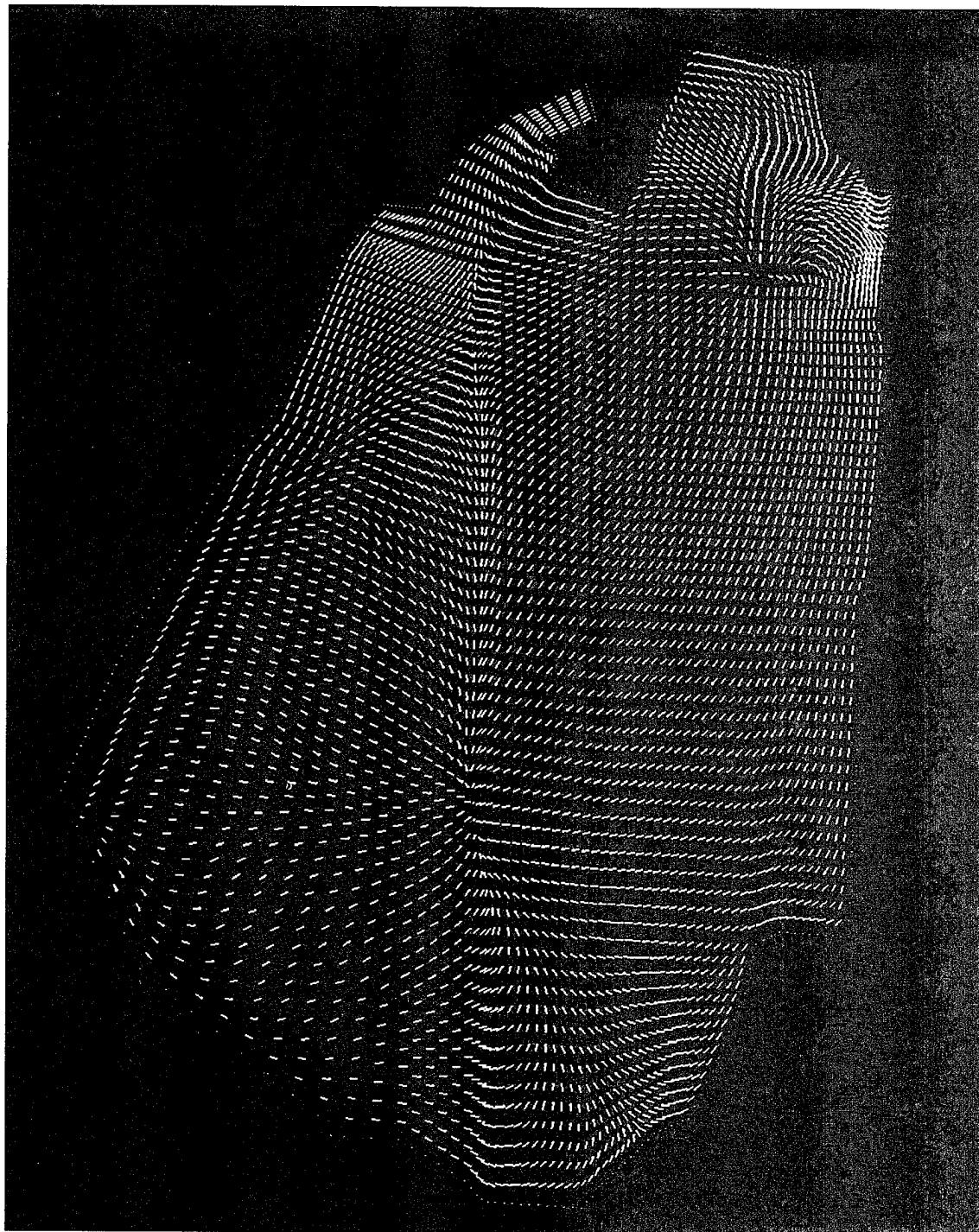
Figure 37. Flow patterns at 80 percent of total depth for stratified reservoir with cold inflow
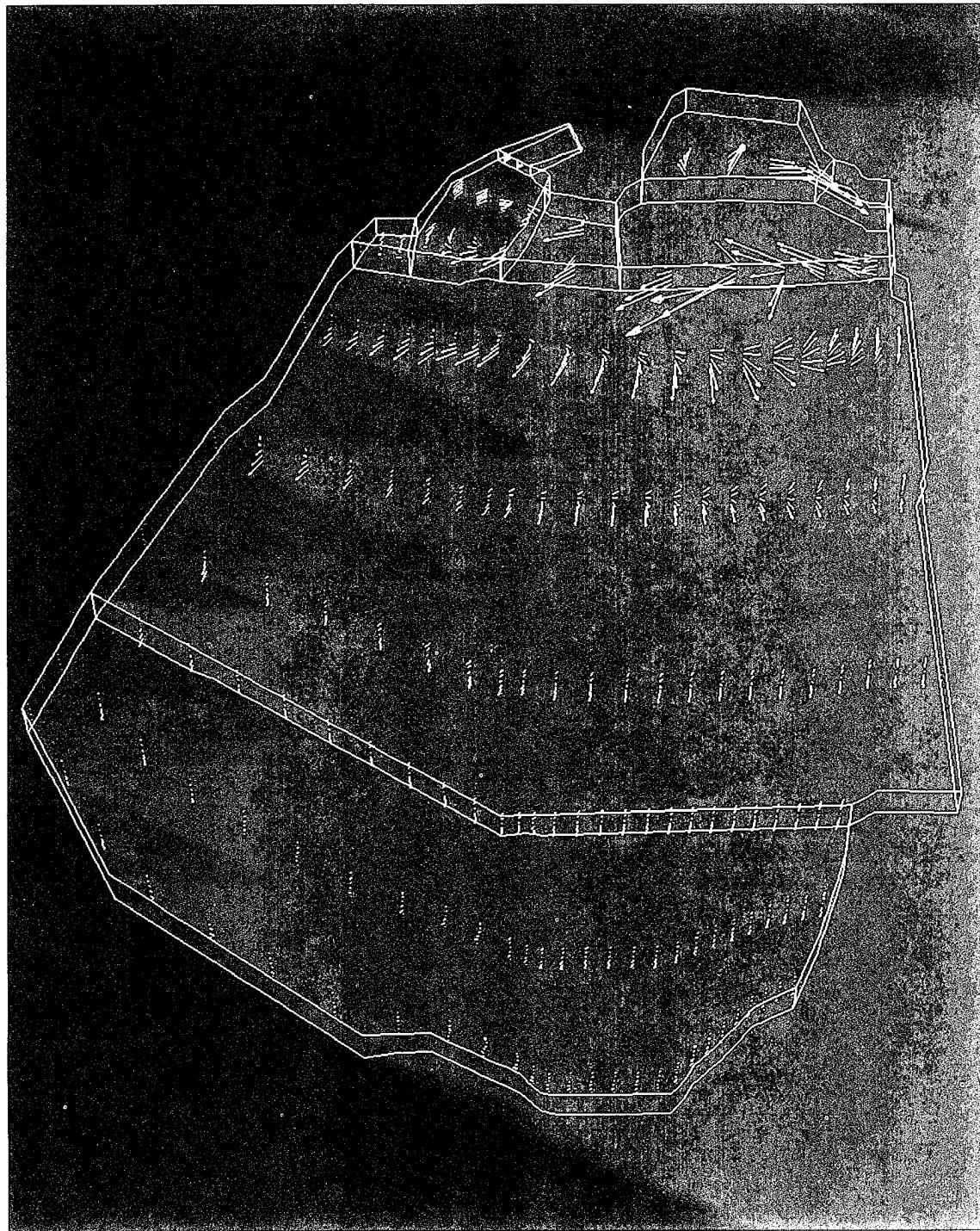
Figure 38. Velocity profiles for stratified reservoir with cold inflow and no background heat conduction
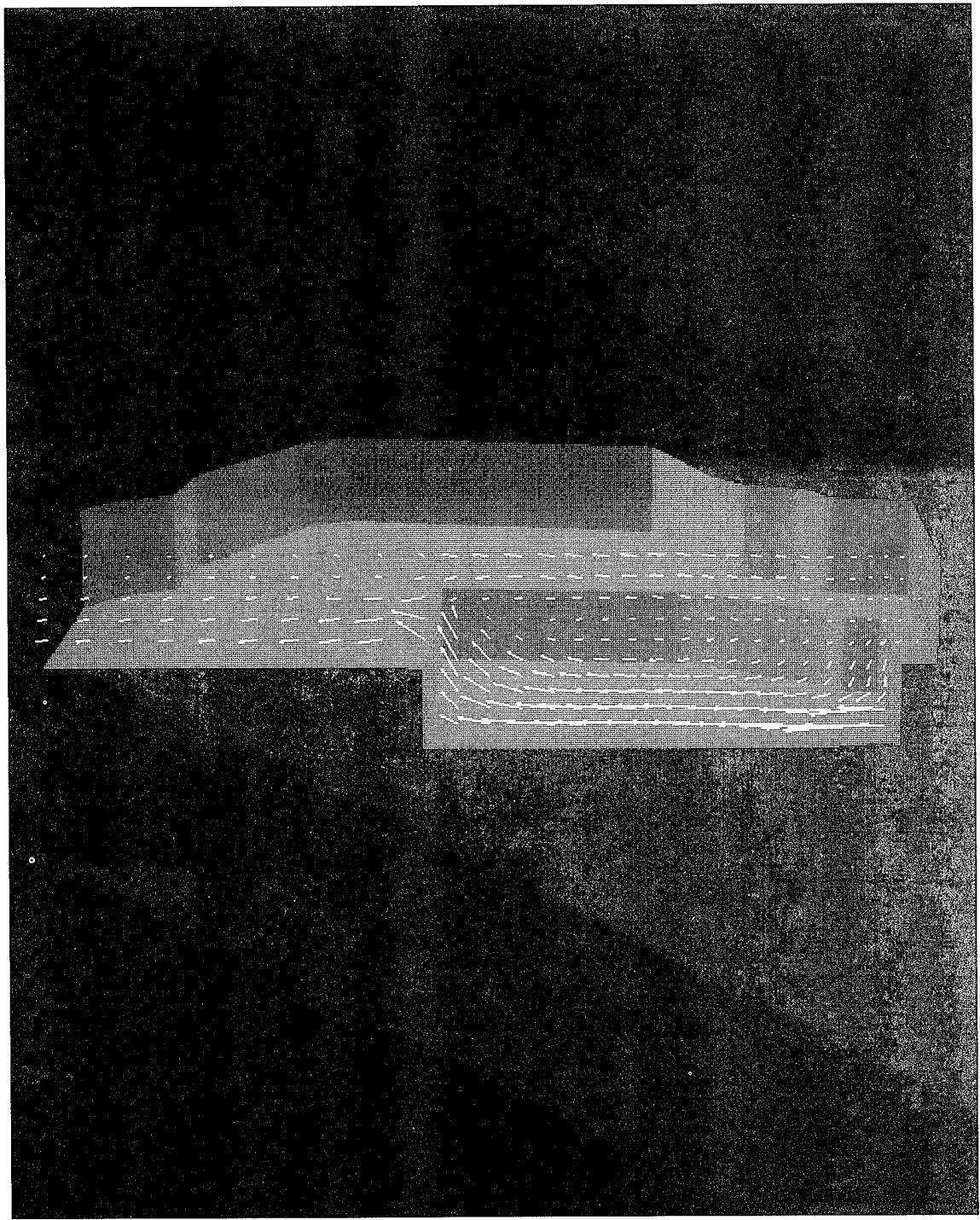
Figure 39. Velocities in elevation plane of sump for stratified reservoir with cold inflow and no background heat conduction
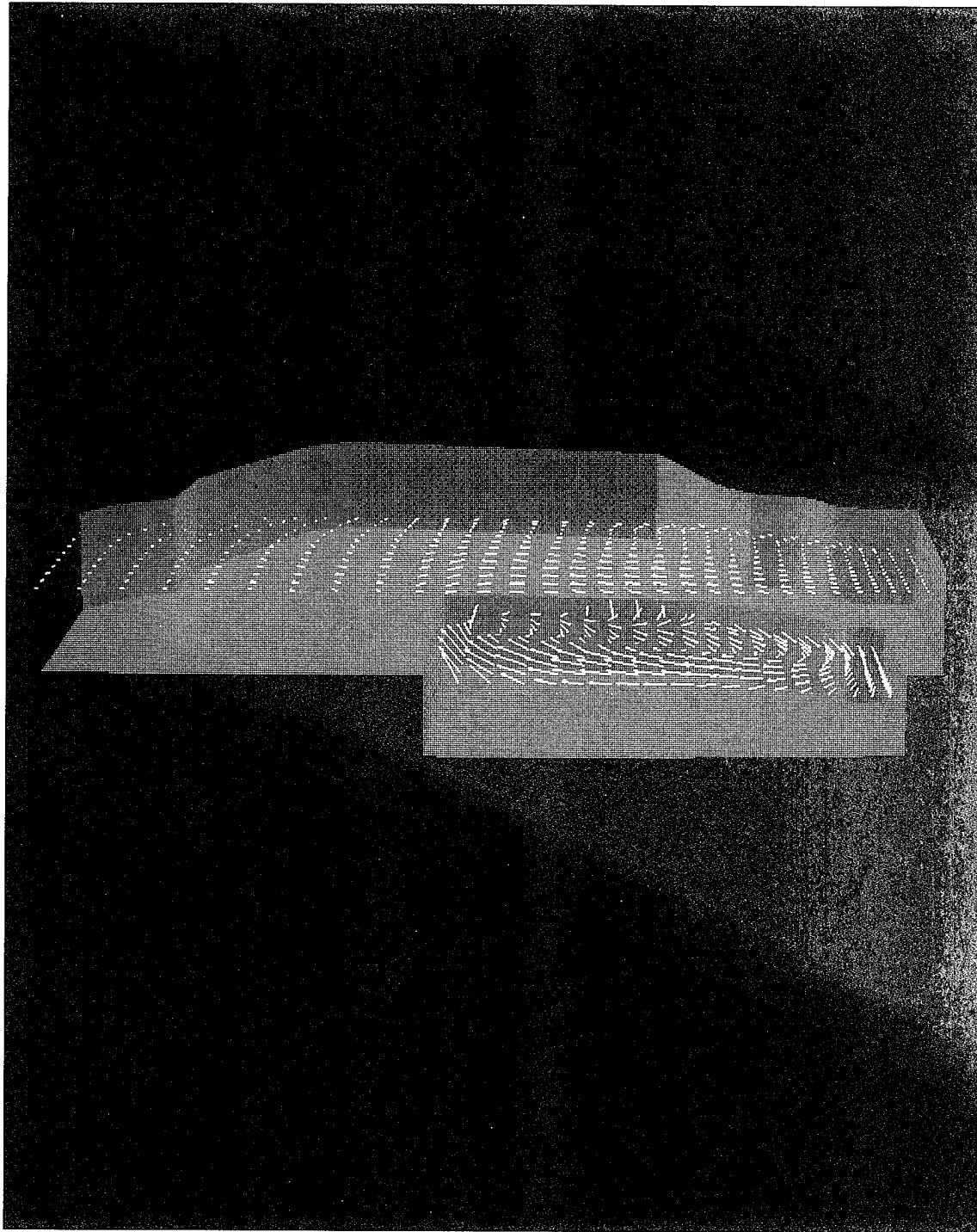
Figure 40. Velocities for horizontal planes in and above sump for stratified reservoir with
cold inflow and no background heat conduction
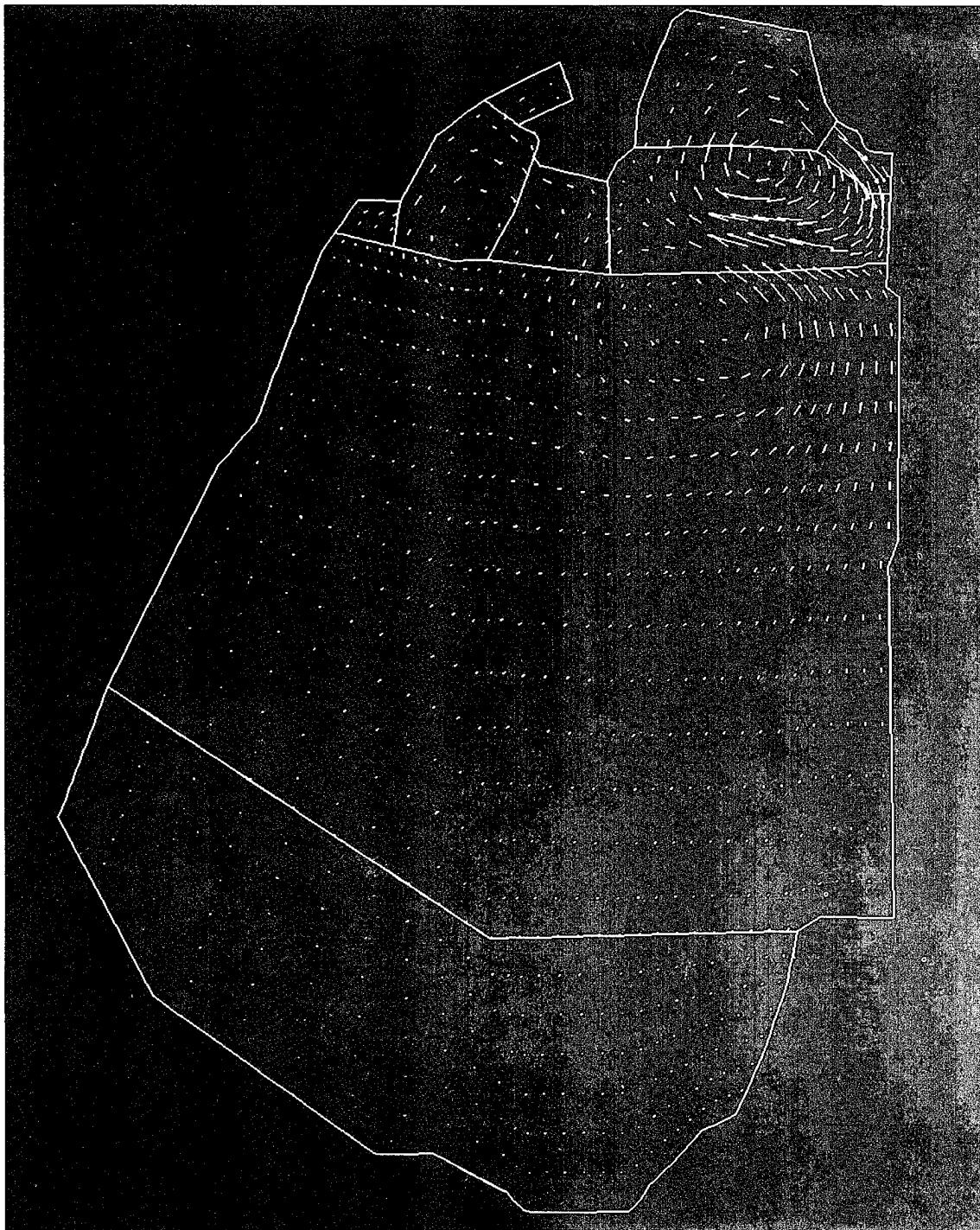
Figure 41. Surface velocities for stratified reservoir with cold inflow and no background heat conduction
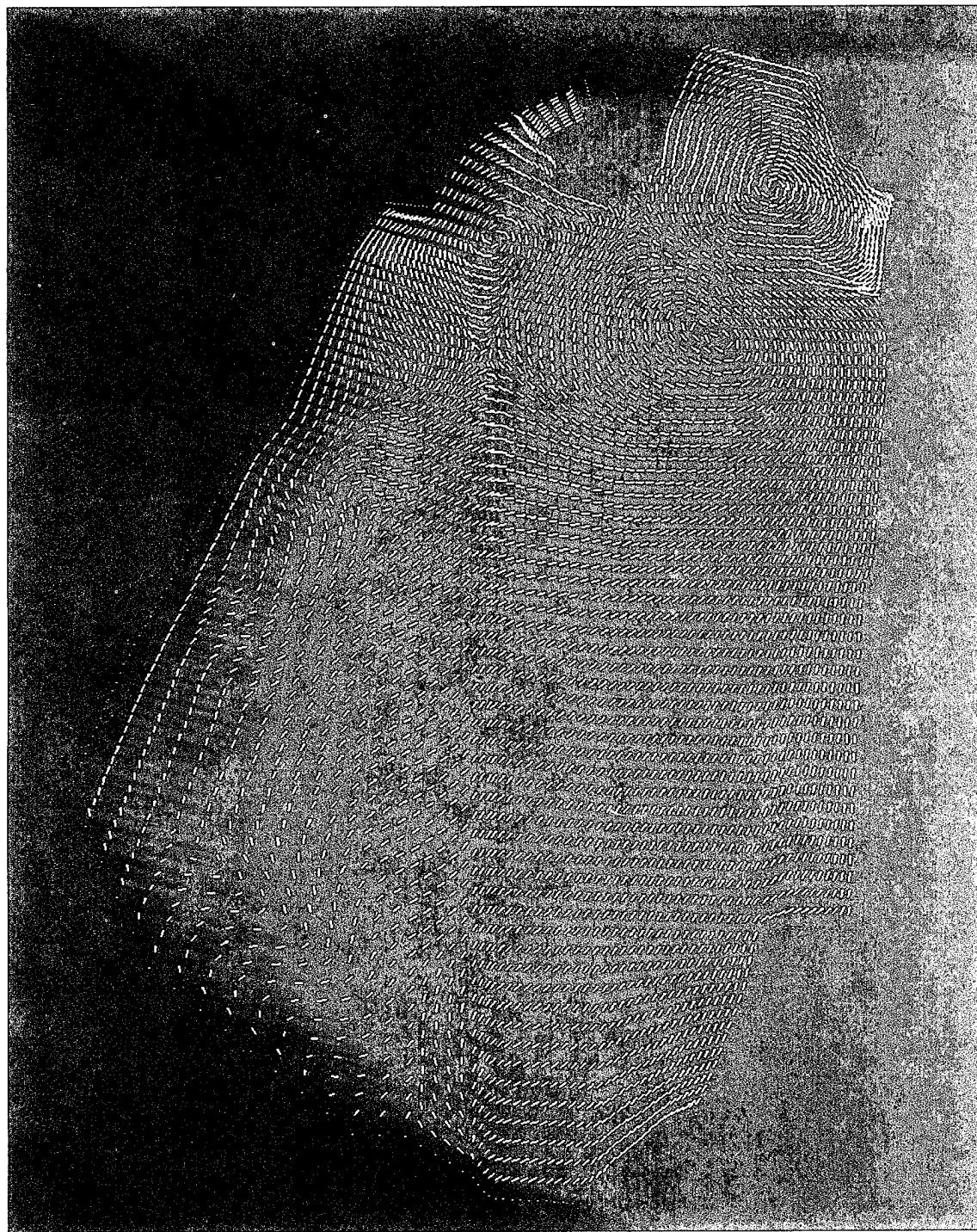
Figure 42. Surface flow patterns for stratified reservoir with cold inflow and no background heat conduction
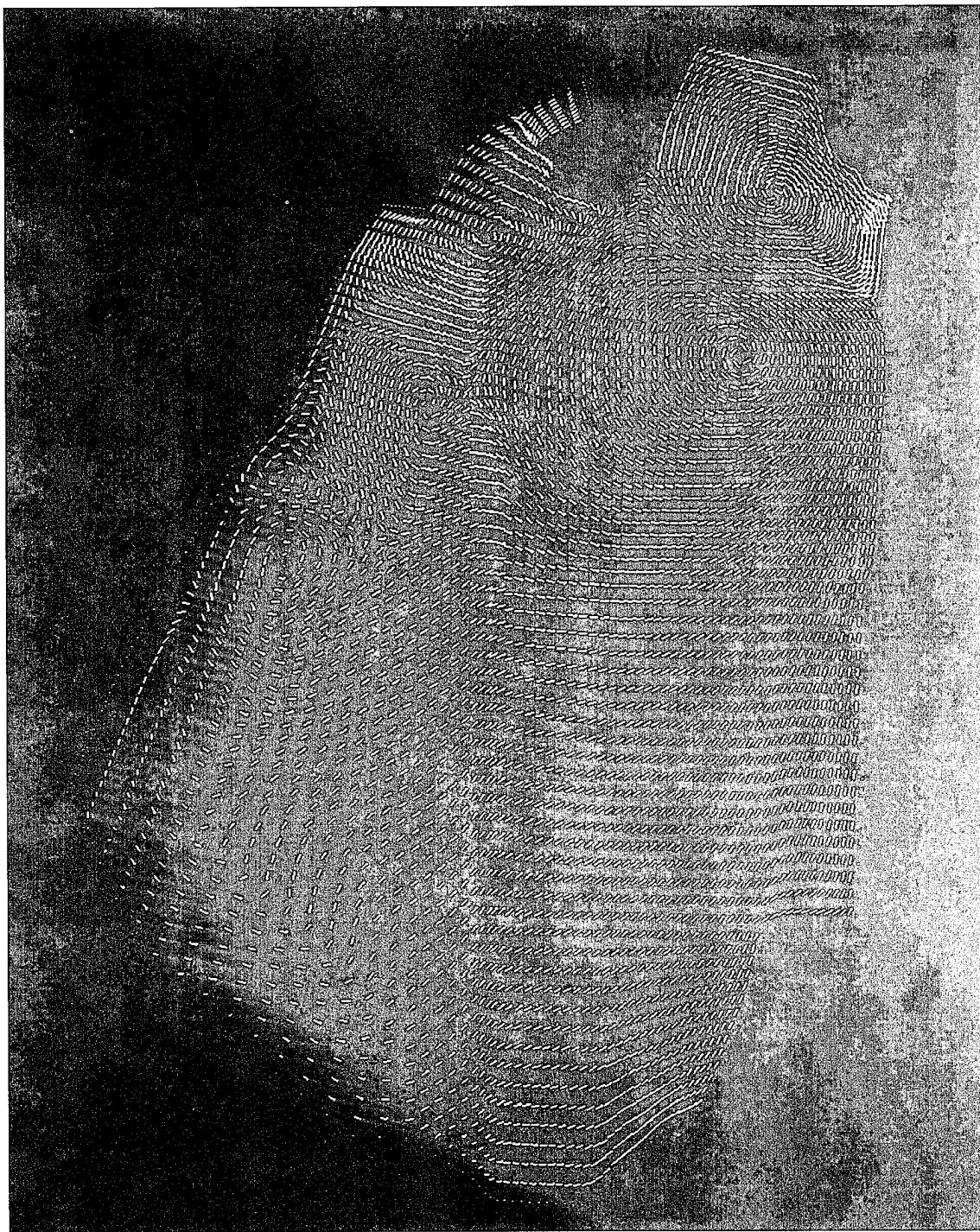
Figure 43. Flow patterns at 20 percent of total depth for stratified reservoir with cold inflow and no background heat conduction
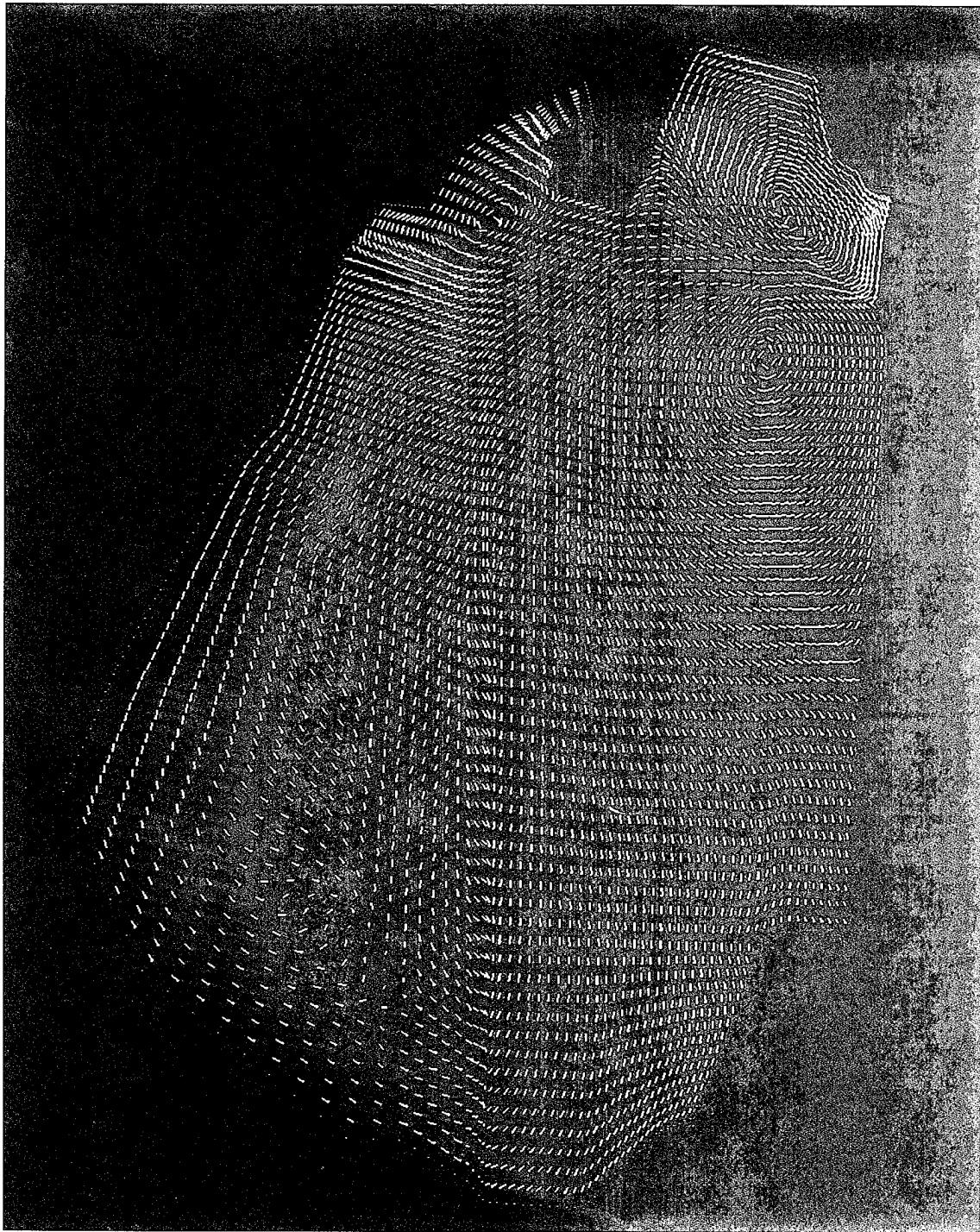
Figure 44. Flow patterns at 40 percent of total depth for stratified reservoir with cold inflow and no background heat conduction
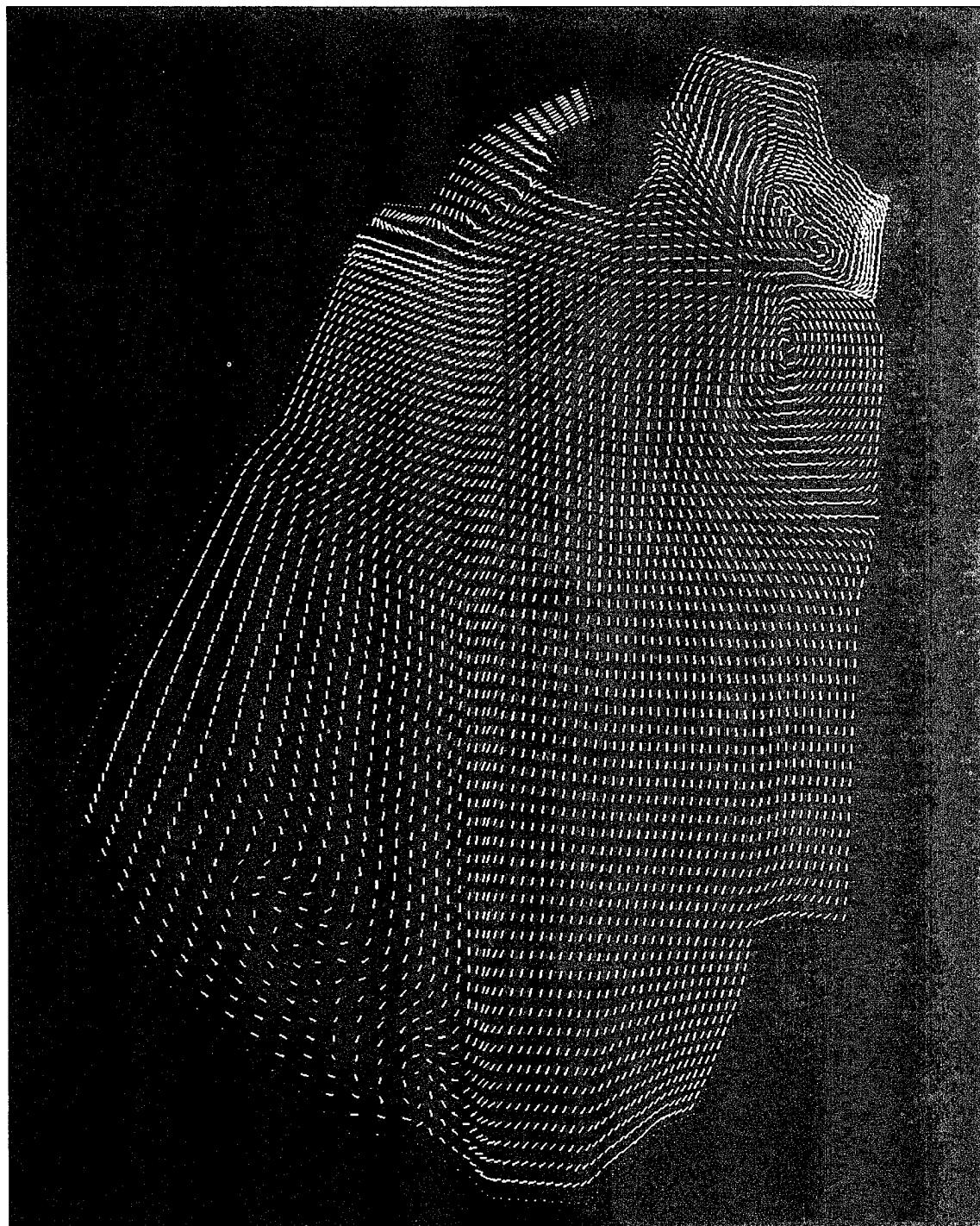
Figure 45. Flow patterns at 60 percent of total depth for stratified reservoir with cold inflow and no background heat conduction
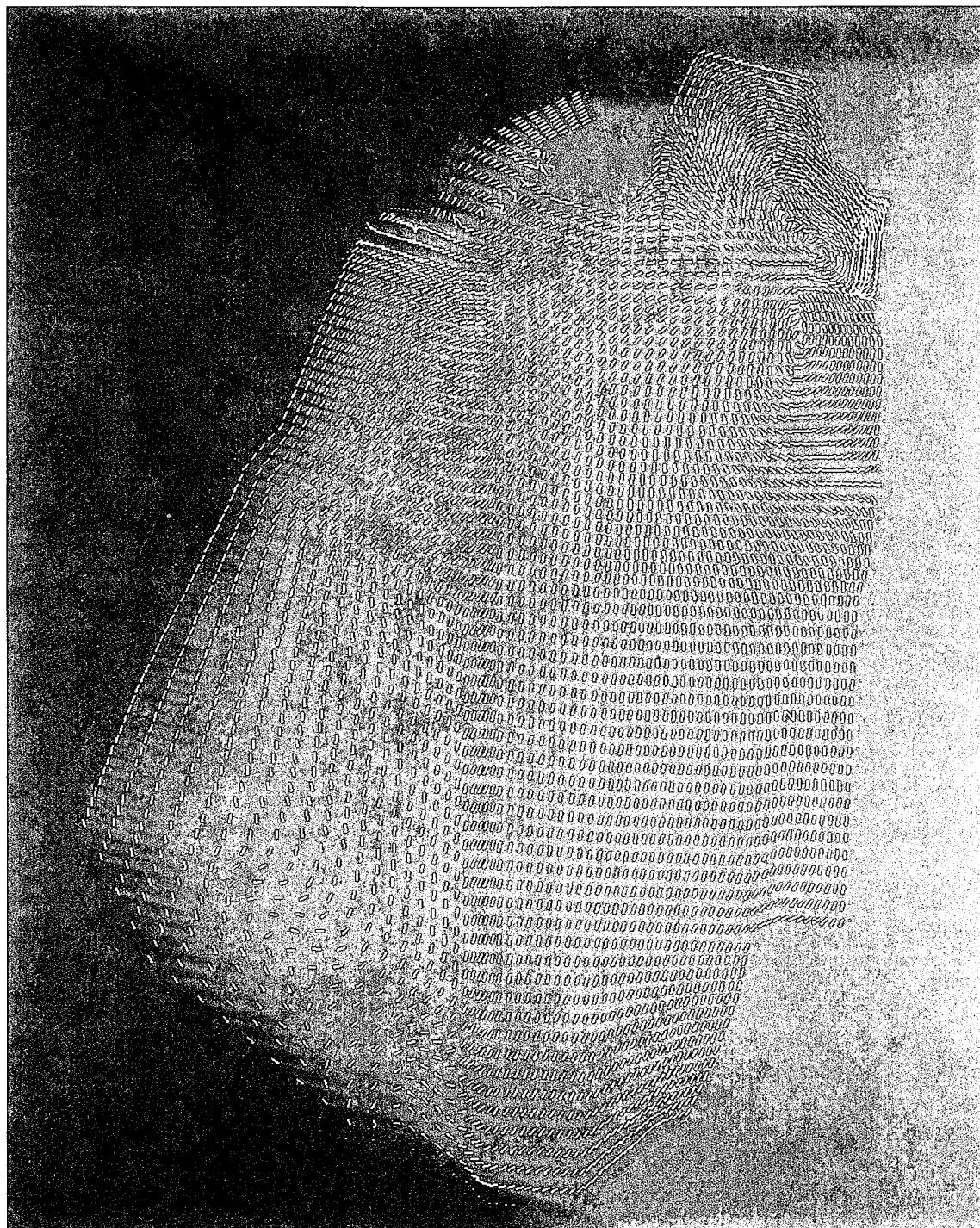
Figure 46. Flow patterns at 80 percent of total depth for stratified reservoir with cold inflow and no background heat conduction
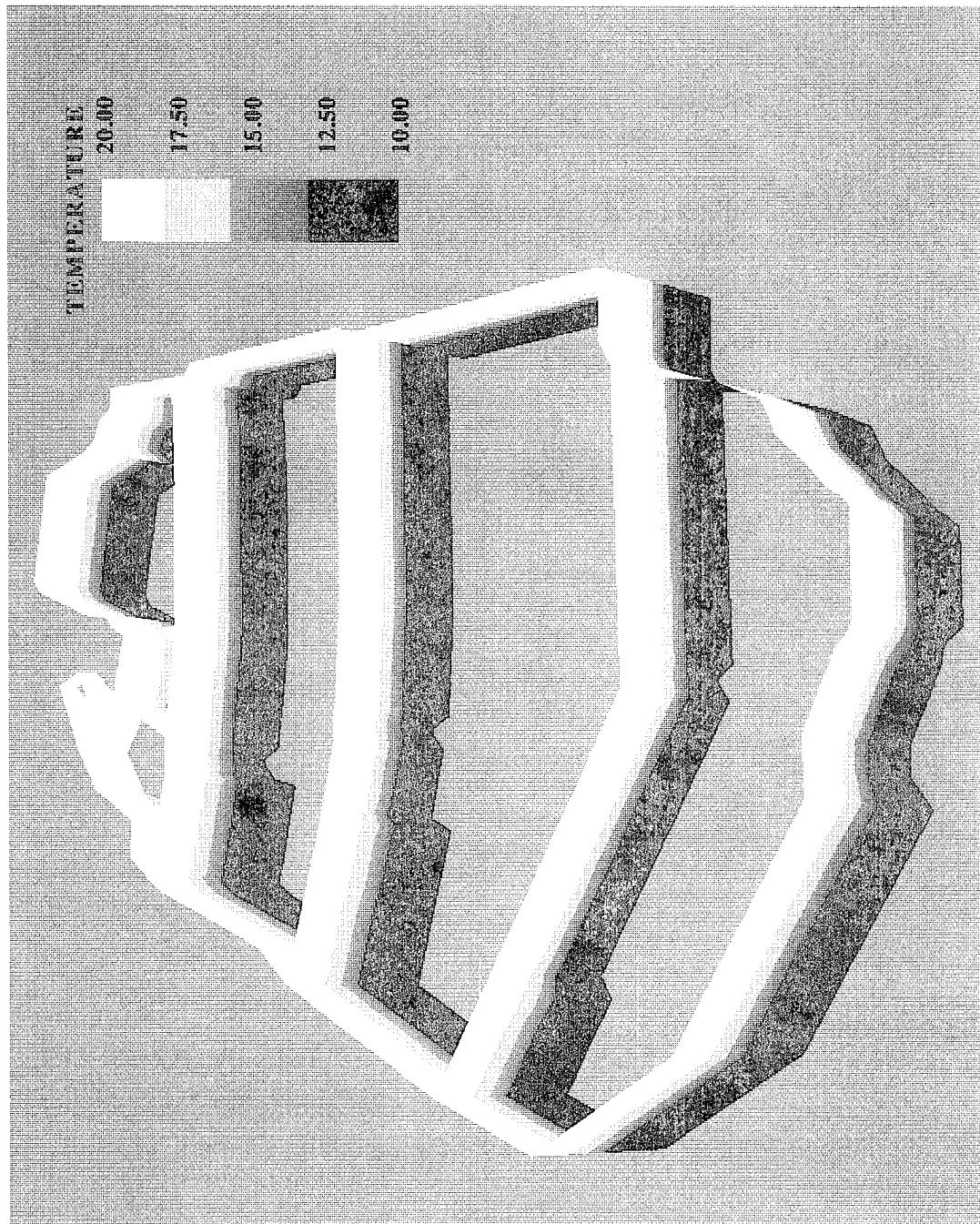
Figure 47. Gray-scale map of initial temperature for stratified reservoir
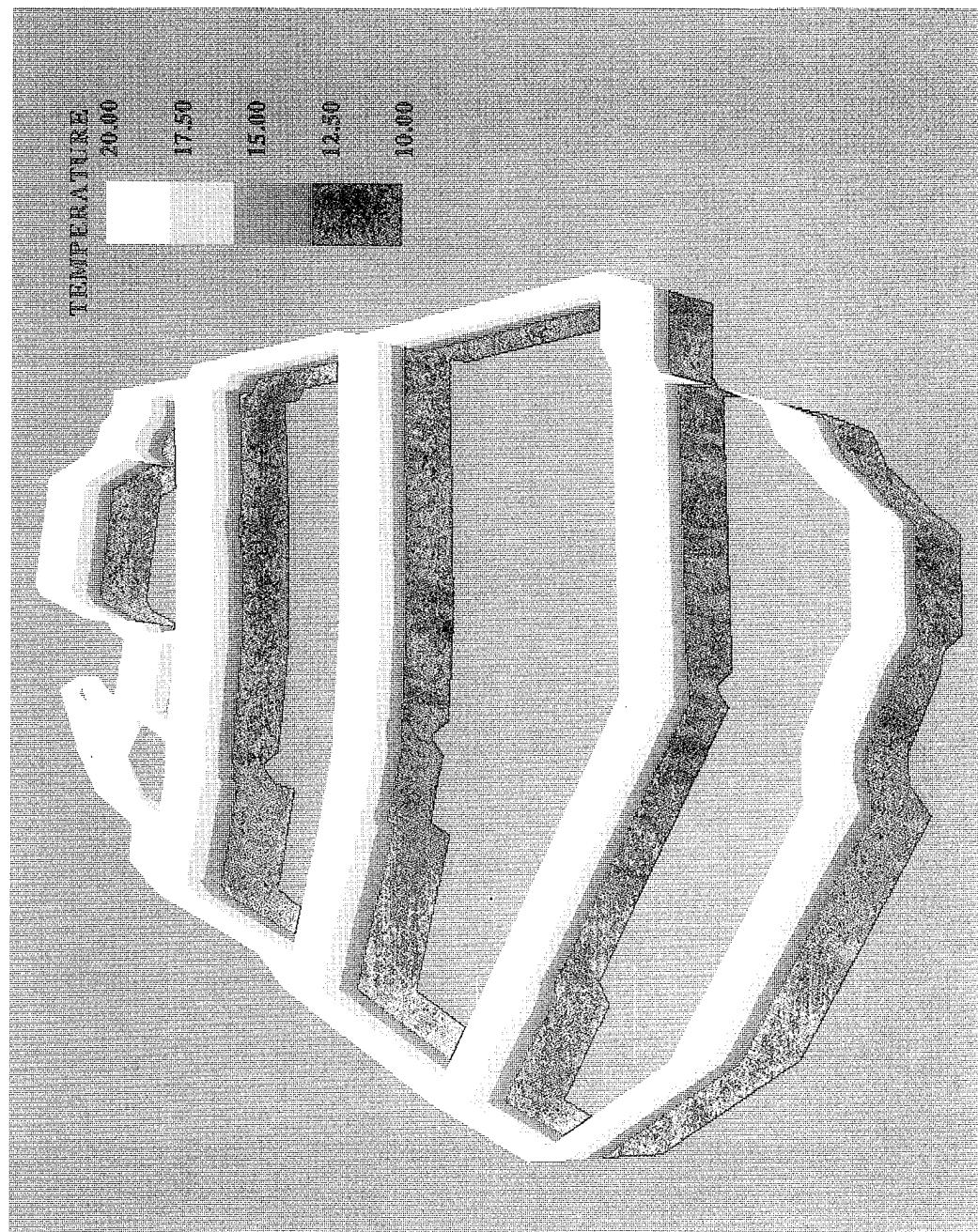
Figure 48. Gray-scale map of final temperature for stratified reservoir without background heat conduction
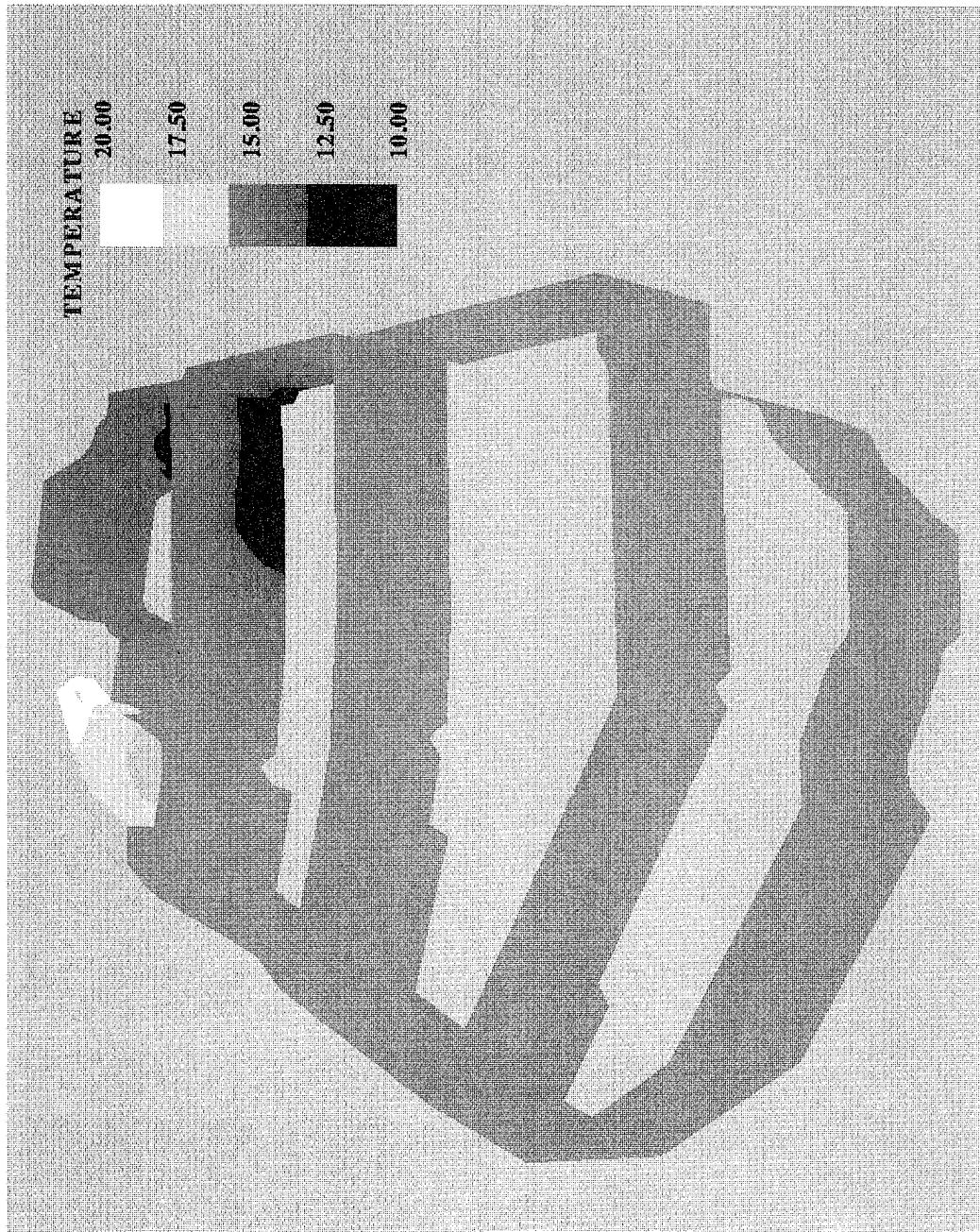
Figure 49. Gray-scale map of final temperature for stratified reservoir with background heat conduction
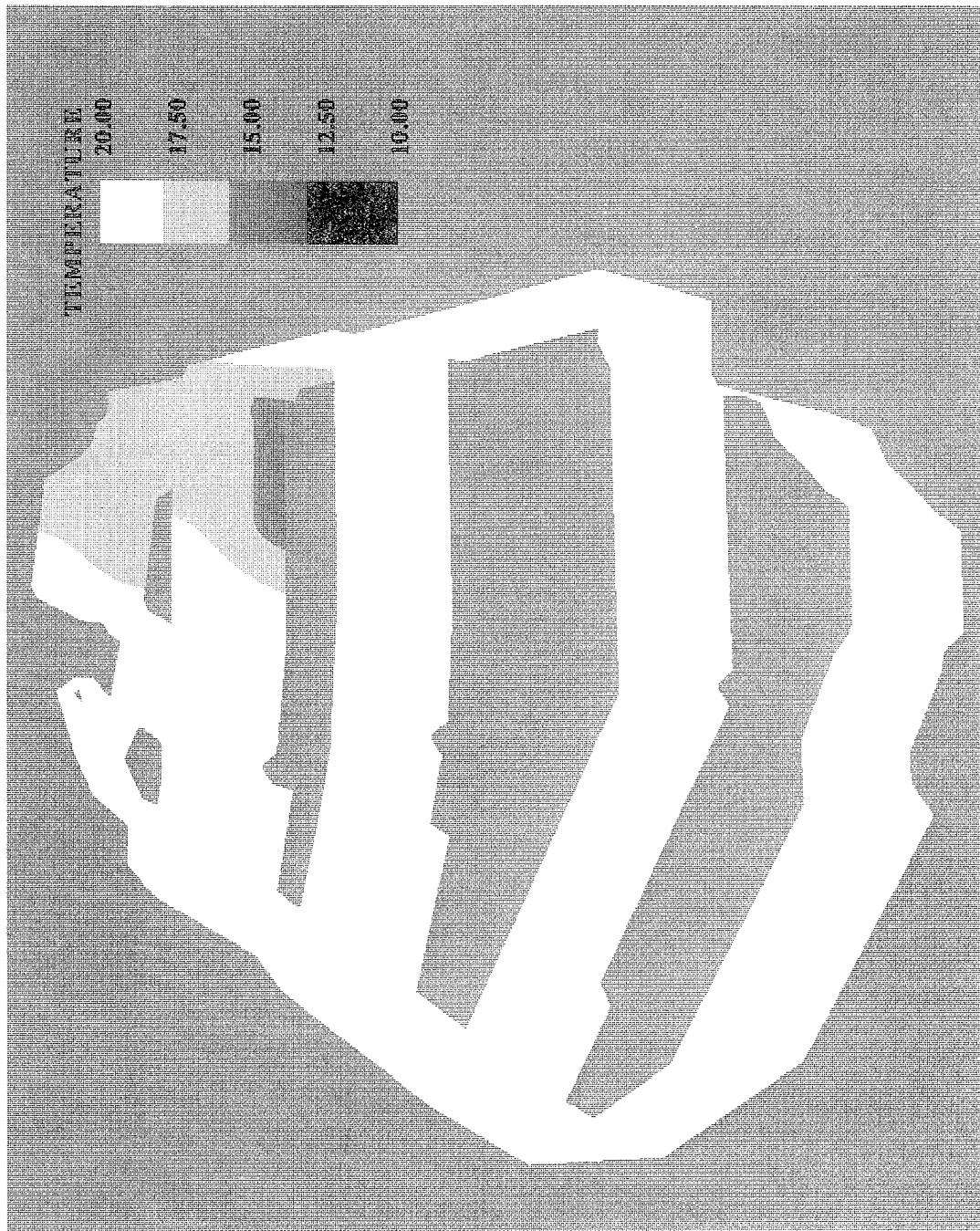
Figure 50. Gray-scale map of final temperature for warm reservoir with cold inflow

Appendix A
Notation

D/Dt	Substantive (total) time-derivative operator
div	Divergence operator
g	Acceleration due to gravity
$grad$	Gradient operator
i,j,k	Integer computational coordinates
J	Jacobian of coordinate transformation
k	Turbulence energy
n	Manning's coefficient
$\underline{n}$	Unit vector normal to boundary
p	Pressure
P_T	Ratio of thermal diffusivity to kinematic viscosity, also known as the Prandtl number
S	Source/sink term
t	Time
T	Temperature
T_S	Static (background) temperature
$\underline{u}$	Vector velocity
u, v, w	Cartesian components of velocity

U, V, W Volumetric fluxes in the ξ-, η-, and ζ-directions, respectively

x, y, z Cartesian coordinates

ϵ Turbulence dissipation rate

θ Relative deviation from reference value

μ Sum of the molecular viscosity μ_M and the eddy viscosity μ_T

ν Kinematic viscosity

ν_ψ Diffusivity for ψ

ξ, η, ζ Curvilinear coordinates

ρ Density

ρ_0 Reference (maximum) density

τ Shear stress

ψ Scalar function or vector component

REPORT DOCUMENTATION PAGE

1. AGENCY USE ONLY (Leave blank)	2. REPORT DATE September 1995	3. REPORT TYPE AND DATES COVERED Final report

4. TITLE AND SUBTITLE

Preliminary Development of a Three-Dimensional Numerical Model for Reservoir Hydrodynamics

5. FUNDING NUMBERS

6. AUTHOR(S)

Robert S. Bernard

7. PERFORMING ORGANIZATION NAME(S) AND ADDRESS(ES)

U.S. Army Engineer Waterways Experiment Station
3909 Halls Ferry Road, Vicksburg, MS 39180-6199

8. PERFORMING ORGANIZATION REPORT NUMBER

Technical Report
HL-95- 9

9. SPONSORING/MONITORING AGENCY NAME(S) AND ADDRESS(ES)

U.S. Army Engineer District, Chicago
111 North Canal Street, Suite 600
Chicago, IL 60606-7206

10. SPONSORING/MONITORING AGENCY REPORT NUMBER

11. SUPPLEMENTARY NOTES

Available from National Technical Information Service, 5285 Port Royal Road, Springfield, VA 22161.

12a. DISTRIBUTION/AVAILABILITY STATEMENT

Approved for public release; distribution is unlimited.

12b. DISTRIBUTION CODE

13. ABSTRACT (Maximum 200 words)

A three-dimensional numerical model has been developed for incompressible flow in reservoirs and other deepwater situations where vertical motion and vertical acceleration are both important. Optional features include k-ϵ turbulence modeling, temperature-driven buoyancy, and passive transport. The developing flow is computed by marching the governing equations forward in time. This is accomplished with a single-step upwind scheme for the turbulence quantities, and a MacCormack predictor-corrector scheme for the remaining flow variables. Pressure is assumed nonhydrostatic and is obtained from the iterative solution of a Poisson equation based on the continuity equation. To enhance geometric flexibility, the model uses composite structured grids assembled from one or more curvilinear subdomains. Flow simulations are presented without confirmation for a provisional design of McCook Reservoir. Empirical validation of the model will be undertaken in future work.

14. SUBJECT TERMS		15. NUMBER OF PAGES 92
Buoyant flow	Reservoirs	
Incompressible flow	Turbulence modeling	16. PRICE CODE
Numerical modeling		

17. SECURITY CLASSIFICATION OF REPORT	18. SECURITY CLASSIFICATION OF THIS PAGE	19. SECURITY CLASSIFICATION OF ABSTRACT	20. LIMITATION OF ABSTRACT
UNCLASSIFIED	UNCLASSIFIED		